CHAPTER

10

Pacific Ocean

10.1. INTRODUCTION AND OVERVIEW

The Pacific Ocean is the largest of the three major oceans. It has well-developed wind-driven circulation systems in the subtropics, subpolar North Pacific, and tropics (Sections 10.1–10.7). In the south, the Pacific circulation transitions to the Southern Ocean, which connects it to the other oceans (Chapter 13). The Pacific is also connected at low latitudes to the Indian Ocean through passages in the Indonesian archipelago. It is connected to the Arctic (Chapter 12) through the very shallow Bering Strait.

The Pacific is the freshest of the three major oceans because of small differences in net evaporation/precipitation between the oceans (Chapter 5). Compared with the North Atlantic, this freshness completely inhibits formation of deep waters and weakens formation of intermediate water in the northern North Pacific (Section 10.9). At this global scale, the Pacific is one of the broad regions of deep upwelling that returns deep waters formed elsewhere back to mid-depths or even the surface. Because of its weak thermohaline circulation, the North Pacific upper ocean circulation is mostly associated with wind forcing. Therefore, it can be useful to study the wind-driven circulation first in the context of the North Pacific and equatorial Pacific, followed by study of the other oceans.

The tropical Pacific is the center of action for the interannual climate mode, El Niño-Southern Oscillation (ENSO: Section 10.8), which impacts much of the globe through atmospheric "teleconnections." Important natural climate variability of quasi-decadal timescale is also observed in the Pacific (Section 10.10; Chapter S15 located in the supplemental material found on the textbook Web site http://booksite.academicpress.com/DPO/; "S" denotes supplemental material).

The Pacific Ocean has numerous marginal seas, particularly along its western side; these are described briefly in the online supplement Section S8.10. The complicated passages through the Indonesian archipelago shunt water from the tropical Pacific to the tropical Indian Ocean. The Bering Strait at the northern end of the Bering Sea allows a small leakage of North Pacific water into the Arctic and hence into the Atlantic Ocean. The Okhotsk Sea in the northwestern Pacific is the site for the densest water formation in the North Pacific; this densest Pacific water is only of intermediate depth and is less dense and much smaller in impact than dense water formation in the North Atlantic and Antarctic, which supply the deepest waters of the global ocean, including the Pacific.

The Pacific Ocean's surface circulation (Figures 10.1, 10.2a and Figure S10.1 in the

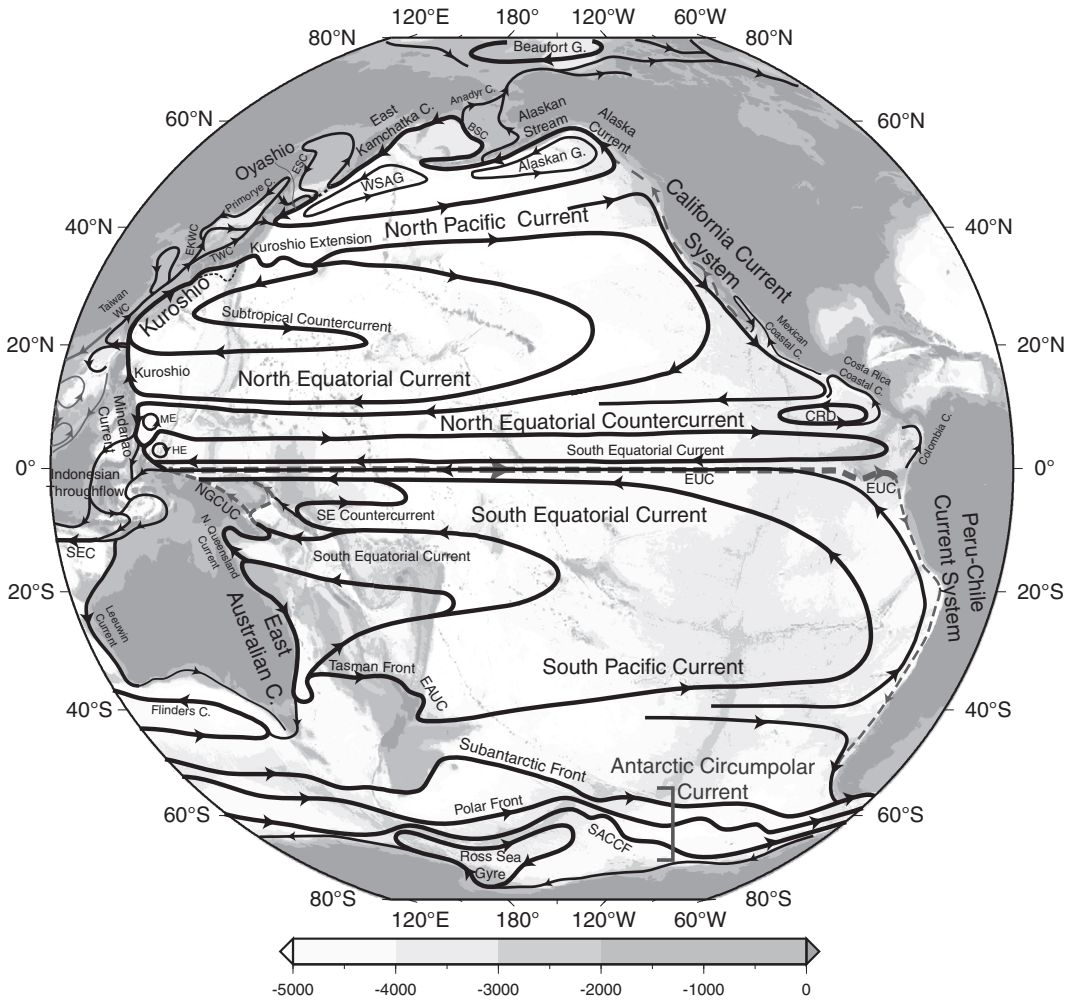

FIGURE 10.1 Pacific Ocean: surface circulation scheme. Major near-surface undercurrents at the equator and along the eastern boundary are also shown (dashed). The South China Sea circulation represents the winter monsoon. Acronyms: SACCF, Southern ACC Front; EAUC, East Auckland Current; NGCUC, New Guinea Coastal Undercurrent; EUC, Equatorial Undercurrent; CRD, Costa Rica Dome; ME, Mindanao Eddy; HE, Halmahera Eddy; TWC, Tsushima Warm Current; EKWC, East Korean Warm Current; WSAG, Western Subarctic Gyre; ESC, East Sakhalin Current; and BSC, Bering Slope Current.

supplementary Web site) includes subtropical gyres in both hemispheres, a subpolar gyre in the North Pacific, and the Antarctic Circumpolar Current (ACC; Chapter 13) in the far south. The western boundary currents for the North and South Pacific's subtropical gyres are the *Kuroshio* and *East Australian Current* (EAC), respectively. The eastern boundary currents for these subtropical gyres are the *California Current* and the *Peru Current*, respectively. The western boundary current for the North Pacific's subpolar gyre is the *Oyashio/East Kamchatka Current* (EKC). The strongly zonal (east-west) circulation in the equatorial Pacific is described

separately (Section 10.7) because of its complexity and dynamics, which differ from mid-latitude wind-driven circulation processes (Section 7.8). The tropical circulation also includes low latitude western boundary currents: the *Mindanao Current* and the *New Guinea Coastal Undercurrent* (NGCUC). The Pacific Ocean's deep circulation (Section 10.6) consists of inflow from the Southern Ocean in a *Deep Western Boundary Current* (DWBC) along the deep plateaus and island chains from New Zealand northward. Much of the deep flow funnels through the Samoan Passage in the South Pacific and then enters the deep tropical ocean. Deep flow crosses the equator in the west and then follows the western boundary's deep trenches northward, filling in the deep North Pacific. The "end" of the deep circulation is reached in the northeastern Pacific, which has the oldest deep waters of the world, as supported by carbon-14 content (Chapter 4, Figure 4.24b).

The inflowing bottom waters upwell through the length of the Pacific, although most of the upward transport occurs in the South Pacific and tropics. Downward diffusion of heat and

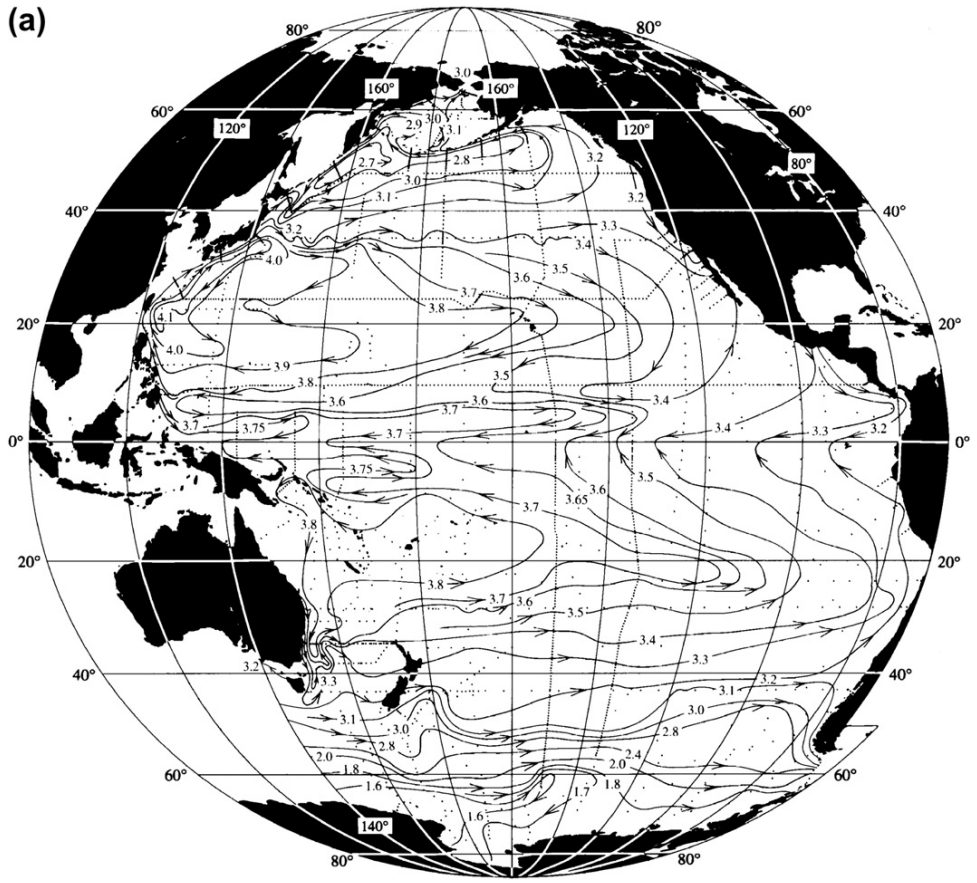

FIGURE 10.2 Adjusted geostrophic streamfunction (steric height, 10 m^2/sec^2) at (a) 0 dbar and (b) 500 dbar. *Source: From Reid (1997).*

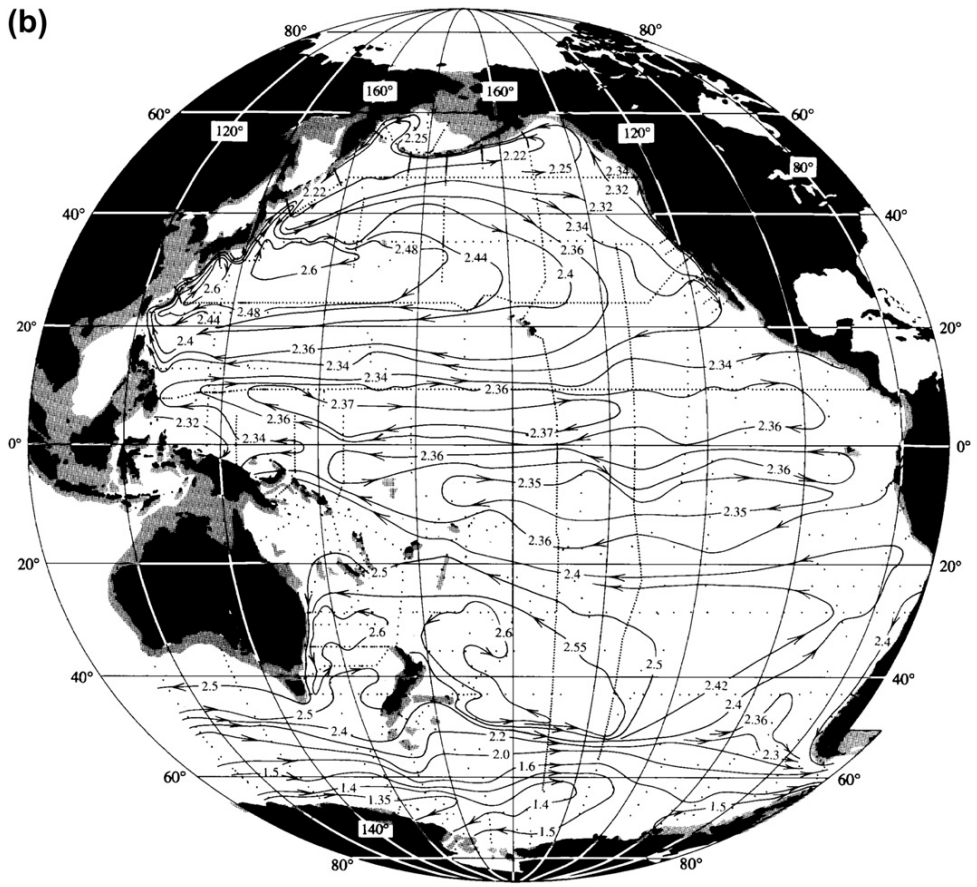

FIGURE 10.2 (*Continued*).

freshwater modify the water density, and the upwelling deep waters create a relatively homogenous and volumetrically large water mass called the Pacific Deep Water (PDW; or Common Water). This returns back to the Southern Ocean where it joins the Indian Deep Water (which is formed similarly) and the North Atlantic Deep Water (which has an entirely different formation mechanism). Within the Pacific, there is also upwelling from the deep waters to shallower layers, including intermediate and upper ocean layers, with outflow in different parts of these layers in all directions: through the Indonesian passages to the Indian Ocean, southwestward around Australia, northward through the Bering Strait, and eastward through the Drake Passage (see Chapter 14).

10.2. WIND AND BUOYANCY FORCING

The Pacific's upper ocean gyres and tropical circulation are mainly wind-driven. The mean surface winds are dominated by the westerlies at latitudes poleward of about 30° (north and

south) and the easterly trade winds at low latitudes (Figure 5.16a–c and supplementary Figure S10.2a). The resulting Ekman transport convergences and divergences drive Sverdrup transport (Figure 5.17 and supplementary Figure S10.2b) and hence the gyres. The anticyclonic subtropical gyres in Figures 10.1 and 10.2a correspond to the Ekman downwelling regions and equatorward Sverdrup transport. The cyclonic gyres in the subpolar North Pacific and south of the ACC in the Ross Sea correspond to the Ekman upwelling regions and poleward Sverdrup transport. A narrow tropical cyclonic cell, centered at about 5°N, stretches across the width of the Pacific; it includes the Mindanao Current and the North Equatorial Countercurrent (NECC). It is associated with Ekman upwelling beneath the Intertropical Convergence Zone (ITCZ).

The alongshore wind stress component at the eastern boundaries creates Ekman transport divergence that is not represented in wind stress curl maps. There is also non-zero wind stress curl in bands along the boundaries, for instance, upwelling-favorable along the California-Oregon coast. Both mechanisms drive the California and Peru-Chile Current Systems (PCCS).

The Pacific's annual mean buoyancy forcing (Figure 5.15) is dominated by heating/cooling (Figure 5.12). The tropical Pacific has the largest mean heating of any region on the globe, over the upwelling cold tongue in the eastern equatorial region. Bands of ocean heat gain are found along the west coasts of North and South America, in the California Current and Peru-Chile Current upwelling systems. The Kuroshio region in the North Pacific is one of the strongest global air–sea heat loss regions (>125 W/m^2). The equivalent region along the Australian coast, in the EAC, also has significant heat loss (>100 W/m^2).

Net evaporation-precipitation (Figure 5.4a) is directly related to the Pacific's surface salinity pattern. There is net precipitation in the ITCZ (5–10°N). A broader region of net precipitation occurs in the western tropical Pacific under the ascending branch of the Walker circulation. Net precipitation is also found throughout the higher latitudes in both the North and South Pacific. Net evaporation is found in the subtropical gyres under the descending branches of the Hadley circulation.

The air–sea flux maps in Chapter 5 do not represent the brine rejection process that creates dense water when sea ice forms. This process is active in the North Pacific in the Okhotsk and Bering Seas, and in the northern Japan (East) Sea. Okhotsk Sea brine rejection is the densest source of North Pacific Intermediate Water (Section 10.9.2)

10.3. NORTH PACIFIC CIRCULATION

The mid-latitude North Pacific surface circulation (Figures 10.1 and 10.2a; Table S10.1 in the online supplement), with its subtropical and subpolar gyres, is the clearest example seen in all of the oceans of the two-gyre circulation driven by the westerly and trade winds. This is because the North Pacific is almost completely closed to the north and has only a weak thermohaline circulation. The gyres have the familiar east-west asymmetry (with strong western boundary currents and weak meridional flow spread over much of the remainder of the ocean), which is understood in terms of meridional Sverdrup transport (Figure 5.17 and Section 10.2). With increasing depth, the North Pacific gyres weaken and shrink, and the subtropical gyre centers (highest pressure) shift westward and poleward (Section 10.6).

10.3.1. Subtropical Circulation

10.3.1.1. General Description

The North Pacific's subtropical gyre, like all subtropical gyres, is anticyclonic (clockwise in

the Northern Hemisphere), associated with Ekman downwelling and equatorward Sverdrup transport (Figure 5.17). Its strong, narrow, northward western boundary current is the *Kuroshio*. After the Kuroshio separates from the western boundary and flows eastward into the North Pacific, the current is referred to as the *Kuroshio Extension*. The broad eastward flow on the northern side of this gyre is called the *North Pacific Current* or the "West Wind Drift." The North Pacific Current also includes the eastward flow of the subpolar gyre; it is also called the Subarctic Current (Sverdrup, Johnson, & Fleming, 1942). The westward flow on the south side of the subtropical gyre is the *North Equatorial Current*, which also includes the westward flow in the elongated tropical cyclonic circulation. The concentrated flow near the eastern boundary is the *California Current System* (CCS), which includes a locally forced eastern boundary current and a poleward undercurrent (Davidson Current); both are forced by coastal upwelling (Section 7.9).

The surface subtropical gyre in the western North Pacific has an overall "C-shape" (Wyrtki, 1975; Hasunuma & Yoshida, 1978). The "C" looks like a large-scale overshoot of the Kuroshio as it becomes the Kuroshio Extension, with a swing back to the west in the *recirculation*, followed by southward flow parallel to the Kuroshio, a turn to the east in the *Subtropical Countercurrent* (STCC) at 20–25°N, and then the westward flow of the North Equatorial Current (NEC) south of 20°N. This C-shape is common to surface flow in all subtropical gyres, but the STCC portion is very shallow; the circulation just 250 dbar below the surface is a simpler, closed anticyclonic gyre.

The broad eastward and westward flows crossing the Pacific include narrow, nearly zonal (east-west) fronts or frontal zones that are narrow (less than 100 km wide). Nomenclature is confusing and contradictory. We adopt Roden's (1975, 1991) terms for the central North Pacific. The *Subarctic Frontal Zone* (SAFZ; or Subarctic Boundary), centered at about 42°N, is embedded in the North Pacific Current; it roughly separates the subtropical and subpolar gyres, being slightly south of the maximum westerly winds. The *Subtropical Frontal Zone* (or convergence), at about 32°N in the central and eastern Pacific, separates the eastward North Pacific Current from the westward NEC.

With increasing depth, the subtropical gyre shrinks toward the west and toward Japan, and decreases in strength. It disappears around 1500 m depth except in the Kuroshio region (Figures 10.10 and 10.14).

10.3.1.2. The Kuroshio and Kuroshio Extension

The Kuroshio (black stream in Japanese, where *shio* means current) arises at the western boundary where the westward flow of the NEC splits at about 15°N into northward and southward boundary currents: the Kuroshio and Mindanao Current, respectively (Figures 10.1 and 10.3). The Kuroshio continues northward, turns to follow the south coast of Japan, then separates and flows out to the mid-subtropical gyre. Maximum surface current speeds in the Kuroshio range between 75 and 250 cm/sec. The width of the current is 80 to 100 km. It has major variability at timescales of weeks to decades.

The Kuroshio velocity decreases with depth (Figure 10.4b). The northward velocity core of the Kuroshio is sometimes flanked on both sides by weak countercurrents (flowing in the opposite direction). Where the Kuroshio begins to leave the western boundary, it passes eastward through Tokara Strait (Figure 10.4a,b), tracks eastward roughly parallel to the south coast of Japan, then passes through gaps in the Izu-Ogasawara (Izu) Ridge, and finally enters the open Pacific at Boso Peninsula (Figure 10.3a). Between Tokara Strait and the Izu Ridge, the Kuroshio exists in one of two (or three) semi-stable states: flowing either nearly directly

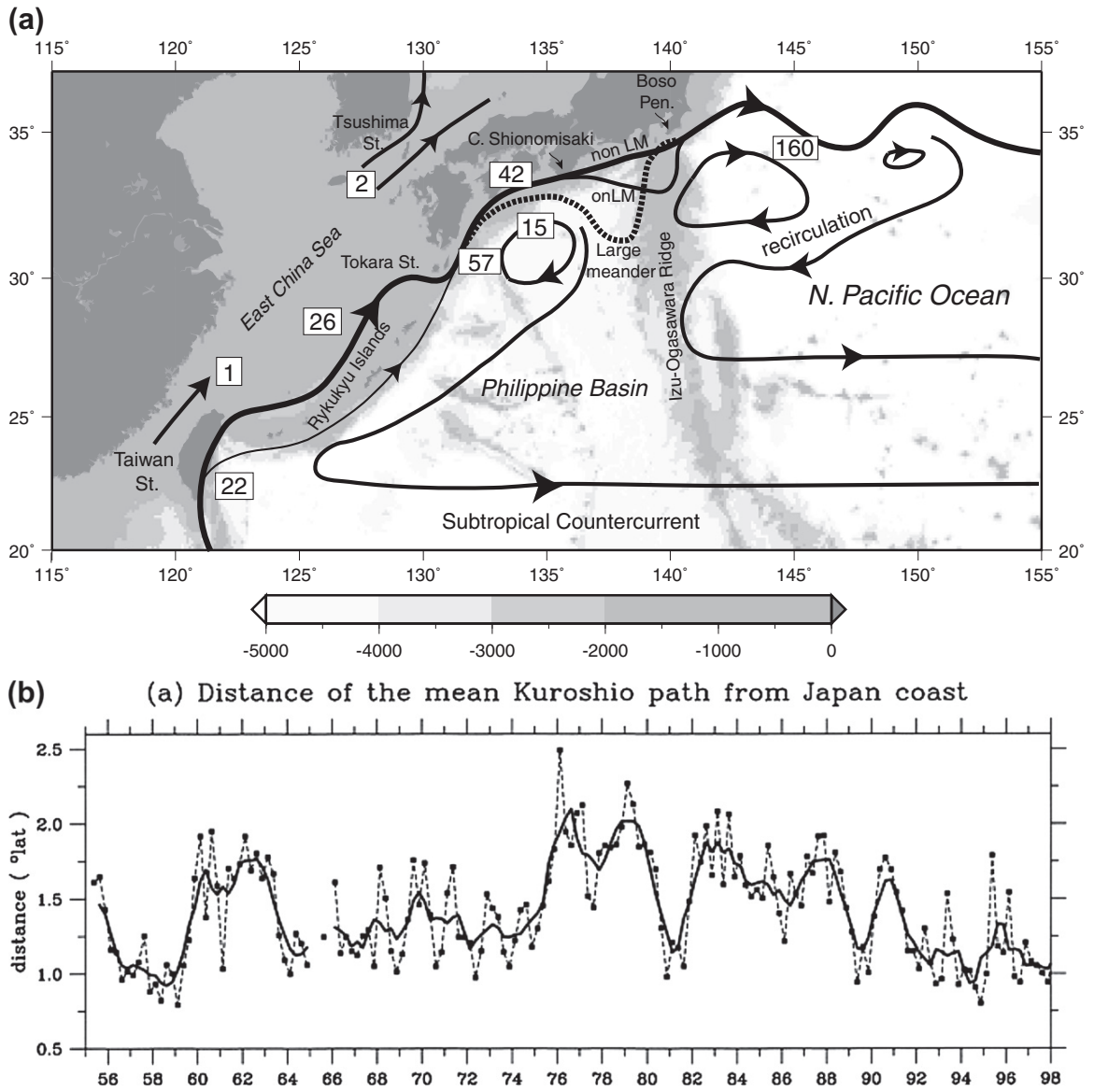

FIGURE 10.3 Kuroshio system in the western North Pacific. (a) Schematic of the large meander (LM), straight (near shore non-large meander) and offshore non-large meander paths (*after Kawabe, 1995*), and recirculation gyre schematics, with transports in Sv (*after Hasunuma and Yoshida, 1978; Qiu and Chen, 2005*). (b) Index of the Kuroshio meander state: distance offshore of the 16°C isotherm at 200 m averaged between 132° and 140°E. *©American Meteorological Society. Reprinted with permission. Source: From Qiu and Miao (2000).*

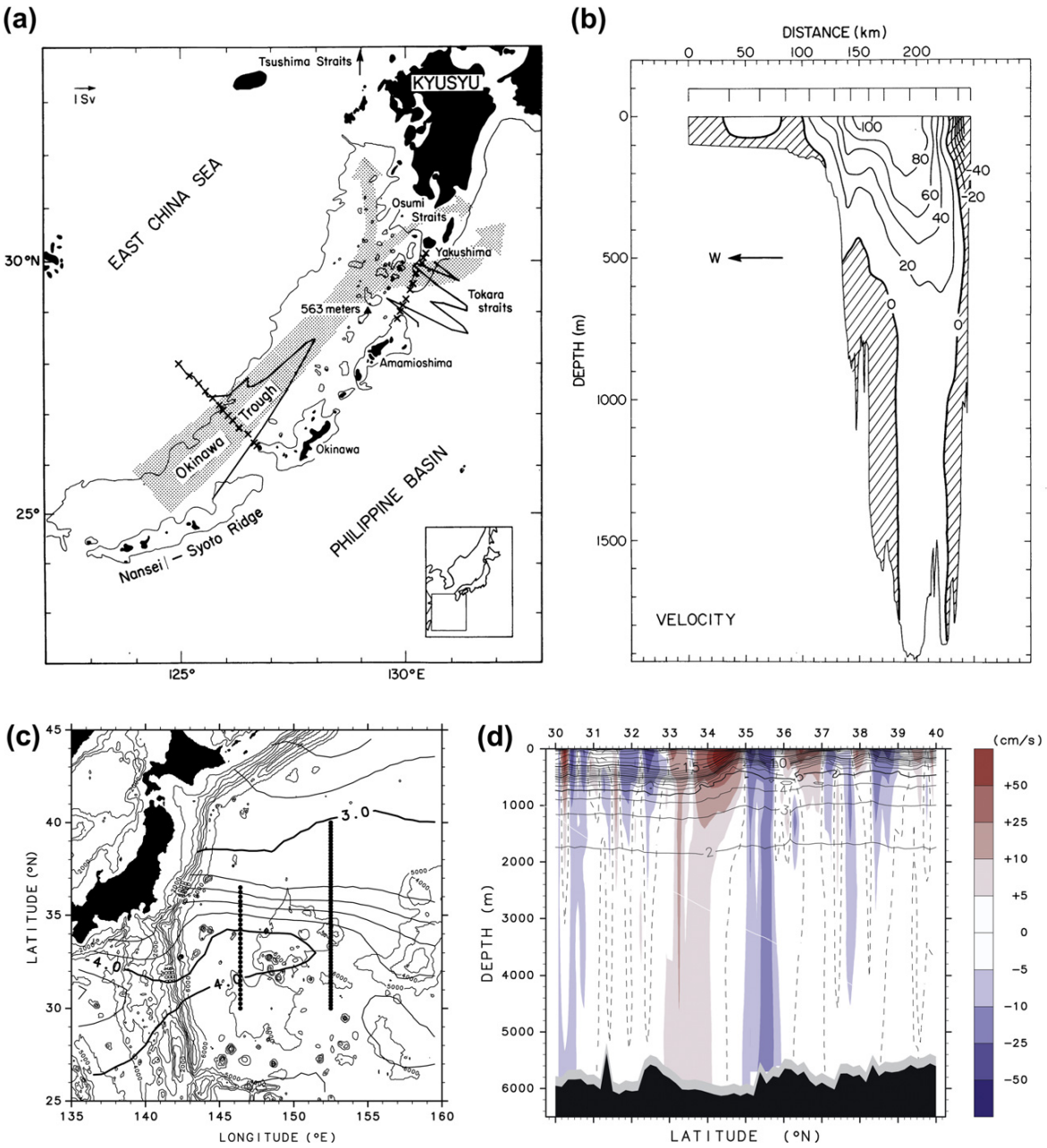

FIGURE 10.4 Kuroshio velocity structure. Vertical sections of (b) northward velocity of the Kuroshio where it is a western boundary current, at 24°N (*Source: From Bingham & Talley, 1991*), and (d) eastward velocity of the Kuroshio Extension at 152° 30′E [red (blue) indicates eastward (westward) flow]. *Source: From Yoshikawa et al. (2004).* Section positions are shown in (a) and (c). Mean temperature at 1000 m is contoured in (c). Figure 10.4d can also be found in the color insert.

along the coast (straight path), or looping far to the south in a meander (large meander path). The Kuroshio remains in one of these states for several years and then switches to the other state (index in Figure 10.3b). The mean eastward-flowing Kuroshio Extension splits close to Shatsky Rise into a southward branch that feeds a westward flow that creates a *recirculation gyre* (*Kuroshio Countercurrent*) and an eastward flow that becomes the North Pacific Current. The recirculation gyre is often split in two by the Izu Ridge, with one gyre west of the ridge and south of Japan, and the other gyre east of the ridge, downstream of the Kuroshio separation point (Figure 10.3a).

Once the Kuroshio crosses the Izu Ridge and enters deep water, its upper ocean structure is like that of the Gulf Stream, with a strong eastward velocity core and marked, but weaker, westward recirculation just to the south. The Kuroshio Extension extends to the ocean bottom in the deepest water downstream of the separation point, with 10 cm/sec velocities even at the bottom (Figure 10.4d). Westward recirculations flank the deep Kuroshio Extension to the bottom.

The volume transport of the Kuroshio increases downstream (Figure 10.3a) from 20 to 25 Sv, where it is a western boundary current east of Taiwan (Johns et al., 2001; Bingham & Talley, 1991), to about 57 Sv east of Tokara Strait but still prior to separation to a maximum of 140 to 160 Sv at 145°E, just to the east of separation. Considerable recirculation causes much of these increases (Imawaki et al., 2001). The transport decreases east of this point, with water lost southward to the recirculation gyre and into the Kuroshio Extension bifurcation fronts (Yoshikawa, Church, Uchida, & White, 2004).

The Kuroshio Extension is highly unstable. It meanders and produces rings when the meanders pinch off. The meanders have somewhat preferred locations, which differs from the Gulf Stream. The first northward meander occurs just downstream of the separation point. This often creates an anticyclonic warm-core ring of about 200 km diameter that moves northward. A second preferred location for northward meandering is at 150°E. Southward meanders, between the northward meanders, form cyclonic cold-core rings south of the Kuroshio Extension. The envelope of paths is several hundred kilometers wide from the separation point out to near 160°E (Shatsky Rise), widening to about 500–600 km with the paths becoming considerably more random (Mizuno & White, 1983; Qiu & Chen, 2005).

10.3.1.3. North Pacific Current and Mid-Latitude Fronts

The *North Pacific Current* is the broad eastward flow of the central and eastern subtropical gyre. The mean speed of the North Pacific Current is small, less than 10 cm/sec. However, synoptic meridional crossings of the North Pacific Current reveal larger geostrophic flows of 20 to 50 cm/sec that reverse direction on the order of every 100 km (at the eddy scale) and are deep-reaching. The difficulty of distinguishing between eddies and permanent flow features obscured observation of the deep penetration of the Kuroshio Extension Front until recently (Figure 10.3d).

The northern and southern "boundaries" of the subtropical gyre can be considered to be the SAFZ (40–44°N) and the Subtropical Front (25–32°N, depending on longitude). In both frontal zones — which are synoptically about 100–200 km wide and often contain at least two sharp fronts — temperature, salinity, and density change rapidly with latitude (Figure S10.3 in the supplementary Web site). The frontal zones are relatively zonal over much of the North Pacific; they veer southward into the CCS in the east.

The SAFZ arises in the western North Pacific from both a branch of the Kuroshio Extension

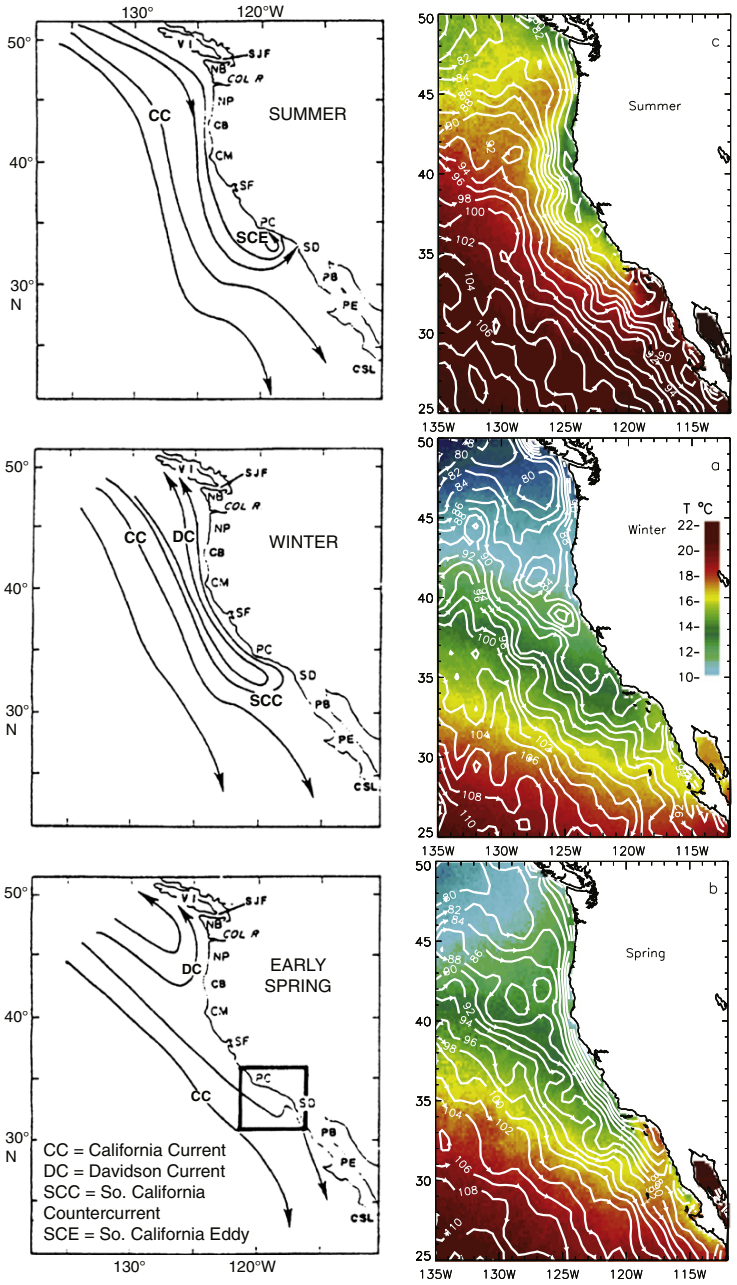

FIGURE 10.5 (a) Schematic of the surface currents in the CCS in different seasons. *Source: From Hickey (1998).* (b) Mean seasonal cycle of satellite-derived surface temperature (color) and altimetric height, showing the geostrophic surface circulation. *Source: From Strub and James (2000, 2009).* This figure can also be found in the color insert.

Front and the STCC. It coincides in the open Pacific with maximum Ekman convergence in the center of the subtropical gyre.

The SAFZ might be partly associated with the separated Oyashio front (Section 10.3.2.2). It coincides approximately with the maximum westerly wind, marking the transition from the Ekman downwelling of the subtropical gyre to the Ekman upwelling of the subpolar gyre. The northern front in the SAFZ is the southernmost limit of the very strong halocline of the subpolar gyre, and the southernmost limit of the shallow temperature minimum in the western subpolar gyre. There is a jump in nutrients across the frontal zone to higher values in the subpolar surface waters (Figure S10.3c,d in the supplementary Web site; surface nitrate map in Figure 4.23).

10.3.1.4. California Current System

The CCS stretches from the Strait of Juan de Fuca to the tip of Baja California (Figures 10.1 and 10.5). We describe the CCS in some detail, because it is the principal example in this text of an eastern boundary current system. In-depth overviews of the CCS and its variability can be found in Wooster and Reid (1963), Huyer (1983), Lynn and Simpson (1987), Hickey (1998), and Marchesiello, McWilliams, and Shchepetkin (2003).

The CCS has two regimes: (1) the southward, shallow, narrow, meandering California Current Front, with upwelling zones along the coast, offshore-advecting jets of upwelled water, and a northward undercurrent or inshore surface countercurrent and (2) the broad southward flow of the subtropical gyre. Dynamically, these two components have entirely different origins: (1) southward flow due to locally wind-driven coastal upwelling with a poleward undercurrent and (2) southward flow that is part of the large-scale subtropical circulation resulting from Ekman downwelling and associated equatorward Sverdrup transport (Figure 5.17). We discuss only the upwelling system here.

A simplified approach to the dynamics of subtropical eastern boundary systems, based on Ekman transport and upwelling, was provided in Section 7.9. This framework is useful for initial broad understanding, but these systems tend to be far more complex than this, which is evident as soon as we look at satellite images of sea-surface temperature (SST) and ocean color in the CCS (Figure 10.6). The CCS upwelling is forced by the alongshore component of the prevailing westerly winds, which results from their southward deflection as they encounter the North American continent (Figure 5.16). The upwelling is apparent off the North American coast from British Columbia to California (50−30°N), as a patchy band of cool surface water within a region 80 to 300 km from shore, strongest from April to August (Figure 10.6a). The upwelled waters are highly productive, which can be observed with satellite ocean color sensors (Figure 10.6b). The upwelled water does *not* originate from great depth because the ocean is stratified. Its source is around 150−200 m depth, but this is deep enough to access the nutrient-enriched waters below the euphotic zone.

The maximum surface velocity of the mean southward California Current is 40−80 cm/sec and its width is 50−100 km. The California Current is in geostrophic balance with the cross-shore pressure gradient force. It decays rapidly with depth and is essentially confined to the top 300 m (Lynn & Simpson, 1987). Thus the CC is much shallower and carries much less transport, on the order of only a few Sverdrups, than a western boundary current such as the Kuroshio. The decrease in geostrophic velocity from the surface to 200 m is evidenced in the upward tilt of isotherms toward the coast (Figure 10.7). The upwelling, surface PGF and upward tilt of the isotherms result from offshore Ekman transport, which has been observed directly by Chereskin (1995) (Figure 7.7).

An idealized steady state requires warming of the upwelled water as it moves offshore. Since the right amount of warming does not generally

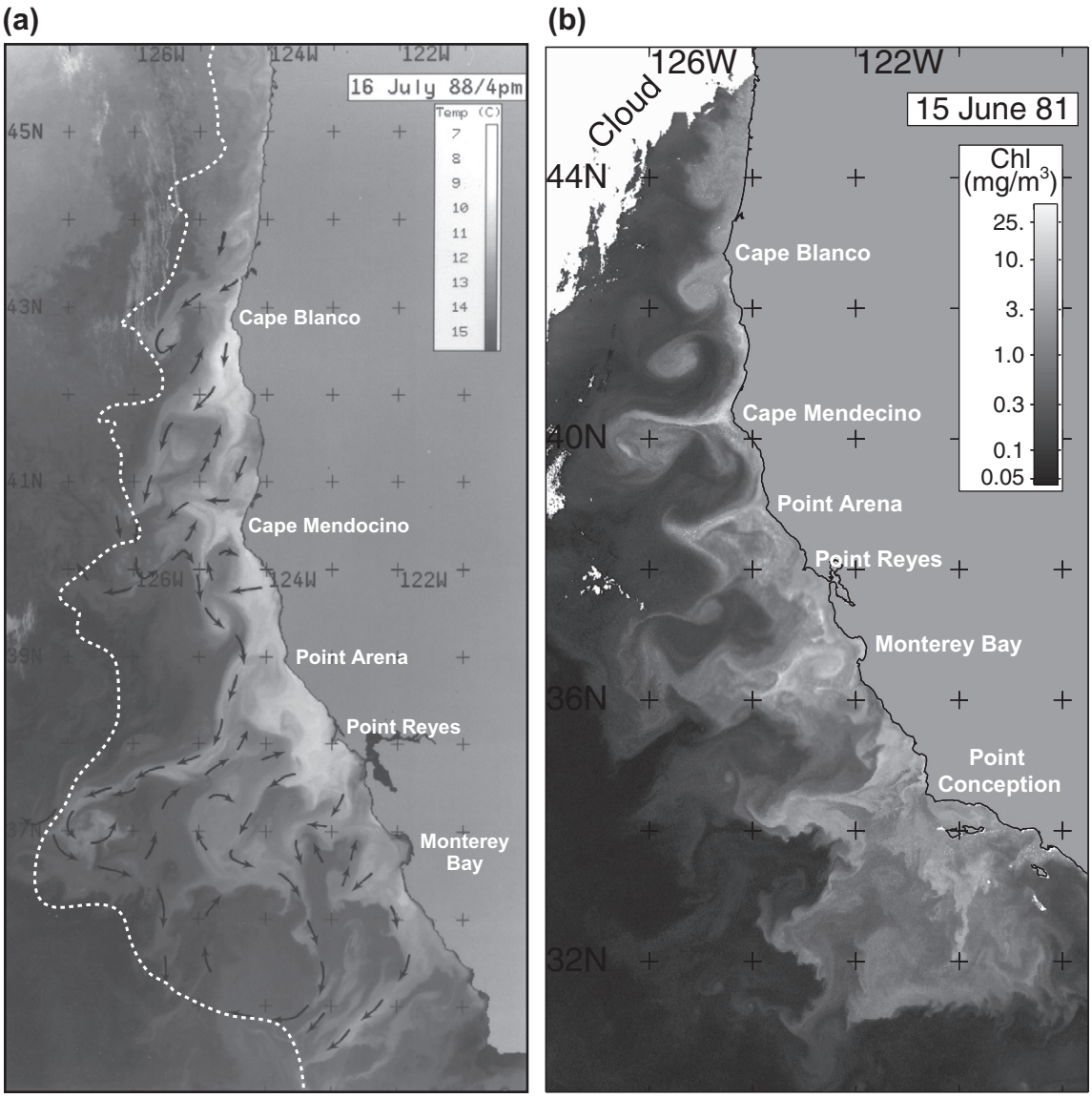

FIGURE 10.6 (a) Satellite SST (July 16, 1988), with subjectively determined flow vectors based on successive images. (b) Surface pigment concentration from the CZCS satellite on June 15, 1981. *Source: From Strub et al. (1991).*

occur at exactly the right time, the actual state is more complicated. The seasonal offshore Ekman transport creates an upwelling front that moves offshore. The California Current's southward core is located at the upwelling front, as seen in Figure 10.7, and moves offshore with the front as it progresses through the upwelling season. The mean location of the California Current is therefore offshore, by about 200–300 km, and not at the coast. This is also evident in the tighter

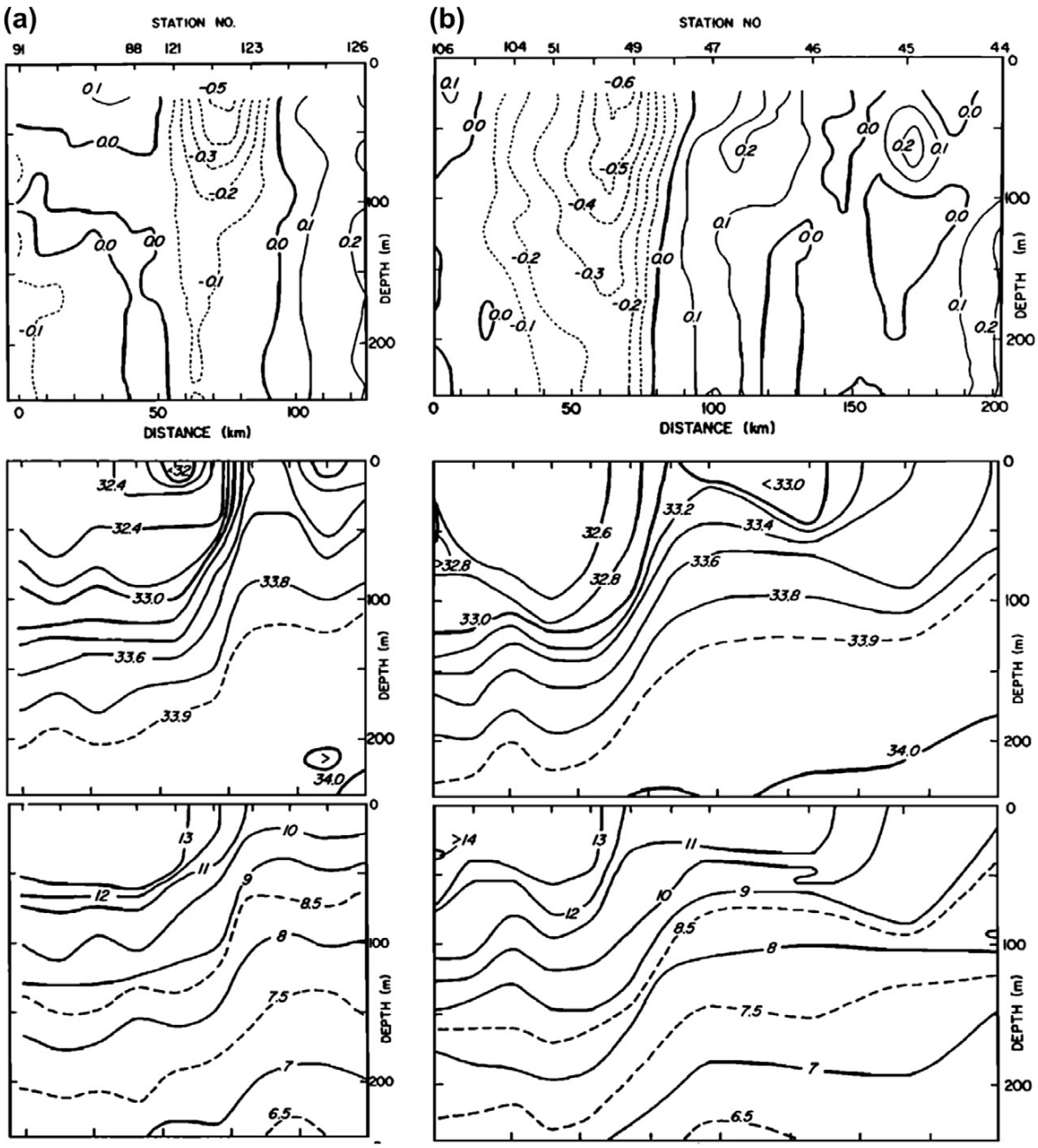

FIGURE 10.7 Sections of (top) velocity (m/sec), (middle) salinity, (bottom) potential temperature (°C) across the CCS at 41.5°N (left) and 40.0°N (right) in June, 1987. The coast is to the right. *Source: From Kosro et al. (1991).*

dynamic height contours in Figure 10.5 and the strong fronts in Figure 10.7.

The mean offshore location of the California Current is also apparent in enhanced dynamic height/sea-surface height variability due to a vigorous eddy field, and in low salinity that reflects the northern source of the surface water (Figure 10.8). Underneath and inshore of the California Current, the mean flow is northward (poleward), centered at the continental shelf break. This is the *California Undercurrent* (CUC). The CUC is approximately 20 km wide and its core lies at about 250 m, although it can extend to more than 1000 m depth. Its maximum speed is more than 10 cm/sec, and its water originates in the warm, saline, low oxygen tropical Pacific. The mean CUC is in geostrophic balance with the offshore pressure gradient force at this depth. The reversal of alongshore geostrophic flow from the southward CC at the surface to the northward CUC requires sloping isopycnals between the two currents. The CUC then weakens below its core. The CUC is thus recognized by a spreading of the isotherms and isopycnals, upward above the undercurrent and downward below it.

During winter, upwelling is weak or inactive. The California Current is far offshore and relatively weak and the coastal flow is northward (the *Inshore Countercurrent* or *Davidson Current*). This poleward flow could be the Sverdrup transport response to the Ekman suction driven by positive wind stress curl in the CCS region; it is overwhelmed by the response to coastal upwelling during the upwelling season (Marchesiello et al., 2003). When upwelling starts up again, an upwelling front appears near the coast as the offshore edge of the Ekman transport. A strong southward California Current jet is associated with the front and moves progressively offshore with time (Figure 10.5; Strub & James, 2000).

The strong seasonal cycle of the wind forcing is quantified with upwelling indices. In Figure 10.9, one index is based on Ekman transport and the

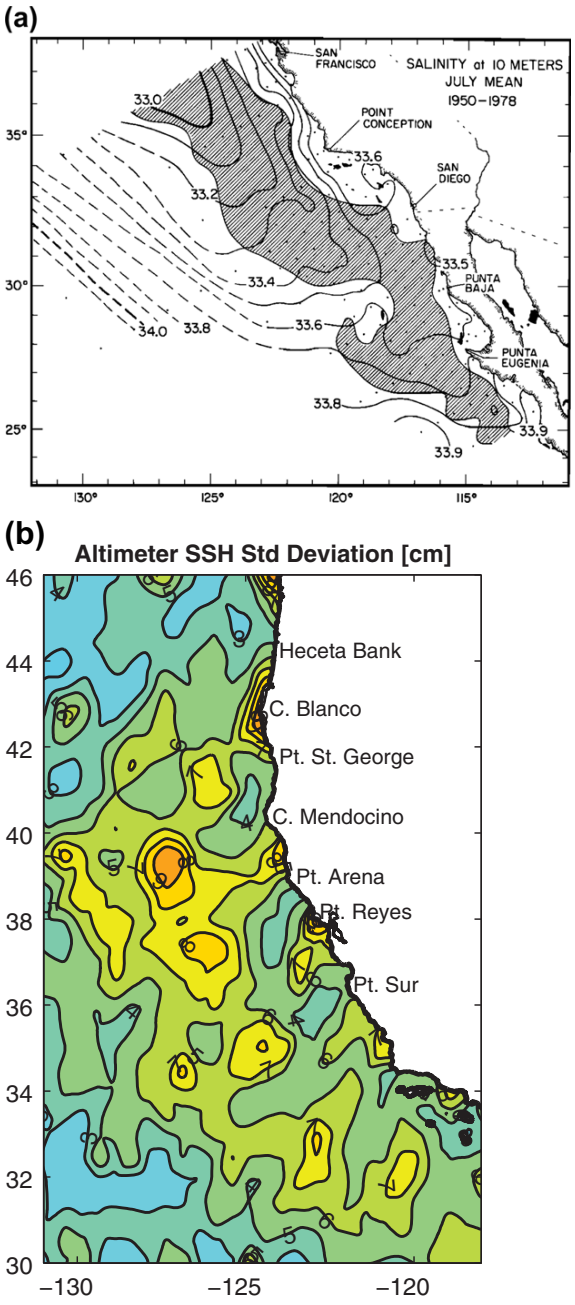

FIGURE 10.8 (a) Mean salinity at 10 m in July (contoured) with dynamic height standard deviations greater than 4 dyn cm in gray. *Source: From Lynn and Simpson (1987).* (b) Sea surface height standard deviation (cm) from satellite altimetry. *©American Meteorological Society. Reprinted with permission. Source: From Marchesiello et al. (2003).*

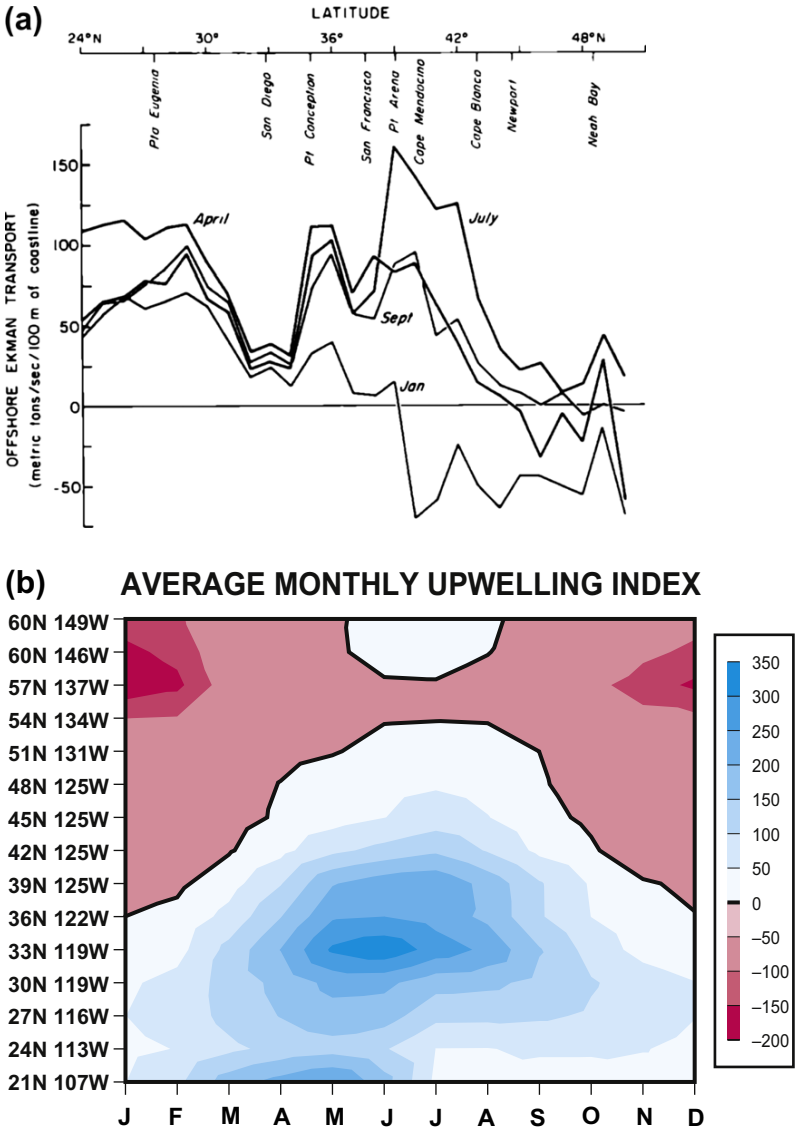

FIGURE 10.9 (a) Offshore Ekman transport based on long-term mean wind stress. *Source: From Huyer (1983).* (b) Upwelling index based on atmospheric pressure distribution (*from Bakun, 1973*), averaged over 1946–1995. Lower shaded region (positive values or blues in the original figure) is upwelling; upper shaded region (negative values or reds in the original figure) is downwelling. *Source: From Schwing, O'Farrell, Steger, and Baltz (1996).*

other on the strength of alongshore wind component.[1] Maximum upwelling occurs in late spring and summer (April through July), as evident from enhanced surface chlorophyll content in summer (Figure 10.6b), and is highest near Point Conception (34°N). North of 40°N, the longshore winds actually cause downwelling in winter as the Aleutian Low expands southward; north of 45°N, there is downwelling in the annual mean (Venegas et al., 2008).

[1] Neither index includes the wind stress curl component of the upwelling, although we have already noted that it can be important (Bakun & Nelson, 1991; Pickett & Paduan, 2003).

The quasi-continuous, alongshore mean circulation described in the previous paragraphs is the simplest view of the CCS. However, as seen in satellite images (Figure 10.6), the upwelled water does not move offshore in a "sheet," but rather in jets at recurring locations associated with capes or points in the coastline. The circulation can be either "squirt-like," in which the jet goes out to sea and dies, or meandering, in which the jet goes out and returns. The high mesoscale eddy activity in the CCS (Figure 10.8) may be created by baroclinic instability of the coastal upwelling current. The eddies spawned by this instability move the upwelled cold water offshore and thus maintain the mean balance, which includes Ekman upwelling (Marchesiello et al., 2003). Recent studies of the California Current are beginning to focus on even smaller spatial scales, called the *submesoscale* (order of 1 to 10 km). These are associated with the actual fronts and their instabilities within the mesoscale eddy field (Capet, McWilliams, Molemaker, & Shchepetkin, 2008).

10.3.1.5. North Equatorial Current

The NEC is the broad westward flow on the southern side of the subtropical gyre. It is between about 8 and 20°N depending on longitude. The NEC forms gradually in the eastern Pacific from southward flow of the subtropical gyre, including the CCS. At the eastern boundary, it has input from the tropical current system (Costa Rica Dome and NECC).

As the NEC flows westward, some of it moves southward and joins the strong eastward flow of the NECC. When the NEC reaches the western boundary, it bifurcates at about 14°N into a northward portion that becomes the Kuroshio and a southward portion that becomes the Mindanao Current (Section 10.7.4). In the western Pacific, the NEC includes a strong zonal surface salinity front that separates saline water that originates in the subtropical gyre from fresher NECC surface water. The location of this front is similar to the latitude of the NEC bifurcation, and it is also an ecological front that is important for fisheries (Kimura & Tsukamato, 2006). These suggest that the front is a boundary between Ekman upwelling in the tropical NEC/NECC cyclonic gyre and downwelling in the anticyclonic subtropical gyre.

Volume transport of the NEC in the western Pacific is up to 50 Sv in the top 500 m and 80 Sv top to bottom (Kaneko, Takatsuki, Kamiya, & Kawae, 1998; Toole, Millard, Wang, & Pu, 1990).

10.3.1.6. Depth Dependence of the Subtropical Circulation

The subtropical gyre shrinks spatially with depth. Like all subtropical gyres, it shrinks toward the most energetic part of its surface flow: westward toward the western boundary, and northward toward the Kuroshio Extension. The Kuroshio Extension extends to the ocean bottom as previously noted.

The gyre shrinkage from the sea surface to about 200 m depth is dramatic (Reid, 1997; represented by Figure 10.2). The boundary between eastward and westward flows shifts from south of 20°N at the sea surface to 25–30°N at 200 m. The C-shape of the western gyre, which includes the STCC, disappears by 200 m. On the other hand, the Kuroshio and Kuroshio Extension do not shift (Figure 10.3d). At 1000–1500 m depth, the anticyclonic subtropical gyre is found entirely in the western North Pacific near the Kuroshio and Kuroshio Extension (Figure 10.10).

Flow in the subtropical regions vacated by the subtropical gyre is very weak. Steric height differences over 1000 km distances are on the order of 1 cm rather than the 10 cm differences within the gyre proper. Dynamically, on isopycnal surfaces that are still within the gyre in the western region, the vacated region is called the shadow zone (Section 7.8.5). Within these regions where there is little direct ventilation from the sea surface, on the eastern and southern flanks of the subtropical gyres, oxygen is depleted to the point where denitrification sets in (Section 10.9.1).

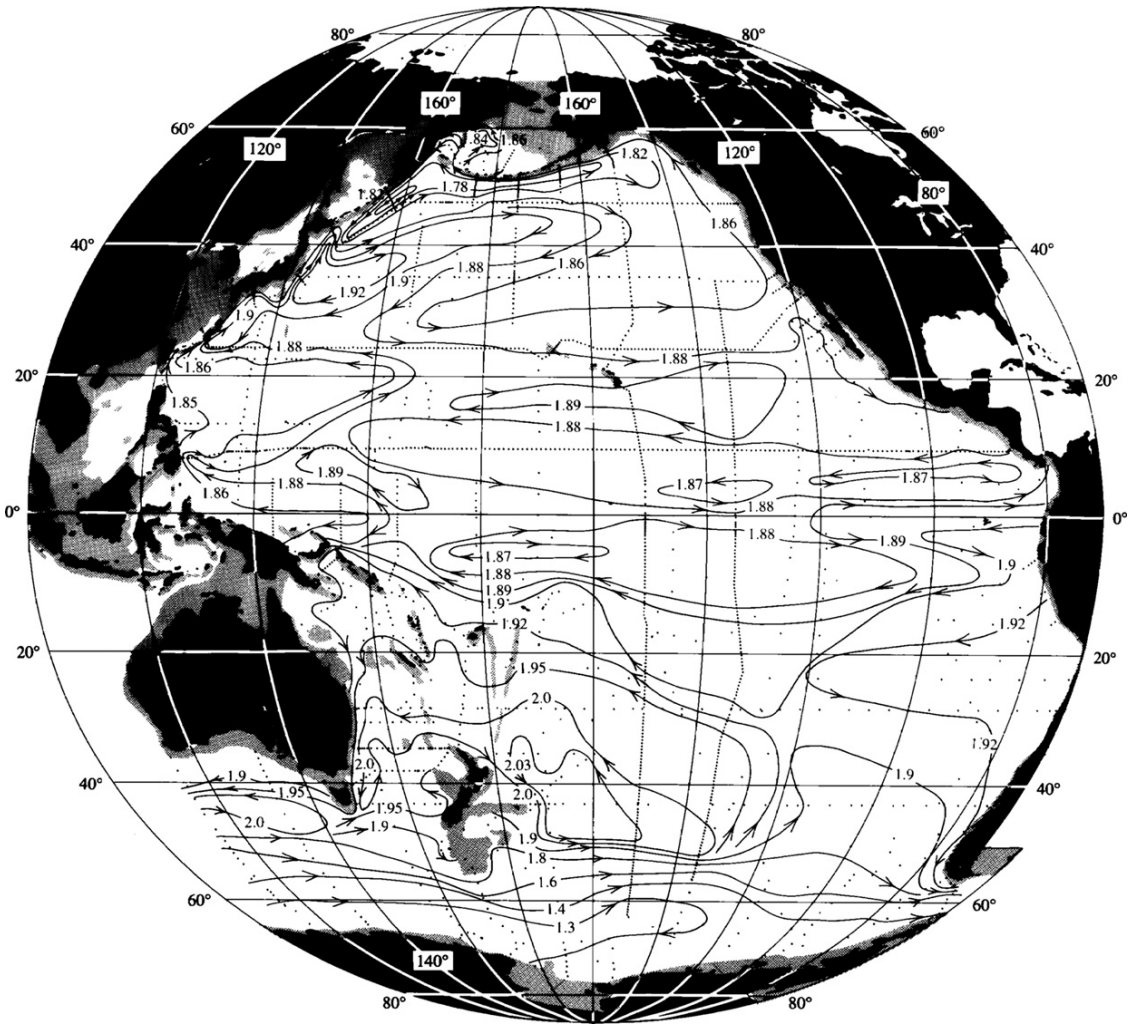

FIGURE 10.10 Steric height (10 m^2/sec^2) at 1000 dbar based on hydrographic data and reference geostrophic velocities adjusted to provide absolute circulation at all depths. *Source: From Reid (1997).*

10.3.2. Subpolar Circulation

10.3.2.1. General Description

The cyclonic (counterclockwise) subpolar gyre in the North Pacific stretches across the width of the basin and is compressed in the north-south direction between about 42°N (Subarctic Front) and the Aleutian Islands/Alaskan coast (Figure 10.1). It has a southward western boundary current, the Oyashio/EKC.

A geographic constriction at the southernmost location of the Aleutian Islands (near the date line) separates the subpolar gyre into two portions. The *Western Subarctic Gyre* is centered east of the Kuril Islands, and the *Alaskan Gyre* is centered in the Gulf of Alaska. They are

connected through eastward flow along the southern side of the gyre (*Subarctic Current*, which is part of the North Pacific Current, Section 10.3.1.3) and westward flow along the Aleutian Islands (*Alaskan Stream*). Completing the nomenclature for the cyclonic gyre, the *Alaska Current* is the northward eastern boundary current along the coast of Canada and Alaska. An older but exhaustive treatment of this circulation is found in Favorite, Dodimead, and Nasu (1976; Figure S10.4 in the supplementary Web site).

Parts of the subpolar gyre circulation loop through the Bering and Okhotsk Seas (S8.10 located in the Web site supplementary text). Transport of 0.8 Sv from the North Pacific to the Arctic and onward to the Atlantic occurs through the Bering Strait at the northern end of the Bering Sea. Both the Bering and Okhotsk Seas have significant ice cover in winter. As a result, important water mass transformation and modification occur in both seas. The Okhotsk Sea produces the densest water in the subpolar North Pacific, mainly through sea ice processes (Section 10.9.2.1).

The subpolar gyre circulation is forced by Ekman upwelling (suction; Figure 5.16d). The winds throughout the region are westerlies, producing southward Ekman transport. The strongest westerly winds are at about 40°N. Southward Ekman transport is largest there and decreases with higher latitude to smaller southward transports. This requires upwelling into the Ekman layer, which creates northward mean Sverdrup transport and the cyclonic gyre (Figure 5.17).

The upwelled water in the subpolar gyre comes from just below the Ekman layer. (It cannot come from greater depth because of the strong pycnocline, mainly due to the low salinity surface layer, hence halocline.) The heightened surface nitrate in Figures 4.22 and 4.23 is a result of this upwelling, which greatly enhances biological productivity. Major fisheries including salmon, halibut, saury, and walleyed pollock are found in the subpolar gyre. Clearly, the Subarctic Front, marking the southern boundary of the subpolar gyre's upwelling, is an important ecosystem boundary.

With increasing depth, the North Pacific's subpolar circulation does not shift location unlike that of the subtropical gyre. It weakens, but its boundary currents reach far down into the water column, even to the bottom. The subpolar gyre is therefore "quasi-barotropic": its surface currents extend to the bottom (barotropic) but weaken (quasi). Near the bottom there are also additional currents associated with the topography and global thermohaline forcing (weak upwelling). The barotropic nature of the gyre is possibly due to geographic restriction, with the Alaskan coast cutting through the region that would be spanned by the gyre if there were no land. On the other hand, similar structure is found in other high latitude cyclonic circulations (North Atlantic subpolar gyre and the Weddell and Ross Sea gyres), suggesting a more general dynamical underpinning.

10.3.2.2. Subpolar Western Boundary Currents

The southward flow in the subpolar western boundary current system includes: (1) the EKC along the Kamchatka peninsula and the northern Kuril Islands and (2) the Oyashio along the southern Kuril Islands and Hokkaido. The division between the two is at Bussol' Strait, which is the deepest strait in the Kuril Island chain. The distinction is drawn because about half of the EKC loops through the Okhotsk Sea, where water properties are greatly modified. This creates a discontinuity in water properties at Bussol' Strait where the Okhotsk Sea waters exit and join the Oyashio.

About 200 km offshore of the Oyashio, there is a northeastward flow called the Subarctic Current (see also Figure S10.4 in the textbook Web site). The Oyashio-Subarctic Current region is very dynamic and includes large (100–200 km diameter), deep-reaching, long-lived anticyclonic eddies with cold, fresh

cores (<3°C, <33.5 psu) that are usually found between Hokkaido and Bussol' Strait (online Figure S10.5). The eddies have two different origins: either locally at Bussol' Strait, from water exiting the Okhotsk Sea, or as warm water from the Oyashio intrusions (see next paragraph) that then propagates northeastward between the Oyashio and the Subarctic Current and is modified by the local cold, fresh subpolar water (Yasuda et al., 2001).

The Oyashio separates from the western boundary at the southernmost cape of Hokkaido. After separation, it usually makes two large meanders called the first (coastal) and second (offshore) Oyashio intrusions (Figure S10.6 from the online supplemental material). These are unrelated to the Kuroshio Extension meanders, which are farther south. Water from the coastal Oyashio intrusion can penetrate southward along the Honshu coast, sometimes as far south as the Kuroshio separation point at around 36°N; this cold coastal water is visible in the SST image of Figure 10.11. The location of southernmost penetration is of great interest to Japanese fisheries since the nutrient-rich Oyashio waters support a more biologically productive ecosystem than the nutrient-depleted Kuroshio waters. Therefore the Oyashio penetration latitude is used as a regional climate index.

The Oyashio/EKC is a relatively weak western boundary current. Maximum surface velocities are 20–50 cm/sec. Total Oyashio transport, based on combined direct current observations and hydrographic data east of

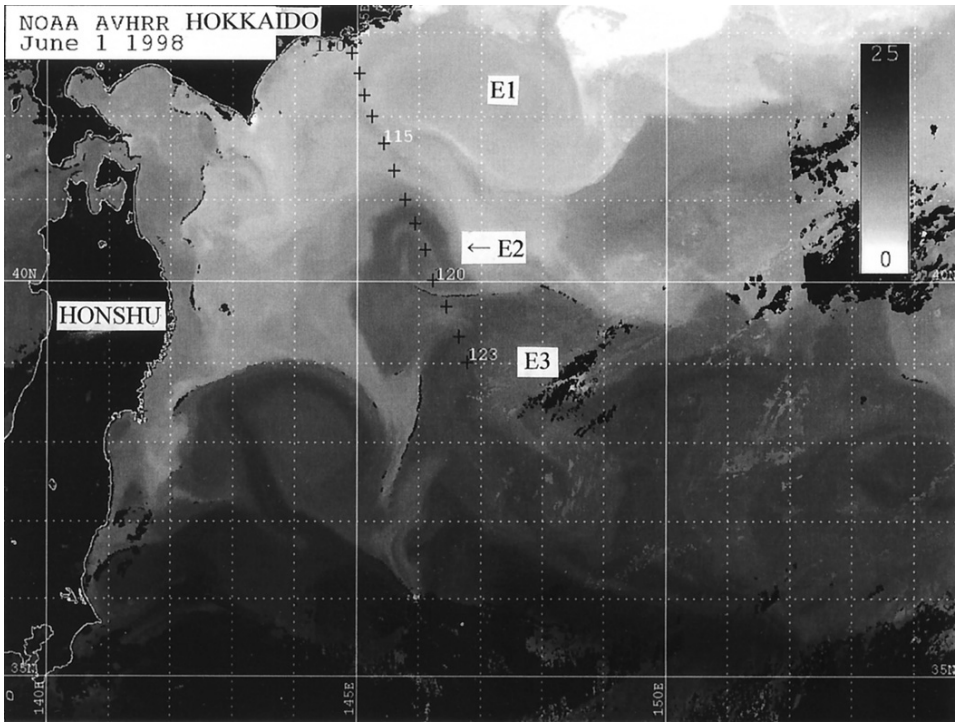

FIGURE 10.11 Oyashio, Kuroshio, and Mixed Water Region east of Japan. Sea surface temperature (NOAA AVHRR satellite infrared image) with temperature scale from 0 to 25°C; E1, E2, and E3 denote anticyclonic eddies. *Source: From Yasuda et al. (2001).*

Hokkaido, ranges from 5 to 20 Sv, with large variability (Kono & Kawasaki, 1997; Yasuda et al., 2001). The EKC transports range from 10 to 25 Sv, relative to various levels of no motion (Talley & Nagata, 1995).[2]

The separated Kuroshio and Oyashio are about 5 degrees of latitude apart (Figure 10.11). The region between them is referred to as the "Transition Region," "Mixed Water Region," or, in older literature, the "Perturbed Area." Water properties in this region are transitional between the Oyashio and Kuroshio properties. Both currents spawn major mesoscale eddy variability, some in the form of "rings," which participate in water mass modification. Sometimes the eddies re-merge with their parent currents, bringing the modified waters back with them.

10.3.2.3. Circulation in the Gulf of Alaska

The North Pacific Current splits as it approaches the North American continent and part turns south into the CCS. The remainder turns north into the Alaska Current, forming the eastern and northern side of the cyclonic Alaskan Gyre in the Gulf of Alaska. Where the coast of Alaska swings southward, at about 143°W, it forms a slanted western boundary along which the swift southwestward Alaskan Stream forms as a western boundary current. The wind field that drives the cyclonic circulation includes intensified Ekman upwelling in the Gulf of Alaska.

Details of the North Pacific Current bifurcation depend on the large-scale wind forcing, which has seasonal variability, and also interannual and decadal variability associated mainly with ENSO and the Pacific Decadal Oscillation (PDO; Sections 10.8 and 10.10; Chapter S15 from the online supplemental material). The position of the North Pacific Current bifurcation is at about 45°N in winter and 50°N in summer (Figure 10.1). The subpolar gyre, including the Alaskan Gyre, intensifies during periods when the atmosphere's Aleutian Low is especially strong such as El Niño years and years of low PDO. When the Aleutian Low and the subpolar gyre are weak, more subpolar water enters the CCS (Van Scoy & Druffel, 1993).

The Alaska Current contains dramatic, large anticyclonic eddies that are permanent, time-dependent components of the circulation. "Sitka Eddies" form west of Sitka, Alaska, at about 57°N and have a diameter of 150–300 km and surface amplitude of 10–20 cm (Tabata, 1982). "Haida Eddies" or "Queen Charlotte Eddies" form west of the Queen Charlotte Islands (Figure S10.7 located in the online supplementary material). The formation sites are related to bottom topography. After formation, these eddies propagate mainly westward into the Gulf of Alaska and are an important means of transporting coastal properties into the interior. Large eddies also populate the Alaskan Stream on the northwest side of the Gulf of Alaska (Crawford, Cherniawsky, & Foreman, 2000).

10.4. SOUTH PACIFIC CIRCULATION

10.4.1. Subtropical Circulation

The South Pacific is dominated by its anticyclonic subtropical gyre, extending from the ACC at about 50°S to the equator (Figures 10.1 and 10.2a; Table S10.2 in the online supplementary material). The gyre is well defined, but its western boundary current is complicated because the western boundary is composed of islands. (Oceanographically, Australia is a large island since it sits entirely within the subtropical gyre latitudes.) Connections with the other Southern Hemisphere oceans occur through the

[2] These transport estimates could be low because (1) velocities are often underestimated due to the use of inappropriately shallow levels of no motion and (2) large anticyclonic eddies can pull much of the Oyashio transport offshore, resulting in a weak coastal Oyashio and a stronger offshore component.

complex passages of the Indonesian archipelago and through the Southern Ocean south of Australia and South America.

The main western boundary current is the EAC, which flows southward along the coast of Australia until reaching the northernmost latitude of New Zealand. The EAC then separates and flows eastward to New Zealand, where it re-attaches to the east coast (as a western boundary current called the *East Auckland Current*) and continues a little farther southward. The EAC is very time-dependent and dominated by a series of cyclonic and anticyclonic eddies.

The broad eastward flow on the south side of the subtropical gyre can be called the *South Pacific Current* (SPC), following Stramma, Peterson, and Tomczak (1995), and consistent with usage of "North Pacific Current" and "North Atlantic Current" for the West Wind Drifts in the Northern Hemisphere. The circulation is bounded to the south by the Subantarctic Front, which is the northernmost front of the ACC (Chapter 13).

The northward flow along the coast of South America is the *Peru-Chile Current*. Like the California Current, the Peru-Chile Current is both the northward flow of the subtropical gyre and a full coastal upwelling system (PCCS) with separate eastern boundary current dynamics driven by alongshore winds. The westward flow of the subtropical gyre is the *South Equatorial Current* (SEC). At the sea surface, the SEC is located from about 20°S northward all the way to and across the equator; its structure at low latitudes is described with the tropical circulation in Section 10.7.3.

10.4.1.1. East Australian Current

The EAC is the southward western boundary current along the coast of Australia (Figure 10.12). A thorough description is found in Ridgway and Dunn (2003). The EAC forms from the westward flow of the SEC as it crosses the Coral Sea and reaches the Australian coast. At the sea surface, the SEC bifurcates at about 15°S into the

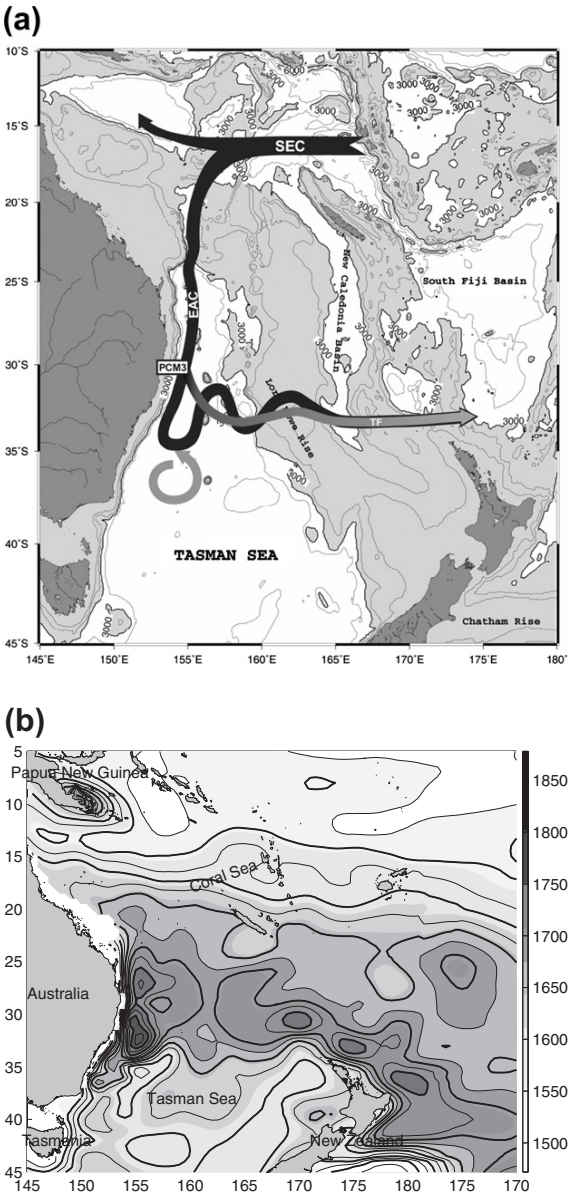

FIGURE 10.12 (a) Schematic of circulation in the western South Pacific (SEC: South Equatorial Current; EAC: East Australian Current; TF: Tasman Front). Eddy shedding from the EAC is depicted in light gray. *Source: From Mata et al. (2006).* (b) Mass transport streamfunction relative to 2000 dbar; contour interval is 25 m^2. *Source: From Ridgway and Dunn (2003).*

southward EAC and northward flow along Queensland. This bifurcation point moves toward the south with increasing depth, reaching 500 m at about 22°S (Figure 10.12b and Figure S10.8 in the supplementary Web site). The EAC transport intensifies as it flows along the Australian coast, reaching a maximum velocity of around 90 cm/sec at 30°S. It begins to separate from the coast around 31 to 32°S. It reaches its maximum transport of about 35 Sv shortly after separation, at 33°S, where it undergoes a southward meander and retroflection with part of the transport returning northward in a tight recirculation. A mean northward recirculation exists offshore of the EAC between latitudes 33°S and about 24°S, and likely has two separate lobes (Figure 10.12).

Most of the EAC flow that does not recirculate turns eastward into the zonal Tasman Front and crosses the Tasman Sea to the northern cape of New Zealand. Transport in the Tasman Front is estimated at 13 Sv. The EAC flow in the Tasman Front re-attaches to the coastline at New Zealand and forms the East Auckland Current (Roemmich & Sutton, 1998). The East Auckland Current continues southward and finally separates from New Zealand at about 43°S (Figure 10.12), where it meets a northward loop of the Subantarctic Front (ACC).

The remainder of the EAC reaches southward through the Tasman Sea to Tasmania. The location of the southernmost penetration of EAC waters along Tasmania is used as a regional climate index, much like the southward penetration latitude of Oyashio waters along Japan (Section 10.3.2.2). A small portion continues southward past Tasmania and turns westward into the Indian Ocean, connecting the westward flow of the South Pacific and Indian subtropical gyres (Speich et al., 2002; Ridgway & Dunn, 2007).

The EAC separates from the coast at about 32°S and meanders strongly southward and then northward. The meander regularly pinches off into a ring. The EAC undergoes major retraction and deformation after such eddy shedding, which occurs about every 100 days (Mata, Wijffels, Church, & Tomczak, 2006).

The EAC has long been understood to be particularly rich in eddies (Hamon, 1965; Godfrey et al., 1980). EAC eddies sometimes appear to dominate the mean circulation. Eddy diameters are 200–300 km, and surface speeds are up to 180–200 cm/sec, with lifetimes of up to a year (Boland & Church, 1981). The eddy centers are well mixed to as much as 300 m depth (Nilsson & Cresswell, 1981). In austral winter, the surface water in an eddy may be as much as 2°C warmer than the surrounding water.

Eddy formation sites in the EAC tend to be recurrent, so the eddies appear in the mean dynamic topographies and altimetric height maps (Figure 10.12 and Figure S10.9 from the online supplementary material). Two are found within the recirculation of the EAC along the Australian coast, and three within the Tasman Front and East Auckland Current. The permanence of these eddy sites suggests topographic control (Ridgway & Dunn, 2003).

10.4.1.2. South Pacific Current and Subtropical Front

The eastward flow of the South Pacific subtropical gyre is the SPC (Stramma et al., 1995; Wijffels, Toole, & Davis, 2001). The broad, weak eastward flow of the SPC was long identified with the ACC, but the SPC is dynamically distinct from the ACC. As an analog of the North Pacific Current, we consider the SPC to be all of the eastward flow of the South Pacific's subtropical gyre north of the Subantarctic Front. The SPC flows into the broad, open-ocean part of the northward Peru-Chile Current, and from there to the westward SEC. These three currents constitute the open ocean part of the South Pacific's subtropical gyre. Maximum Sverdrup transport for the subtropical gyre occurs around 30°S and is about 35 Sv (Figure 5.17, Figure S10.2b in the online supplementary materials, and Wijffels et al., 2001).

The SPC forms as eastward outflow from the East Australian and East Auckland Currents. In mid-ocean, it has a somewhat bowed structure, with a slight northward excursion from offshore of the EAC to mid-gyre, around 170°W, then southward to about 140°W and finally, northward in the main Peru-Chile gyre flow. This structure appears to be permanent.

The eastward flow of the SPC bifurcates at the eastern boundary between 40°S and 45°S. The northward flow joins the Peru-Chile Current and the southward flow joins the ACC through Drake Passage.

Within the SPC there is a marked, nearly zonal Subtropical Front, called the Subtropical Convergence in earlier works, including earlier editions of this text. The Subtropical Front is identified by large meridional gradients in temperature and salinity in the upper ocean, with a northward increase of 4°C and 0.5 psu, sometimes over just a few kilometers (Deacon, 1982; Orsi, Whitworth, & Nowlin, 1995). North of the Subtropical Front lies the saline, warm water of the central subtropical gyre; salinities are greater than 34.9 psu just north of the front. South of the Subtropical Front is the fresher, cooler water of the poleward part of the gyre.

Transport of the SPC has not been estimated as such. An estimate for the Subtropical Front alone is less than 5 Sv (Stramma et al., 1995). Otherwise the transport of the broad subtropical gyre has been mainly estimated from the meridional (north-south) component through east-west sections across the gyre, which are described in the next subsection.

10.4.1.3. Northward Flow of the Subtropical Gyre and the Peru-Chile Current System

Northward flow in the subtropical South Pacific consists of the broad subtropical gyre and the swifter, narrow eastern boundary current system along the coast of South America, referred to as the PCCS (Figures 10.1 and 10.13). The northward transport is estimated to be 15 Sv between 180° and the eastern boundary (Wijffels et al., 2001). Within the broad gyre, denser surface waters from the south subduct northward under lighter low latitude waters. This creates the stratified structure of the central South Pacific pycnocline (Section 10.9.1), and the salinity/oxygen layering in the vertical that facilitates identification of various water masses.

At the eastern boundary, the PCCS (Figure 10.13) is a typical eastern boundary current upwelling system (Sections 7.9 and 10.3.1.4), forced by the alongshore component of the large-scale winds and an offshore band of positive wind stress curl. It includes the northward Peru-Chile Current (also called the Peru Current and formerly called the Humboldt Current). The Poleward Undercurrent (also called the Gunther Current) is found along the coast beneath the surface layer, as expected for a typical eastern boundary current system. The PCCS also contains other currents: a poleward Peru-Chile Countercurrent 100–300 km offshore, and an equatorward Peru Coastal Current on the inshore side. The Peru-Chile Current and Peru Coastal Current connect to the equatorial SEC and the cold tongue in the eastern equatorial Pacific (Figure 10.13). The Equatorial Undercurrent (EUC) feeds into the Poleward Undercurrent and Peru-Chile Countercurrent (Strub et al., 1998).

Maximum upwelling, extending southward along the Chilean coast to 45°S, occurs in austral summer. The PCCS upwelling is well known because of the rich fisheries there. Satellite ocean color images (Figure S10.10 in the online supplemental text) vividly show the effects of coastal upwelling, which lifts nutrients to the euphotic zone, resulting in high biological productivity. The permanent upwelling region extends from about 32°S northward to the equator; seasonal upwelling occurs south of this to about 40°S.

Vertical sections across the PCCS at 33°S (Figure 10.13) show the isotherm structure

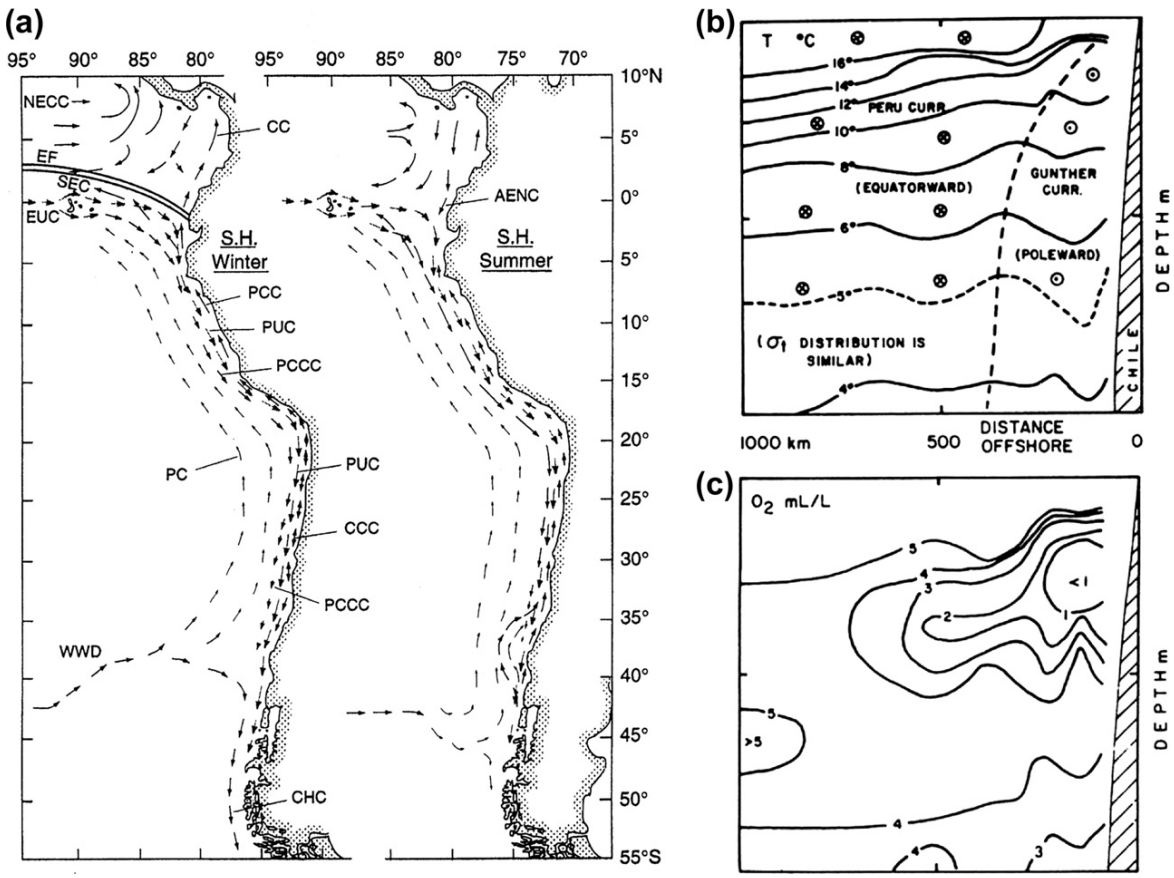

FIGURE 10.13 Peru-Chile Current System. (a) Maps in austral winter and summer. Acronyms: WWD, West Wind Drift; PC, Peru Current; PCCC, Peru-Chile Countercurrent; PUC, Poleward Undercurrent; PCC, Peru Coastal Current; CCC, Chile Coastal Current; and CHC, Cape Horn Current. Also, near the equator: CC, Colombia Current; AENC, Annual El Niño Current; NECC, North Equatorial Countercurrent; SEC, South Equatorial Current; EUC, Equatorial Undercurrent. *Source: From Strub et al. (1998).* (b, c) Eastern South Pacific zonal vertical sections at 33°S: temperature (°C) with meridional current directions and dissolved oxygen (ml/L); companion salinity and phosphate sections appear in Figure S10.11 on the textbook Web site.

typical of a geostrophic eastern boundary current system, including the equatorward Peru-Chile Current above about 500 m and the poleward subsurface Peru-Chile Undercurrent (PCUC) near the coast. The undercurrent is characterized by low oxygen which comes from the tropics and from local high productivity that traps high nutrients and low oxygen just beneath the surface layer (Montecino et al., 2006). High nutrient content, associated with the low oxygen, helps to create the characteristic high biological productivity of this eastern boundary region.

The PCCS is strongly affected by ENSO (Section 10.8). Collapses of the PCCS fisheries resulting from changing upwelling conditions were among the earliest dramatic evidences for ENSO, which is now known to encompass the entire equatorial Pacific. During normal conditions, the Peru-Chile Current extends to a few degrees south of the equator before

turning west into the SEC. The low temperature of the Peru-Chile Current surface waters contrasts with higher equatorial temperatures to the north. During an El Niño (warm phase), the high temperatures extend 5 to 10 degrees farther south than usual and the thermocline deepens by 100 m or so. Upwelling either weakens or simply draws on warmer water from this thicker warm layer, thus causing the surface temperatures to increase. The increase in temperature was thought to kill fish, but recent studies have shown that the fish merely descend below the abnormally warm surface layer. In every austral summer there is a slight warming of the sea surface along with an increase in precipitation. During El Niño years, however, the warming and the rainfall far exceed the norm.

10.4.1.4. South Equatorial Current

The SEC is the broad westward geostrophic flow in the northern limb of the South Pacific's subtropical gyre (Figures 10.1 and 10.12). The SEC forms in the eastern Pacific as the northward flow of the subtropical gyre turns westward. The narrow eastern boundary current (Peru-Chile Current) also feeds into the SEC close to the equator.

As it reaches the western South Pacific, the SEC carries water into the Coral Sea off northeastern Australia. The many islands in the region complicate the SEC, including intense zonal jets with large east-west extent (Webb, 2000; Qu & Lindstrom, 2002; Ganachaud, Gourdeau, & Kessler, 2008). When the SEC reaches the Australian coast, it bifurcates into the southward EAC and the northward North Queensland Current. The latter feeds the NGCUC, bringing South Pacific water to the western equatorial Pacific and feeding the EUC (Section 10.7.4).

The SEC also includes the frictional equatorial surface flow (Section 10.7), which is bounded to the north by the powerful eastward NECC. Because the SEC extends across the equator, whereas the NEC is separated from the equator by the NECC, the South Pacific subtropical gyre is much more directly connected to the equator than is the North Pacific gyre. Subtropical anomalies in heat or salinity can more easily reach the equator from the South Pacific than from the North Pacific because of this direct SEC connection (Johnson & McPhaden, 1999).

10.5. PACIFIC OCEAN MESOSCALE EDDY VARIABILITY

The ocean circulation focused on in this text is the mean of a highly time-dependent, turbulent flow. Mesoscale eddy variability at timescales of weeks to months is easily detected with instruments such as satellite altimeters, which measure the surface height variability. At depth, eddy variability is measured with moored observations at point locations and using Lagrangian floats that are usually deployed at a single depth.

Surface EKE and horizontal eddy diffusivity in the Pacific are shown in Figures 14.16 and 14.17 and also in Figure S10.12 on the textbook Web site. High EKE is mostly associated with strong mean flows: the Kuroshio Extension (30−40°N), the EAC (25−40°S), the ACC (south of 50°S), and the NECC (5−10°N). Two zonally elongated regions of high eddy energy, at 20°N and 25°S, are associated instead with weak eastward surface flows. These are the STCCs in both hemispheres; the flow just below the surface, even at 200 dbar, is westward (Figure 10.2). The energy in these unstable mean flows is mainly released through baroclinic instability, creating the high EKE (Stammer, 1998; Qiu, Scott, & Chen, 2008; Section 7.7.5).

High eddy variability in the Pacific in Figures 14.16 and S10.14 also occurs at the locations of recurrent rings, including the Tehuantepec eddies in the eastern tropical Pacific (Section 10.7.6), the Kuroshio rings, the EAC rings, and the rings along the boundaries of the subpolar

gyre (Haida & Sitka eddies; eddies in the Oyashio).

10.6. DEPTH DEPENDENCE OF THE PACIFIC OCEAN CIRCULATION AND MERIDIONAL OVERTURN

Below the wind-driven subtropical gyres, and coexisting with the deep-reaching North Pacific subpolar gyre, the Pacific circulation is weak, mostly less than several centimeters per second except in the tropics. Faster currents (>10 cm/sec) occur in the deeper parts of the upper ocean western boundary currents and in the DWBCs, but transports are nevertheless relatively small, of the order of 10 Sv or less.

As we leave the sea surface, the subtropical gyres shrink away from the equator, away from the eastern boundary, and toward the energetic western boundary currents. The Kuroshio gyre shrinkage was described in Section 10.3.1.6. In

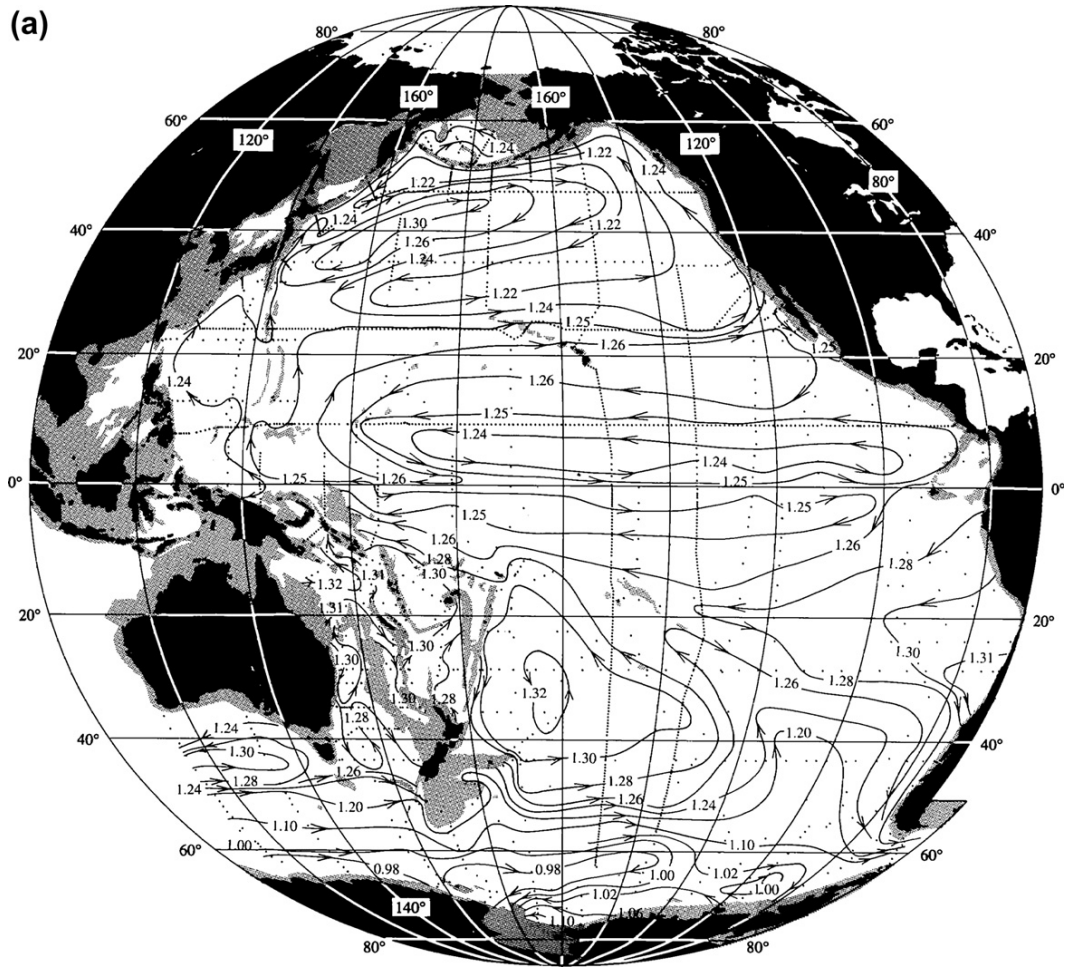

FIGURE 10.14 Adjusted geostrophic streamfunction (steric height, 10 m^2/sec^2) at (a) 2000 dbar, (b) 4000 dbar. *Source: From Reid (1997).*

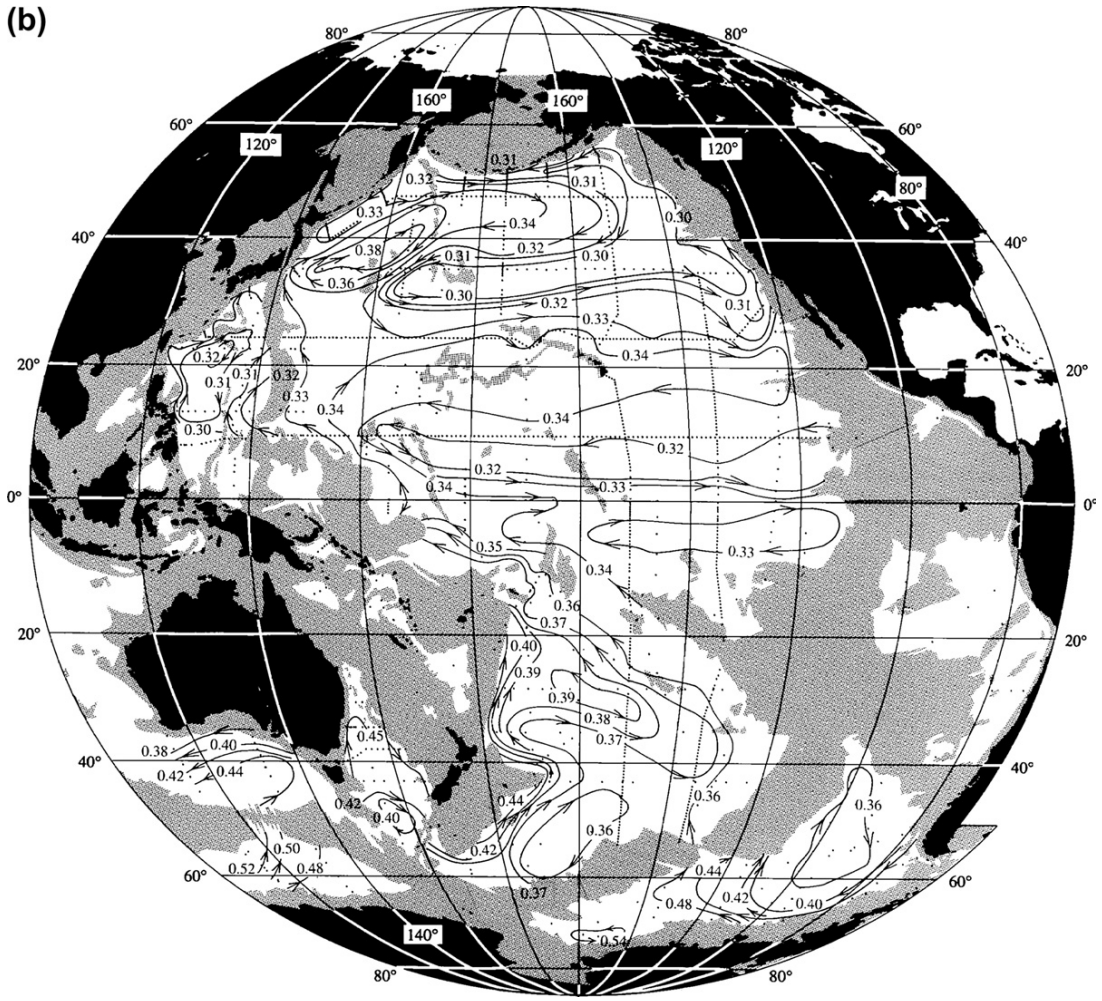

FIGURE 10.14 (*Continued*).

the South Pacific, the subtropical gyre shrinks into the Southwest Pacific Basin, east of New Zealand and the Tonga-Kermadec Ridge.

On the tropical side vacated by these shrinking gyres, the flows are nearly zonal except close to the western and eastern boundaries (Figures 10.2b, 10.10, 10.14 and Figure S10.13 on the textbook Web site). This zonal flow pattern persists down to the tops of the major mid-ocean ridges, roughly between latitudes 20°N and 20°S. Outside the tropics, the deep flow patterns are influenced by the overlying gyres, the underlying topography, and the DWBCs (Figure 10.14). In the southwest Pacific below 2000 dbar, the circulation is a combination of a northward DWBC and an anticyclonic flow that fills the rest of the basin to the east and north. In the southeast Pacific, in the Bellingshausen Basin, the flow is weak and cyclonic from about 800 dbar to the ocean bottom, with a southward eastern boundary current that carries the thick, low oxygen layer of PDW southward to the Southern Ocean (Shaffer et al., 1995;

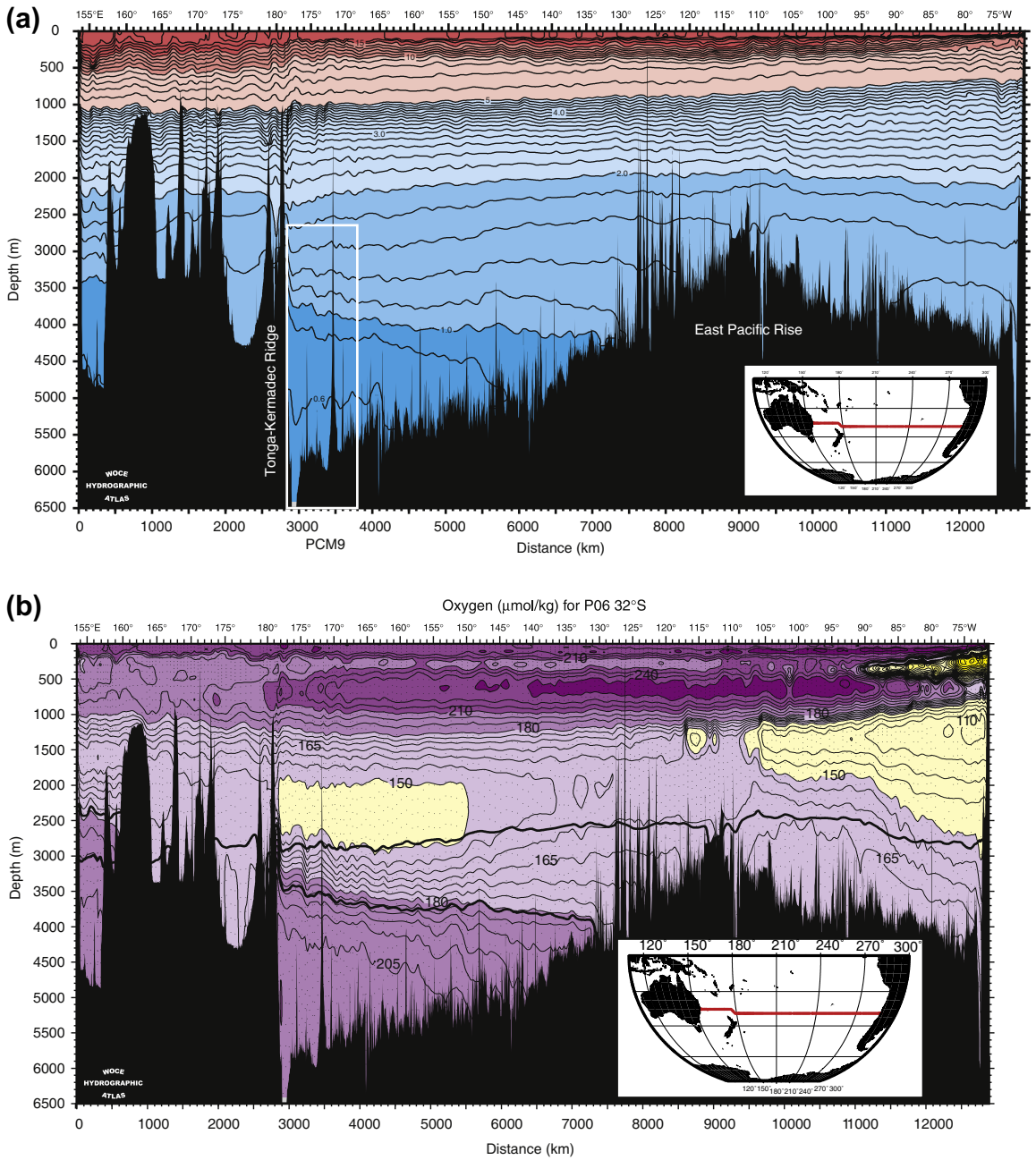

FIGURE 10.15 South Pacific sections at 32°S and DWBC. (a) Potential temperature and (b) oxygen (µmol/kg). Neutral densities 28.00 and 28.10 kg/m^3 are superimposed in (a). *Source: From the WOCE Pacific Ocean Atlas, Talley (2007).* (c) Mean northward velocities (cm/sec) from current meters at 32° 30′S northeast of New Zealand in 1991–1992. The array location is within the white box in (a). *Source: From Whitworth et al. (1999).*

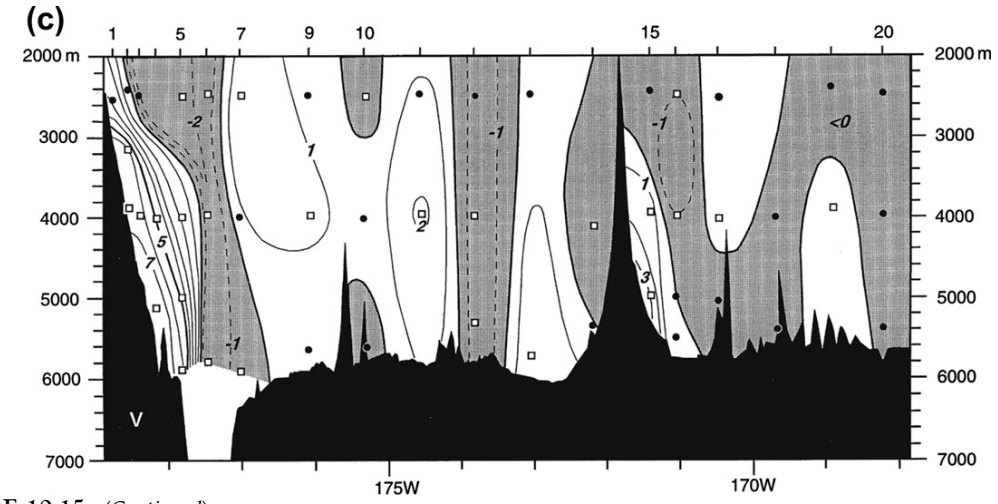

FIGURE 10.15 (*Continued*).

Figure 10.15b; Section 10.9.3). In the deep North Pacific north of about 10°N, the abyssal flow consists of two anticyclonic circulations, one centered south of the Hawaiian Islands, and the other centered at about 45°N (Figure 10.14b). These two gyres are also evident in silica distributions on deep isopycnals (Talley & Joyce, 1992).

The deep flows include well-delineated DWBCs (Section 7.10.3). In the southwest Pacific, the DWBC carries deep and bottom waters from the Southern Ocean northward into the Pacific, as seen in observations at 32°S (Whitworth et al., 1999). Large upward slopes in isotherms within several stations just east of the Tonga-Kermadec Ridge indicate the narrow DWBC, from the bottom up to 1.8°C (~2500 m; Figure 10.15). Northward transport of 16 Sv was measured in a narrow, banked band at the ocean bottom, mostly colder than 1°C. This DWBC continues northward to the tropics. Its most constricted location is at the Samoan Passage at 10°S, 169°W (Figure 10.16). Observed transport of all waters colder than 1.1°C, including those within the passage and banked against the Manahiki Plateau, was 11.7 Sv (Roemmich, Hautala, & Rudnick, 1996). The mean northward transport below 4000 m, within the Samoan Passage, was 6.0 Sv; velocities were shown in Figure 6.7 (Rudnick, 1997).

The DWBC proceeds northward from the Samoan Passage region and crosses the equator at the deep western boundary (Figure 10.17 and Figure S10.14 on the textbook Web site). Here it splits into two branches, one following the western boundary and the other heading toward the Wake Island Passage (168° 30′E, 18° 20′N). The western boundary branch is observed to carry both Lower Circumpolar Deep Water (LCDW; 1 Sv) and Upper Circumpolar Deep Water (UCDW; 11 Sv). The flow in the Wake Island Passage is up to 10 cm/sec within several hundred meters of the bottom, with a transport of 4 Sv of LCDW (Kawabe, Yanagimoto, Kitagawa, & Kuroda, 2005; Kawabe, Yanagimoto, & Kitagawa, 2006).

North of the Wake Island Passage, the deep flow moves westward to the boundary and then northward to an encounter with the Kuroshio Extension. Further north along the subpolar boundary, abyssal circulation theory indicates that the DWBC should flow southward (even though there is no local source of deep water; Figure 7.16). The western and northern boundaries are complicated by a very deep trench, in

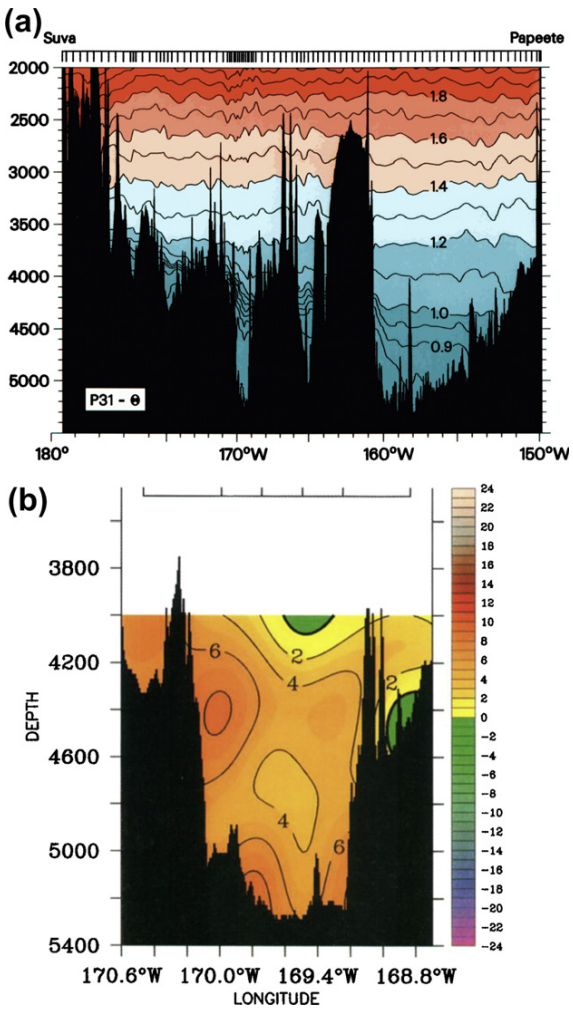

FIGURE 10.16 DWBC in the Samoan Passage. (a) Potential temperature (°C) on WOCE P31 across the passages. (b) Mean northward velocity (cm/sec) through the passage measured by current meters (1992–1994). *Source: From Roemmich et al. (1996).*

which the observed flow is southward/westward at the continental boundary and northward/eastward along the offshore side of the trench (Figure 10.17; Owens & Warren, 2001). The net DWBC transport is small (order 3 Sv) and southward/westward, matching theory. The net meridional overturning in the Pacific consists of northward transport from the Southern Ocean in the abyssal layers and southward outflow in the deep to intermediate layers (e.g., Figures 10.18, 14.6, and Figure S10.15 on the textbook Web site). Estimates of the northward transport of the deepest water into the South Pacific (LCDW or Antarctic Bottom Water; AABW) range from 7 to 20 Sv, but the large range might simply be due to layer choices. Most of this water upwells into the PDW and returns southward. Most of the upwelling occurs in the South Pacific and tropics; at 24°N in the North Pacific the bottom upwelling cell is much weaker and much more confined to the bottom layers.

10.7. TROPICAL PACIFIC CIRCULATION AND WATER PROPERTIES

10.7.1. Introduction

The Pacific equatorial current system is dominated by strong zonal (east-west) flows with weak meridional (north-south) currents in the ocean interior (Figure 10.2a; Table S10.3 and Figure S10.1 located on the textbook Web site). At the sea surface there are three major zonal currents. Below the surface there is a complex set of reversing zonal flows. At the western boundary, strong meridional currents connect the zonal flows.

The three major zonal surface currents are (1) the westward-flowing NEC between about 8°N and 20°N, (2) the westward SEC from about 3°N to 10°S, and (3) the narrow NECC flowing to the east between them, centered at about 5°N. These were well-known components of the Pacific surface circulation before 1940. The other major equatorial current lies just below the thin surface layer of the SEC and it is the eastward-flowing EUC, which is one of the fastest permanent currents in the world. The eastward *South Equatorial Countercurrent* (SECC) in the western South Pacific between 10 and 12°S is much weaker and more time-dependent than these. Then

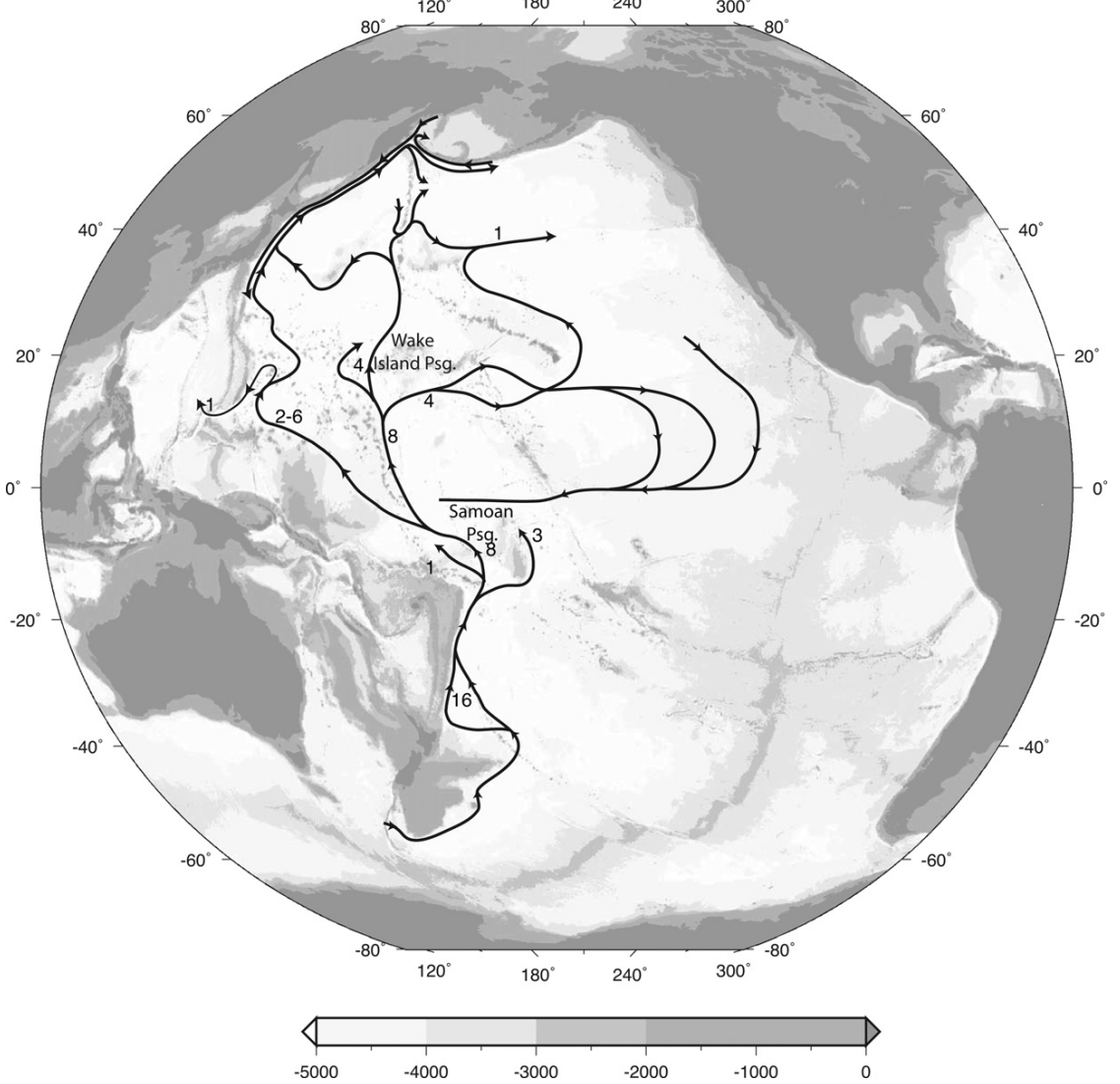

FIGURE 10.17 Abyssal circulation schematics. *After: Owens and Warren (2001), Johnson and Toole (1993), Kato and Kawabe (2009), Komaki and Kawabe (2009), Yanigomoto, Kawabe, and Fujio (2010), Whitworth et al. (1999), and Roemmich, Hautala, and Rudnick (1996).*

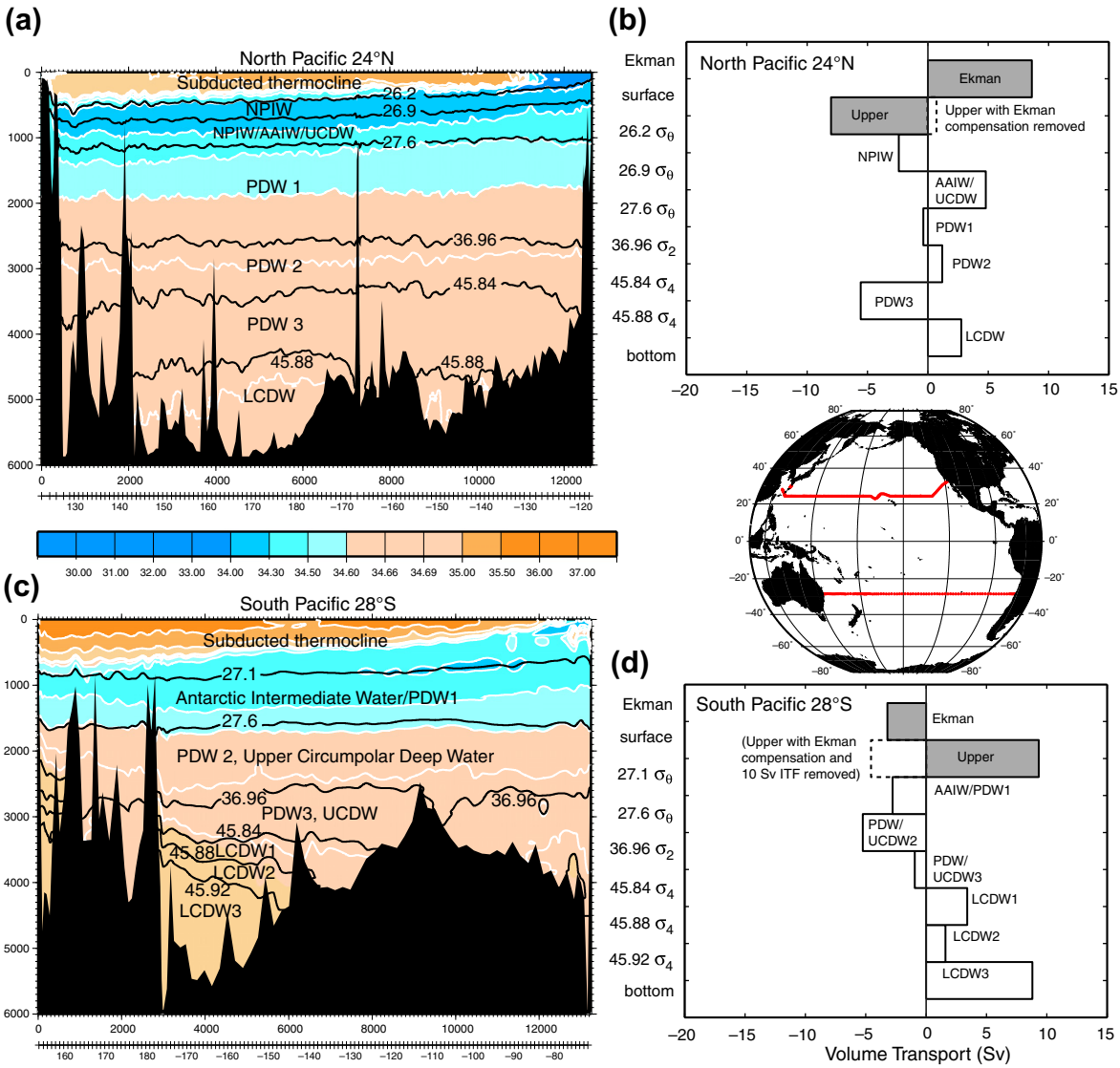

FIGURE 10.18 Salinity and meridional transport in isopycnal layers at 24°N (a, b) and at 28°S (c, d). Inset map shows section locations. The isopycnals (σ_θ, σ_2, σ_4) that define the layers are contoured on the salinity sections. *After Talley (2008).* Overturning transports from Ganachaud (2003) are shown in Figure S10.15 on the textbook Web site.

Subsurface Countercurrent, NSCC; and South Subsurface Countercurrent, SSCC), and also crossing the equator to meet the southward flow of the Mindanao Current and feed the NECC.

Dynamics of the wind-driven equatorial surface currents and the EUC were presented briefly in Section 7.9.2, and directly on the equator, flow is in the direction of wind stress (in the frictional surface layer) and pressure gradient force. Moving slightly away from the equator, the Coriolis force quickly becomes important; the currents are almost geostrophic

and the upper ocean circulation can be considered in terms of the usual Sverdrup dynamics driven by convergence of the wind-driven Ekman layer (Section 7.5).

10.7.2. Tropical Wind and Buoyancy Forcing

The tropical surface current system is driven by the easterly trade winds at the ocean's surface (Figure 5.16, Figure S10.16 located on the textbook Web site, and also the stick plot in Figure 10.20b). The trade winds are part of the atmosphere's Walker and Hadley cells (Section 7.9.2). The trade winds are not uniformly westward; these surface winds converge at the ITCZ north of the equator. (A weak, secondary ITCZ is found in the western South Pacific.) The wind stress curl associated with the ITCZ is positive, creating Ekman suction (Figure 5.16d). This drives cyclonic circulation that is very zonally elongated. This includes westward flow on the northern side (part of the NEC), and eastward flow on the southern side, which is the NECC (Yu, McCreary, Kessler, & Kelly, 2000). The SECC, which appears in the western South Pacific tropics, is driven by a similar mechanism associated with the Southern Hemisphere ITCZ.

Seasonally, the trade winds are stronger in the winter hemisphere (Figure 5.16). The Northern Hemisphere ITCZ lies closer to the equator, at about 5°N in the east, in February than in August. In August, the northern ITCZ shifts northward to 10°N across the whole Pacific. In the western tropical Pacific, there is a seasonal monsoon, which is a reversal in winds in the Northern Hemisphere and equatorial regions. This especially impacts the surface equatorial circulation (Section 10.7.3.1).

Air–sea fluxes of heat and freshwater in the tropical Pacific are important for the global balances of both of these quantities (Figures 5.4, 5.12). The tropical oceans warm due to high solar radiation (Figure 5.11a). The greatest warming is in the equatorial cold tongue in the eastern Pacific (see next section), where lower surface temperatures result in reduced latent and longwave heat losses, hence higher net heating.

The tropical Pacific is also a region of net precipitation. The precipitation is not uniform (Figure 5.4). Beneath the ITCZ of the Northern Hemisphere is a band of net precipitation. The western Pacific is also a region of net precipitation, concentrated in two bands centered at the northern and Southern Hemisphere ITCZs. The eastern tropical Pacific is a region of net evaporation. These patterns are directly related to the Hadley and Walker circulations, with more precipitation where air rises along the ITCZ and in the western tropical Pacific.

The net precipitation in the western tropics creates a low salinity surface layer, with a strong halocline beneath. The mean stratification here consists of a so-called *barrier layer*, in which warm surface temperature extends to greater depth than the fresh surface water. The mixed layer stratification, therefore, is dominated by salinity.

10.7.3. Equatorial Pacific Current Structure

10.7.3.1. Zonal Currents and Associated Mid-Ocean Meridional Flows

Zonal flows dominate meridional flows in the tropics, except at the western boundary. Average upper ocean zonal velocity, temperature, and salinity structure in the central Pacific (154°W) is shown in Figures 10.19 and 10.20 (Wyrtki & Kilonsky, 1984; WK). The deep equatorial currents are described for a nearby longitude (Figure 10.21). These zonal currents are geostrophic except directly on the equator,[3] and are therefore reflected in sloping surface dynamic

[3] Geostrophy is valid to within about one-quarter degree of the equator with sufficient temporal averaging. A 12-month set of 43 sections was used for the mean structure in WK.

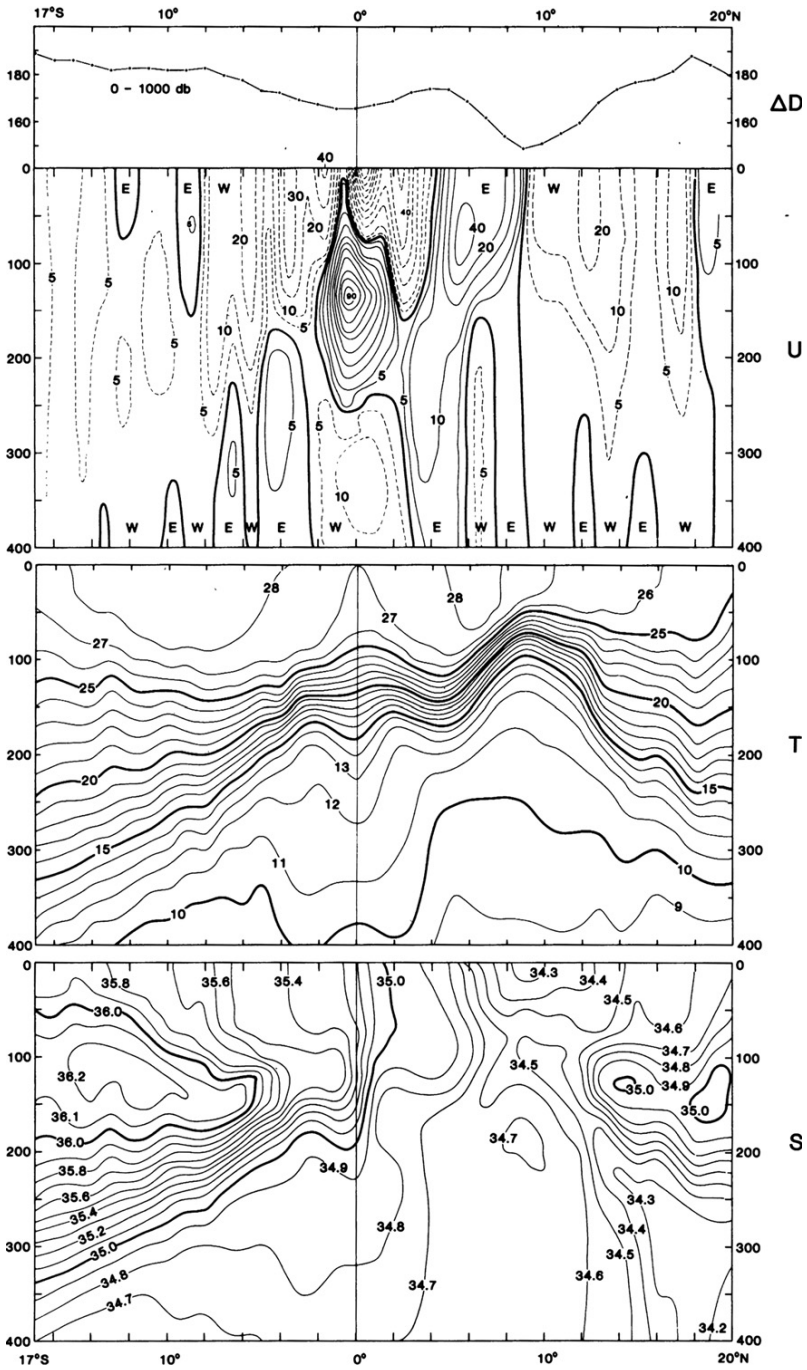

FIGURE 10.19 Mean distributions of surface dynamic height (△D dyn cm) relative to 1000 db (dyn cm) and vertical meridional sections of zonal geostrophic flow (U in cm/sec), temperature (T in °C), and salinity (S) between Hawaii and Tahiti, for 12 months from April 1979. ©*American Meteorological Society. Reprinted with permission. Source: From Wyrtki and Kilonsky (1984).*

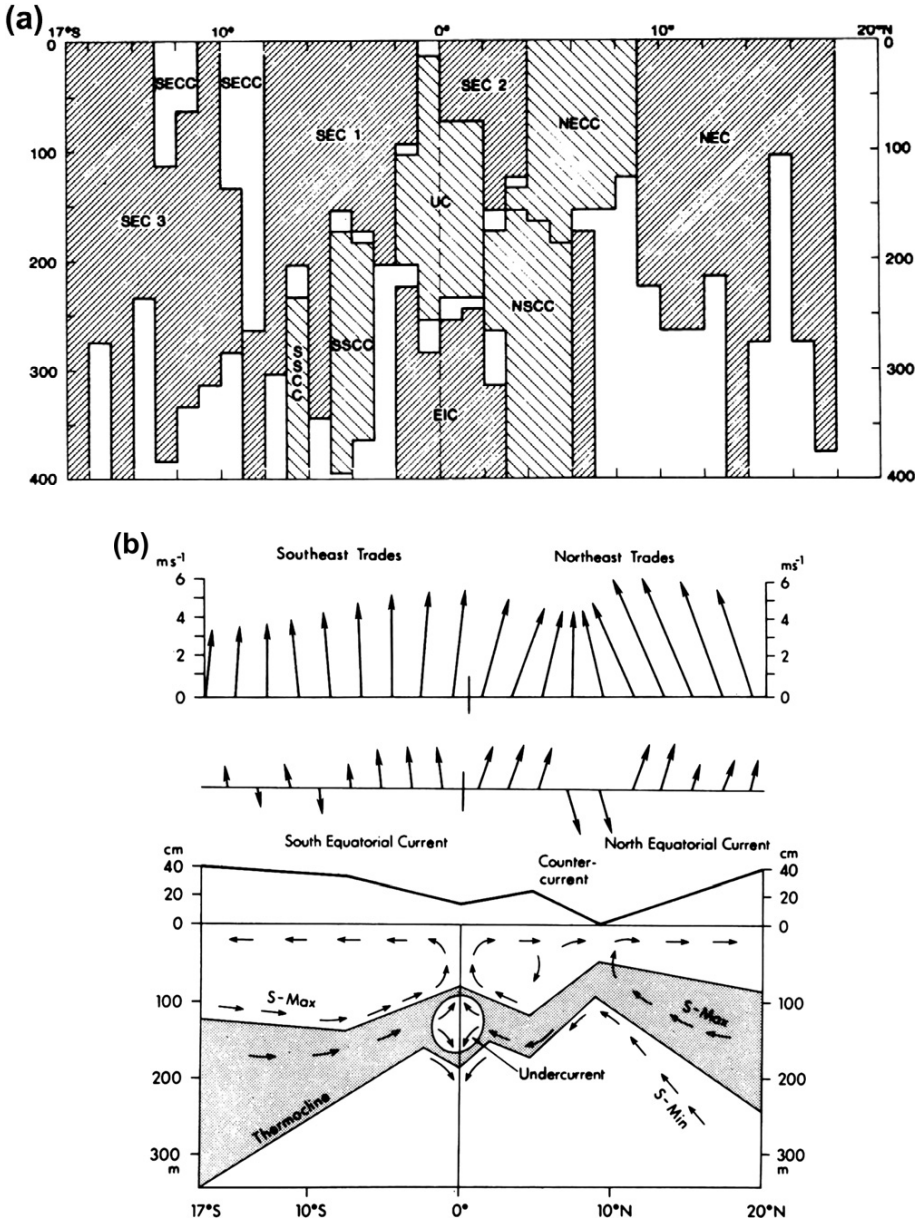

FIGURE 10.20 (a) Schematic of mean areas occupied by zonal currents between Hawaii and Tahiti for 12 months from April 1979. Dark shading indicates westward flow, light shading indicates eastward flow, blank areas have zonal speeds less than 2 cm/sec. Acronyms: NEC, North Equatorial Current; NECC, North Equatorial Countercurrent; SEC, South Equatorial Current (three sections); SECC, South Equatorial Countercurrent; UC, Equatorial Undercurrent (EUC in our notation); EIC, Equatorial Intermediate Current; and NSCC/SSCC, Northern/Southern Subsurface Countercurrents (Tsuchiya jets). (b) Schematic meridional section across the equator showing (top) the mean trade winds, (middle) surface circulation, and (bottom) schematic surface dynamic topography, temperature structure, and meridional circulation below the surface. ("Countercurrent" = "NECC" in our notation.) *Source: From Wyrtki and Kilonsky (1984).*

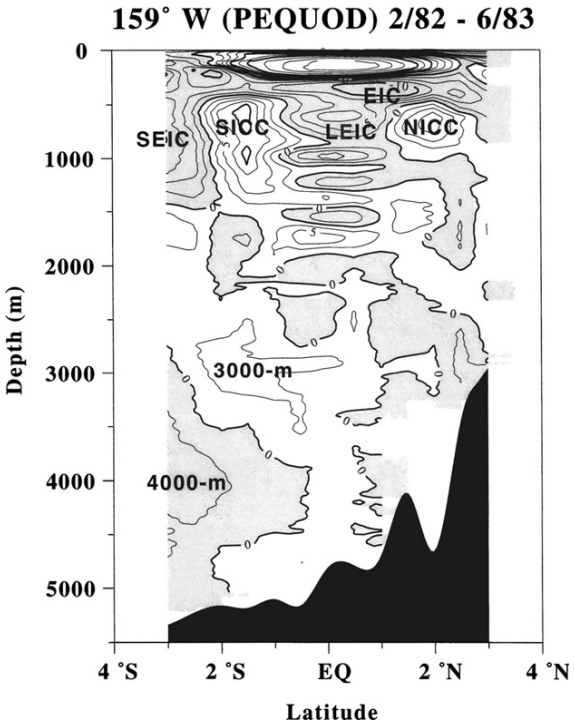

FIGURE 10.21 Zonal velocity (cm/sec) in the equatorial Pacific, averaged from 41 sections of direct current measurements collected in 1982–1983. White is eastward flow, gray is westward. *Source: From Firing, Wijffels, and Hacker (1998).*

height ($\triangle D$; Figure 10.19), and in isopycnal slopes, which produce the vertical shear of the geostrophic currents. The westward NEC and the southernmost part of the westward SEC (SEC-3) are the primary westward flows of the North and South Pacific's subtropical gyres (Figure 10.1) and extend down through the thermocline. Their dynamic heights slope downward and isotherms tilt upward toward the equator.

The eastward NECC is a strong, permanent current that stretches across the whole width of the Pacific with associated large dynamic height and isotherm slopes in the opposite direction to those of the NEC/SEC. In contrast, the weak, eastward SECC is mostly restricted to the western Pacific with only a weak expression in the central Pacific seen as a slight reversal in surface dynamic height slope (Figure 10.19).

At the surface on the equator, the surface flow is westward (SEC-1). This equatorial SEC is in just a thin layer above the EUC. The equatorial SEC's flow is the downwind, frictional equatorial response to the westward trade winds, in the absence of the Coriolis force and hence an Ekman layer (Section 7.9.2). It can disappear at times since it is driven directly by the wind, and in any case responds quickly to changes in winds; a reversal to eastward occurs regularly during westerly wind bursts at the onset of El Niño (Section 10.8; Hisard & Hénin, 1984).

At the equator, the EUC lies just beneath the SEC. Its maximum velocity core at this central Pacific location lies at 130 m, with average speeds greater than 90 cm/sec.[4] The EUC was considered to be weak during the WK measurement period; it can regularly reach speeds of 120 cm/sec. Despite its thinness in the vertical, its large speeds are reflected in large transport (32.3 ± 3.5 Sv in WK's annual average). The EUC is easily identified in isotherm structure at the equator: the 13–26°C isotherms spread upward above it and downward below it. It has no expression in surface dynamic height since it is not a surface current. This creates the necessary geostrophic vertical shear on

[4] The EUC was first discovered in 1951 when researchers from the U.S. Fish and Wildlife Research Service in Honolulu found that their "long-line" deep fishing equipment drifted strongly eastward in spite of the westward surface currents. Their gear traveled eastward at speeds of about 1.5 m/sec, which was about three times that of the westward surface current. A subsequent cruise to investigate this phenomenon was led by Townsend Cromwell; the EUC is also called the "Cromwell Current." Unfortunately Dr. Cromwell died the next year in a plane crash on the way to an oceanographic expedition. See Knauss (1960).

both sides of the equator to create a subsurface eastward flow with westward flows both above it (SEC) and below it (Equatorial Intermediate Current; EIC).

The eastward NSCC and SSCC are just to the north and south of the equator and slightly deeper than the EUC. The NSCC is not always easily distinguishable from the deeper part of the surface-intensified NECC. In the isotherms (Figure 10.19), the SCCs are apparent in the strong upward slopes of the 10 and 11°C isotherms away from the equator. The SCCs were first identified from maps of properties on isopycnals by Tsuchiya (1975). They transport salinity, oxygen, and nutrients characteristic of the western Pacific toward the east. In honor of this first description, the SCCs are often referred to as "Tsuchiya jets".

The westward EIC is a weak but persistent flow along the equator beneath the EUC. Beneath the EIC, the reversing eastward and westward flows between 1000 and 2000 m are referred to as the *equatorial stacked jets* (Figure 10.21). Off the equator, around 700–900 m depth, there are also reversing zonal flows, but in thicker layers with speeds around 15–20 cm/sec. The deepest equatorial flows in Figure 10.21 have small mean speeds, <5 cm/sec, but might be permanent features.[5] Given the local topography at 159°W, which rises to 3000 m in the north, the robust currents are south of the equator. Transports of each of these flows is on the order of several Sverdrups. Farther from the equator, within 15–20° of the equator and above the topography of the mid-ocean ridges (above 3000 m), the intermediate and deep circulation remains dominantly zonal compared with flow at higher latitudes. The zonal nature of the flows is clear in float trajectories at 900 m (Davis, 2005; Figure S10.13 on the textbook Web site), in steric height maps for these mid-depths (Figure 10.2b), and in ocean properties on isopycnals. At 2500 m, flow includes a narrow eastward tongue at about 2°S and broad flanking westward flows centered at 5–8°N and at 10–15°S (Talley & Johnson, 1994). At the bottom, the westward equatorial flow is possibly fed by broader eastward flow north of the equator (Johnson & Toole, 1993). These complex, zonal deep flows are likely wind-forced (Nakano & Suginohara, 2002).

Returning to the upper ocean, meridional flows in the equatorial Pacific (Figure 10.20b) are associated with the major zonal currents. At the sea surface, the easterly trade winds cause Ekman transport to the north in the Northern Hemisphere and to the south in the Southern Hemisphere. This results in equatorial divergence, which creates *equatorial upwelling*. (There is equatorial downwelling if the winds shift to westerly, as in the western equatorial Pacific at the beginning of an El Niño event.)

The equatorial upwelling is fed by equatorward subsurface flow. The inflow is in the thermocline, based on water properties, including salinity (Figure 10.19 "S" panel). The equatorward inflow can be geostrophic, due to the west-to-east pressure gradient force set up by the westward flow of surface water along the equator to the western boundary. This creates high pressure in the west and low pressure in the east.

10.7.3.2. Zonal Structure of the Equatorial Currents

The equatorial current system extends from at least 143°E (north of Papua, New Guinea) to the Galapagos Islands (90°E) and then eastward to the coast of Ecuador, a distance of approximately 15,000 km. The sea surface is high in the west and slopes down to the east in the equatorial band (Figure 10.2 and Figure S10.1 on the textbook Web site). The west-east difference in surface height is 40–60 cm, with significant interannual variability associated with ENSO; the largest slopes occur during La Niña (Figure 10.22c). Surface dynamic height shows

[5] According to Firing (1989), "a 10 year time-series would be ideal for studying annual and interannual variations."

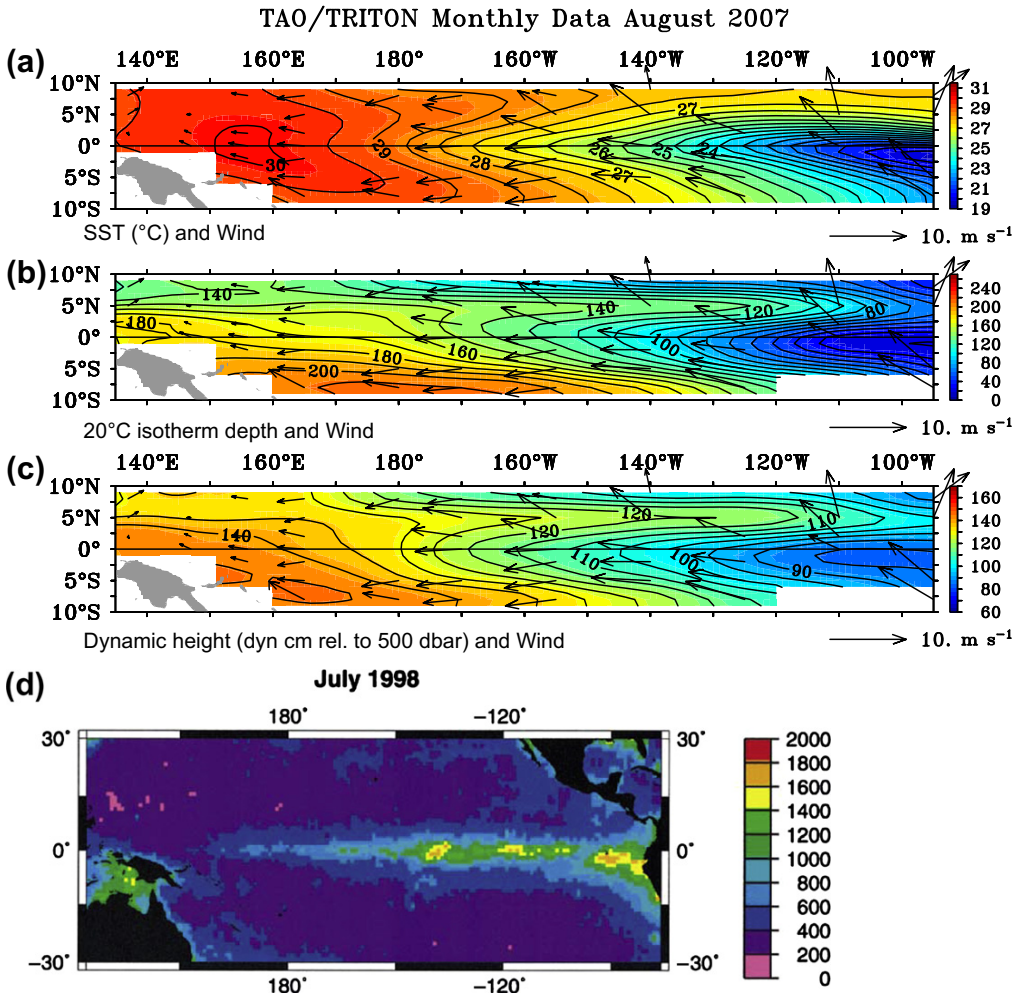

FIGURE 10.22 (a) SST; (b) depth of the 20°C isotherm, which is an indicator of thermocline depth; and (c) dynamic height (dyn cm), with superimposed wind velocity vectors, during a period of a well-developed cold tongue (La Niña; August 2007). *Source: From TAO Project Office (2009a)*. (d) Primary productivity (mg C m^{-2} day^{-1}) based on ocean color, during a La Niña (July 1998). *Source: From McClain et al. (2002).*

the same west-east contrast of about 40 dyn cm (Figure S10.17 on the textbook Web site). The equatorial sea-surface height slope is due to the wind-driven westward flow of surface water in the SEC along the equator. This piles warm water up in the west, in the region called the *warm pool*. The westward equatorial flow is also associated with equatorial upwelling in the east. The cold, upwelled surface water in the east is called the *cold tongue*. These structures are obvious in mean SST (Figures 4.1 and 10.22). Along-equatorial sections of potential temperature, salinity, and potential density show the warmer, lighter water to the west and colder, denser surface water to the east. Surface nutrients have a similar structure, with higher nutrients in the cold tongue and nearly complete depletion in the warm pool (Figure 4.22).

Cold water along the equator has two sources: upwelling in the eastern Pacific due to the westward surface flow (SEC) driven along the equator by the trade winds, and upwelling due to divergent Ekman transport just off the equator, also due to the trade winds, which can occur at all longitudes. Because the warm pool in the western Pacific is so thick, the Ekman divergence component of the upwelling does not bring cold water to the sea surface there.

The pileup of water in the west causes an eastward pressure gradient force along the equator. This pressure gradient force drives the eastward flow of the EUC. The west-to-east pressure gradient force also creates equatorward geostrophic flow that feeds the equatorial upwelling.

The equatorial pycnocline is deep in the west and tilts upward toward the east (Figure 10.23). This upward tilt compensates the downward sea-surface tilt such that the pressure gradient force along the equator beneath the pycnocline is very weak. In fact the equatorial flow beneath the EUC is weakly westward (EIC). The EUC is located within the pycnocline (Figure 10.23c). It shoals toward the east along with the pycnocline (Figure 10.23). It is weak in the western equatorial Pacific, with speeds less than 40 cm/sec. It speeds up east of the date line, and reaches maximum strength around 140°W. This corresponds to longitudes of greater eastward pressure gradient force, evident in surface height and dynamic height. Its transport peaks at about 2.5 Sv in the central Pacific (Leetmaa & Spain, 1981).

At the western boundary, the EUC is fed by the saline NGCUC (Section 10.7.4). As the EUC flows eastward it encounters the Galapagos Islands, located on the equator at 91–89°W. The EUC splits upstream of the islands at about 92°W and flows north and south around the islands. The southern part is stronger; the main core of the EUC core is actually slightly south of the equator from 98°W. East of the Galapagos, part of the EUC penetrates southeast to 5°S and joins the Peru Countercurrent at the surface and the PCUC at the South American coast (Section 10.4.1.3; Lukas, 1986).

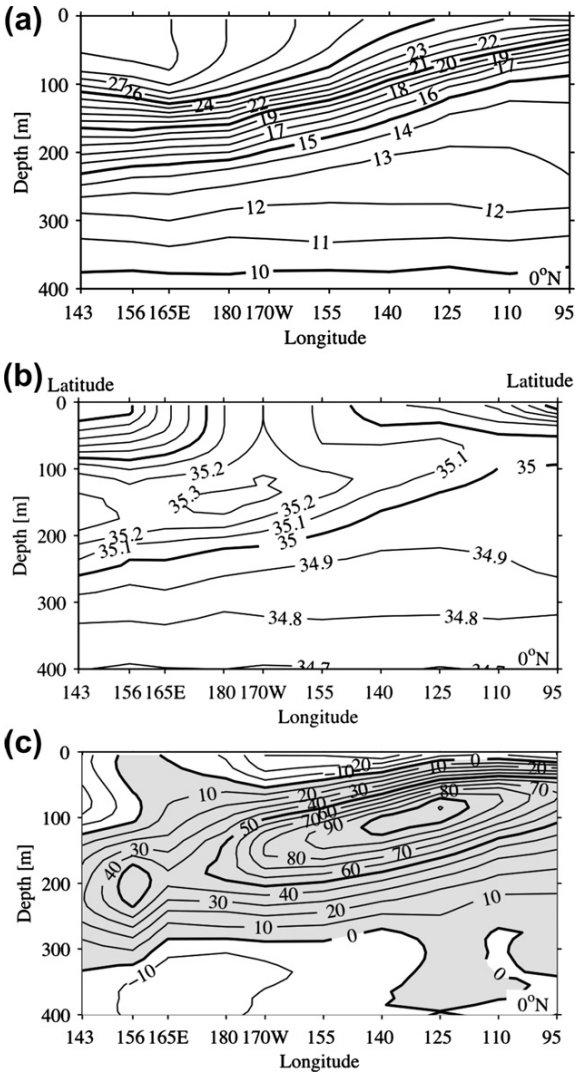

FIGURE 10.23 Mean equatorial (a) potential temperature (°C), (b) salinity, and (c) zonal velocity (cm/sec). Eastward velocities are shaded. *Source: From Johnson et al. (2002).*

Other zonal "asymmetries" are apparent in the other major tropical currents. The eastward NECC shifts northward toward the east. The

eastward NSCC and SSCC both shift poleward as well. The SECC is present permanently only in the western Pacific and disappears by the mid-Pacific.

10.7.3.3. Equatorial Upwelling and Biological Productivity

The Pacific equatorial SST structure is strongly influenced by upwelling of cold water from the pycnocline/thermocline. Where the thermocline is shallow, upwelling creates cold surface temperature; where and when the thermocline is deep, upwelling is not as effective in cooling the surface. The cold tongue and warm pool are evident in satellite images in non-El Niño years (Figures 4.1 and 10.24). Coastal upwelling along Ecuador is also evident, joining with the equatorial cold tongue.

Upwelled water is often richer in nutrients than the displaced surface water. Global maps of surface nutrients show a maximum in the Pacific cold tongue (nitrate in Figure 4.24), because of the eastward shoaling of the pycnocline, which is also the nutricline. This nutrient maximum promotes biological production. Biological productivity, measured in amount of carbon produced per area per day, is high in the upwelled water of the cold tongue (Figure 10.22d, from a La Niña period of enhanced upwelling). This calculation of productivity was based on ocean color from the SeaWIFs satellite (Figure S10.318 on the textbook Web site).

10.7.4. Low Latitude Western Boundary Currents

The Mindanao Current is a 200 km wide western boundary current that flows southward along the western boundary of the tropical North Pacific. Dynamically, it is the western boundary current associated with the Sverdrup transport of the elongated tropical cyclonic gyre. The Mindanao Current carries subtropical North Pacific waters toward the equator, including saline water from the subtropical thermocline and traces of North Pacific Intermediate Water (Bingham & Lukas, 1994).

The Mindanao Current forms near 14°N where the westward-flowing NEC splits, with the northward flow forming the Kuroshio (Figure 10.1 and Figures S10.1 and S10.19 on the textbook Web site). It turns eastward at about 5°N and feeds the NECC. Mindanao Current speeds are typical of western boundary currents, reaching a maximum of 100 cm/sec. Volume transport estimates range from 20 to 40 Sv, consistent with the calculated Sverdrup transport (Wijffels, Firing, & Toole, 1995).

The Mindanao Eddy (ME in Figure 10.1) is a recirculating cyclonic feature at the western boundary of the cyclonic tropical gyre. It forms between the westward NEC and the eastward NECC. Its western side is the Mindanao Current. The Halmahera Eddy (HE in Figure 10.1) is an anticyclonic feature at the western boundary just north of the equator between the eastward NECC and the westward SEC. The Halmahera Eddy mixes waters from the North and South Pacific. The properties of waters that enter the Indonesian Throughflow (ITF) may therefore depend on the activity of this eddy (Kashino et al., 1999). Both eddies are highly dependent on wind forcing.

The NGCUC is the northward western boundary current of the tropical South Pacific. The NGCUC is the northernmost part of the western boundary current that forms from the westward flow of the SEC (Qu & Lindstrom, 2002), which splits at the Australian coast, with the southward flow forming the EAC (Section 10.4.1.1). The split is at 15°S at the sea surface and shifts poleward to 23°S at 800 m. The northward boundary current north of 15°S is referred to as the *North Queensland Current* (NQC). (The northward subsurface flow between 23°S and 15°S is called the *Great Barrier Reef Undercurrent* (GBRUC).) The NQC flows through the Coral Sea, through the Solomon Sea, and then through the Vitiaz Strait between New Guinea and New Britain. Beyond that

point it is referred to as the NGCUC. The NGCUC turns north and then east along the equator at about 143°E to feed the EUC. The NGCUC has speeds of 50 cm/sec centered at 200 m depth and a transport of 7 Sv at 2°S, which are equivalent to those of the EUC at the equator.

Lastly, the tropical Pacific and Indian Oceans are connected via the Indonesian Throughflow, through the complex passages of the Indonesian archipelago (Figure 11.11; Section 11.5). Approximately 10–15 Sv flow through the passages, with significant variability, much of it due to ENSO. The Pacific's low latitude western boundary currents are the source of the ITF. The flow through the Makassar Strait originates in the Mindanao Current. South Pacific waters from the NGCUC enter the Halmahera Sea; deeper South Pacific waters from the same source enter through Lifamatola Strait (Hautala, Reid, & Bray, 1996).

10.7.5. Equatorial Property Distributions

Although most of the Pacific water mass description is in Section 10.9, we briefly review the tropical upper ocean distributions in this section because they are so clearly linked to the equatorial current system.

The temperature structure is highly symmetric about the equator (Figure 10.19). The thermocline is most intense a few degrees north and south of the equator, with the isotherms spreading apart north and south of the 10°N and 10°S parallels. At the equator, the spreading of the isotherms marks the core of the EUC. Below the thermocline, between about 5°S and 12°N, there is a marked thermostad (low vertical gradient).

For salinity, there is little symmetry across the equator (Figure 10.19), because the South Pacific is more saline, because the SEC reaches the equator and the NEC does not, and because of the Northern Hemisphere location of the ITCZ. Salinity maximum layers are subducted equatorward from both the South and North Pacific subtropical evaporation maxima; their core salinities are 36.2 psu and 35.0 psu, respectively. (These are the Subtropical Underwaters, also called Tropical Waters in Johnson & McPhaden, 1999.) Because the SEC extends to the equator, the salinity maximum at the equator comes directly from the South Pacific subtropical gyre. The South and North Pacific salinity maxima are separated laterally by lower salinity arising from the California Current and downward diffusion beneath the rainy ITCZ (Johnson & McPhaden, 1999). The lowest surface salinity is in the NECC, which lies directly below the ITCZ. The subsurface low salinity water entering at about 20°N at 300 m is the North Pacific Intermediate Water (Section 10.9.2.1).

10.7.6. Intraseasonal and Seasonal Variability

The equatorial Pacific includes temporal variability at intraseasonal (20–30 days), seasonal, monthly-to-interannual, interannual (3–7 years), and interdecadal (10–30 years) timescales. The most energetic intraseasonal variations are the *Tropical Instability Waves* (TIWs). Seasonal variability includes response to changes in location and strength of the ITCZs in both hemispheres. Other variability at weekly to interannual periods is associated with Rossby and Kelvin waves (Section 7.7) and at interannual and longer periods, with ENSO and other climate modes (Section 10.8 and Chapter S15 on the textbook Web site).

TIWs are large cusp-like spatial oscillations in SST along the northern edge of the cold tongue (Figure 10.24) (Legeckis, 1977). The oscillations are also apparent in ocean color/chlorophyll (McClain et al., 2002). TIWs have wavelengths of about 1000 km. The TIW pattern propagates westward at an average phase speed of 30 to 50 cm/sec, resulting in a period of about 20 to 30 days. The TIWs are principally

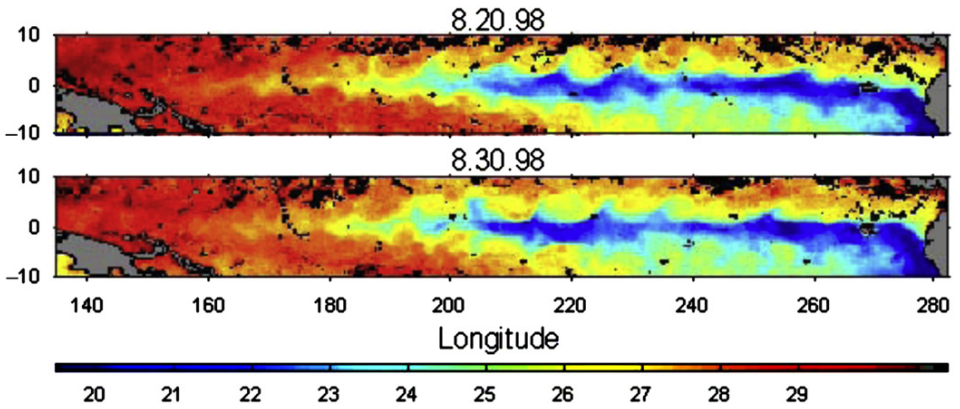

FIGURE 10.24 Tropical instability waves. SST from the Tropical Rainfall Mapping Mission (TRMM) Microwave Imager (TMI) for two successive 10-day periods in August 1998, after establishment of the cold tongue during a La Niña. A more complete time series (June 1–August 30, 1998) is reproduced in Figure S10.20 on the textbook Web site. This figure can also be seen in the color insert. TMI data are produced by Remote Sensing Systems and sponsored by the NASA Earth Science MEASURES DISCOVER Project. Data are available at www.remss.com. *Source: From Remote Sensing Systems (2004).*

due to (barotropic) instability arising from the horizontal shear between the SEC and the NECC (Philander, 1978). TIWs are shallow (100–200 m thick) because the high velocities of the currents that create them are surface-intensified.

TIWs appear in summer (June) when the ITCZ migrates northward and the trade winds accelerate the portion of the SEC that lies north of the equator (Vialard, Menkes, Anderson, & Balmaseda, 2003). In the time series leading to Figure 10.24 (Figure S10.20 on the textbook Web site), the equatorial cold tongue emerges in early June; by June 10 the tongue shows north-south oscillations due to TIWs. Closed anticyclonic vortices are found in the troughs of the waves. Seasonal wind forcing in the tropical Pacific directly affects SST and the surface and upper ocean currents (Figure 10.25). The cold tongue is strongest in August-September, during the period of strongest trade winds, accompanied by warmest temperatures in the warm pool; the west-east contrast is as much as 10°C. By March, both temperature features are much weaker and the west-east contrast is reduced to about 5°C. (The large interannual variability superimposed on the annual cycle in Figure 10.25 is due to ENSO.)

The equatorial part of the SEC, which responds frictionally to the wind stress, varies mostly in phase with the seasonal winds. The EUC, which responds to the west-east pressure gradient set up by the SEC, has a more complicated response that lags the winds. Johnson, Sloyan, Kessler, and McTaggert (2002) provided detailed discussion of the seasonal variability of each of the upper ocean currents, phasing with the winds, and spatial structure. Dramatic seasonal variability occurs just offshore of the Central American mountain chain (Figure 10.26). Trade winds from the Atlantic funnel through three major gaps in the mountains, with wintertime winds reaching 20 m/sec during several 5- to 7-day-long events. The wind jets (Tehuantepec, Papagayo, and Panama) that emerge over the Pacific force dramatic local circulations and upper layer mixing, resulting in cool SST (Chelton, Freilich, & Esbensen, 2000) and ocean color anomalies; the effects are visible even in the global mean wind stress curl map from Chelton et al. (2004; Figure 5.16d).

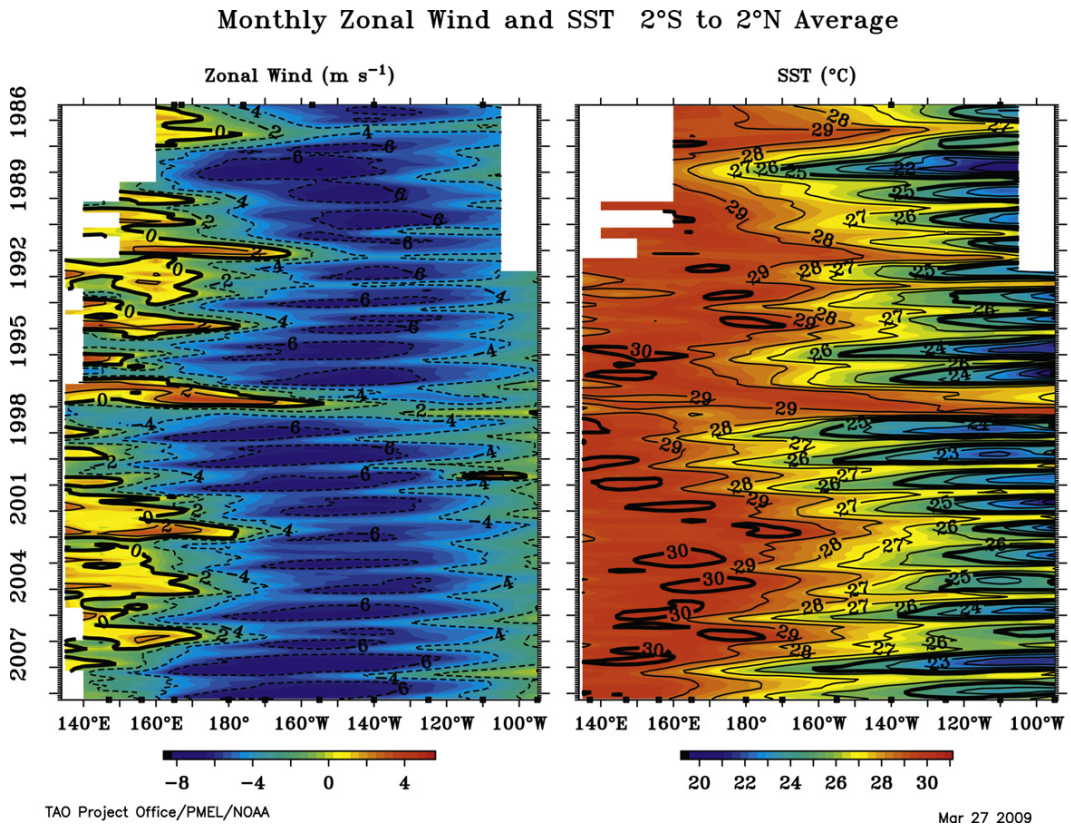

FIGURE 10.25 Zonal wind speed and SST in the equatorial Pacific to illustrate the annual cycle. Positive wind speed is toward the east. Climatological means in February and August and an expanded time series for 2000–2007 are shown in Figure S10.21 on the textbook Web site, to emphasize the seasonal cycle. This figure can also be found in the color insert. *Source: From TAO Project Office (2009a).*

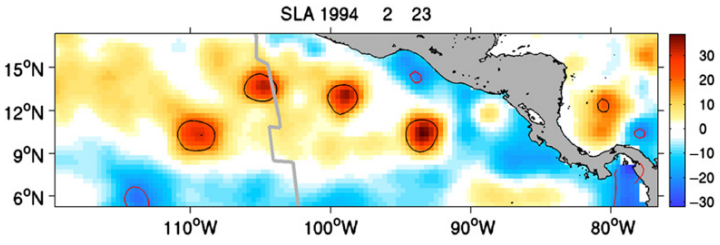

FIGURE 10.26 Tehuantepec eddies evident in sea surface height anomalies from satellite altimetry in February, 1994. *Source: From Palacios and Bograd (2005).*

Anticyclonic eddies are produced by the wind jets, as a combination of eddy shedding from the coastal circulation system (coastally trapped waves) and the strong wind stress curl in the jets. The eddies propagate offshore. The best known are the Tehuantepec eddies (Figure 10.26 and Figure S10.22 on the textbook Web site). Three to four Tehuantepec eddies and two to three Papagayo eddies form each year between October and July with greater

frequency and intensity during El Niño years (Palacios & Bograd, 2005).

10.8. EL NIÑO/ LA NIÑA AND THE SOUTHERN OSCILLATION (ENSO)

El Niño/La Niña is a natural climate variation that is dynamically centered in the tropical Pacific. Its "interannual" timescale is 3 to 7 years for quasi-periodic alternation between the El Niño and La Niña states. The *Southern Oscillation* is an index based on the pressure difference between two tropical South Pacific locations, and is closely related to the El Niño state. Because this index is so closely related to El Niño events, the full climate phenomenon is often referred to as El Niño-Southern Oscillation (ENSO). The ocean and atmosphere are fully coupled in this climate "cycle." The coupling is referred to as the Bjerknes feedback (Section 7.9.2; Bjerknes, 1969).

An El Niño event is marked by an unusual excursion of warm water (>28°C) to the east in the equatorial zone, associated with weakened southeast Trade Winds in the east and stronger westerlies in the west. La Niña is the opposite — stronger southeast Trades in the east (and weak westerlies in the far west) with resulting cool water (<25°C) extending much further westward along the equator than usual. The alternation between states is not regular since there are many different oceanic and atmospheric phenomena linked in the full system plus random, short-term forcing. Therefore, ENSO predictability is not like that of, say, the tides, which are forced by very regular, predictable progressions in the orbits of the earth, moon, and sun.

El Niño/La Niña events have large and sometime devastating impacts on ocean ecosystems, particularly along the South American coast, but also as far north as the CCS. ENSO impacts air temperature and precipitation on global scales (Figures S10.24 and S10.25 on the textbook Web site), via propagation of large-scale waves through the atmosphere and propagation of Kelvin waves (Section 7.7.6) along the eastern boundary of the Pacific. Precipitation anomalies during a composite El Niño include regions of anomalously low precipitation that are susceptible to drought and fire and high precipitation that are susceptible to flooding. Although it is not located in the tropics, U.S. air temperatures are affected by ENSO; El Niño signatures include anomalous warmth over the northwest and high plains; cool temperatures in the south and Florida; anomalously dry conditions in the northwest, east, and Appalachians; and wet conditions from California through the southeastern U.S.

Early ideas about the cause of El Niño centered on local mechanisms along the South American coast, for instance that the alongshore winds off Peru changed to lessen or stop the coastal upwelling. More intensive studies in the early 1970s, motivated by a major El Niño event in 1972 that resulted in the collapse of the Peru/Ecuador anchovy fishery, showed that El Niño has a much larger geographic scale. Rasmusson & Carpenter's (1982) canonical description of ENSO, based on El Niño's from 1949 to 1980, was the underpinning for an international project (Tropical Ocean Global Atmosphere; TOGA) to study ENSO (1985–1995). TOGA planning was underway when the strong El Niño event of 1982/83 provided additional impetus for the experiment. The importance of ENSO analysis and prediction is such that a massive permanent observing system has been deployed in the tropical Pacific since the 1980s (TAO and TRITON; Section S6.5.6 on the textbook Web site).

Excellent, regularly updated information, including background information on dynamics and impacts, forecasts, and links to many different ENSO products, is available from several different Web sites administered by the National Oceanic and Atmospheric Administration.

10.8.1. ENSO Description

We first recall the "normal" ocean and atmosphere conditions in the tropical Pacific (Section 7.9.2; Figure 10.27b). The easterly trade winds pile up warm equatorial water in the western tropical Pacific and cause upwelling along the equator. This causes the cold tongue in SST in the eastern tropics, and causes the thermocline to be inclined upward from west to east (Section 10.7.3). The warm-to-cold SST difference along the equator maintains the Walker circulation in the atmosphere, thus sustaining this component of the trade winds. This is an equilibrium state of the simple coupled ocean-atmosphere, and the system would remain in this state if it did not include large-scale propagating waves such as Kelvin and Rossby waves.

The exaggerated, strong version of the normal state is the La Niña state (Figure 10.27a). In La Niña, the warm SST shifts slightly more to the west, the thermocline is a bit deeper in the west, the sea surface is higher in the west and lower in the east, and the Walker circulation in the atmosphere is stronger.

In an El Niño state, the trade winds are weaker, because the Walker circulation is weak or reversed, and the thermocline is more level (Figure 10.27c). The cold tongue in the east weakens and disappears, due to both relaxation of the thermocline and eastward movement of warm water from the central and western tropical Pacific. This does not indicate an absence of upwelling but rather that warm water is now occupying the eastern tropical Pacific; the schematic shows easterly trades in the eastern Pacific, but these upwell only warm water from the now thicker and warmer surface layer.

In the time series of SST along the equator (Figure 10.25), warm SST and weaker trade winds mark several El Niño events, with the opposite markers for La Niña events. Time series indicating the occurrence of El Niño and La Niña are constructed in various ways. The first index, the *Southern Oscillation Index* (SOI) is the difference in atmospheric pressure between the western and eastern tropical South Pacific; meteorological stations at Darwin, Australia, and Tahiti are used in the SOI because observations have been made in these locations for a very long time. Every El Niño event is associated with low SOI. However, not every SOI low corresponds to an El Niño. Several indices are based on SSTs averaged spatially over portions of the eastern tropical Pacific because this reflects conditions in the cold tongue (e.g., Oceanic Niño Index in Figure 10.28). A multivariate index based on SST, sea level pressure, surface air temperature, surface wind, and cloudiness is also useful (Wolter & Timlin, 1993; Wolter, 2009). Very long time series have been reconstructed from proxies of temperature measured in coral heads (Cobb, Charles, Cheng,

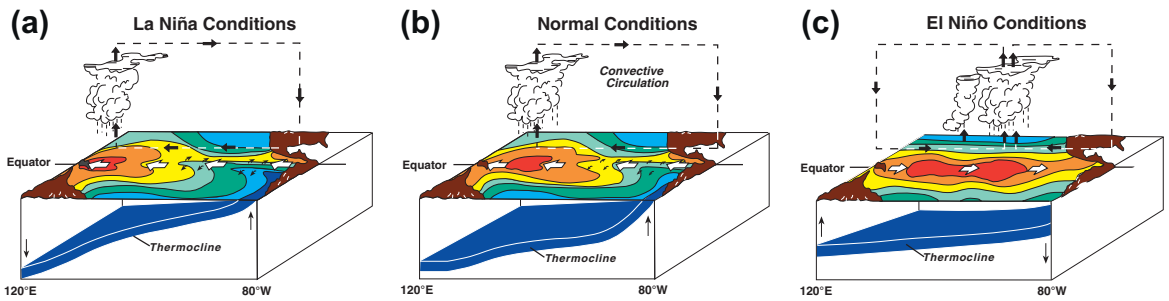

FIGURE 10.27 (a) La Niña, (b) normal, and (c) El Niño conditions. This figure can also be found in the color insert. *Source: From NOAA PMEL (2009b).*

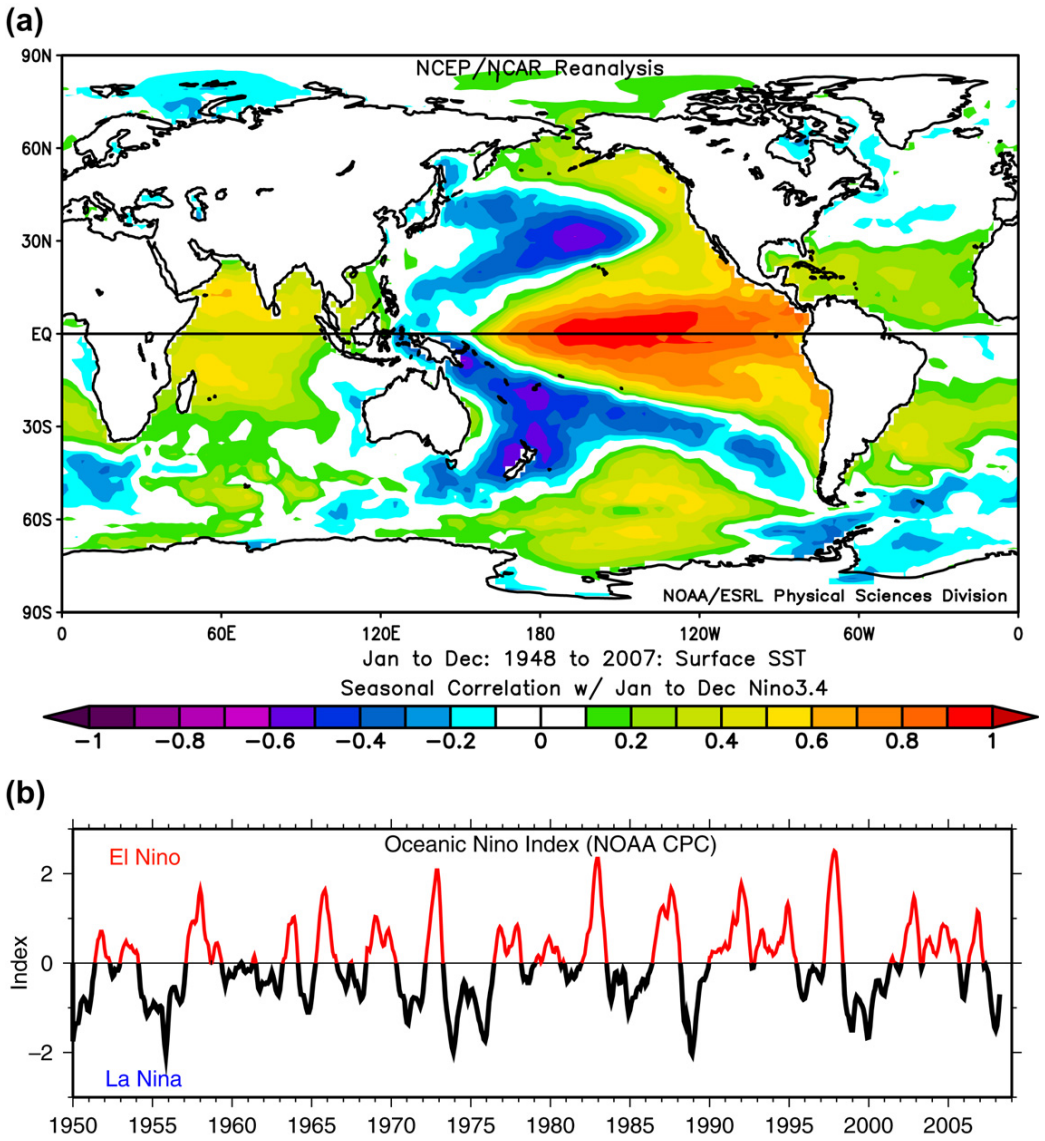

FIGURE 10.28 (a) Correlation of monthly SST anomalies with the ENSO Nino3.4 index, averaged from 1948 to 2007. The index is positive during the El Niño phase, so the signs shown are representative of this phase. (*Data and graphical interface from NOAA ESRL, 2009b.*) This figure can be found in the color insert. (b) "Oceanic Nino Index" based on SST in the region 5°N to 5°S and 170°W to 120°W. (*Data from Climate Prediction Center Internet Team, 2009*). Gray and black correspond to El Niño and La Niña, respectively. Additional indices representing ENSO and the correlation of monthly sea level pressure anomalies with the ENSO Nino3.4 index are shown in Figure S10.23 on the textbook Web site.

& Edwards, 2003). Long-term reconstructions of tropical Pacific SST show that El Niño events at 2–7 years are ubiquitous, although intensity and duration have varied. Well-documented El Niño events took place in 1941–1942, 1957–1958, 1965–1966, 1972–1973, 1977–1978, 1982–1983, 1997–1998, and 2002–2003. The events of 1982–1983 and 1997–1998 were the largest recorded since the 1880s.

The global reach of ENSO is apparent in correlations of SST and sea level pressure with an ENSO index (Figure 10.28b and Figures S10.23d on the textbook Web site). SST in the equatorial Pacific shows the pattern previously described of anomalously warm eastern equatorial waters during the El Niño phase. The even simpler sea level pressure pattern extends well into the ACC region in an alternating zonal pattern that is similar to that of the Southern Annular Mode (Section 10.10 and Chapter S15 on the textbook Web site).

10.8.2. ENSO Mechanisms

The Bjerknes (1969) feedback is at the heart of ENSO (Section 7.9.2), but it does not describe how each stage of ENSO develops or why there is a transition from one state to another with an "oscillation" timescale of 3 to 7 years. Bjerknes speculated that the transition results from ocean dynamics but could go no further. An oscillation with a period of several years can be produced with a model that includes an eastward-propagating equatorial Kelvin wave that reflects at the eastern boundary, producing westward-propagating Rossby waves (Cane, Münnich, & Zebiak, 1990; Jin, 1996; Van der Vaart, Dijkstra, & Jin, 2000).

The ENSO cycle, based on Rasmusson & Carpenter (1982), Jin (1996), and Van der Waart et al. (2000), is very briefly summarized here. Moving from normal conditions toward a full-blown El Niño, the steps are (1) changes of the trade winds to westerly winds in the western Pacific, often associated with the atmosphere's 30–60 day Madden-Julian oscillation; (2) an oceanic Kelvin wave shooting eastward along the equator in response; (3) resultant warm SST anomalies in the eastern and central equatorial Pacific; and (4) disruption of the Walker circulation through SST feedback on the atmosphere. The "recharge oscillator" that transitions this back toward a La Niña occurs when: (1) the Kelvin wave reflects at the eastern boundary and produces westward-propagating Rossby waves, (2) the Rossby waves move warm water away from the equator which weakens the equatorial SST warm anomaly, (3) the trade winds strengthen a little in response to the somewhat cooler SST, (4) the strengthened trades begin pushing the thermocline back toward a normal state, and (5) Bjerknes feedback then creates a La Niña state.

The adjustment timescale of this nearly free oscillation yields the 3–7 year ENSO timescale. An important property of this system is a delay between the change in thermocline depth in the western Pacific and the SST warming in the eastern Pacific, which can be explained partially by the Kelvin wave propagation (Jin, 1996).

The actual ENSO system is nonlinear and messy. Fedorov et al. (2003) described it as a "slightly damped, swinging pendulum sustained by modest blows at random times." The switch from one state to another, and the intensity and duration of the resulting state, depend on many factors. These include phasing of the shifts relative to the seasonal cycle and also to the occurrence, timing, and intensity of westerly wind bursts in the western tropical Pacific that are associated with the intraseasonal (30–60 day) Madden-Julian Oscillation in the atmosphere. Predictability of onset, intensity, and duration of events is therefore limited.

Because of the widespread economic impacts of ENSO, skillful prediction several months ahead has been a goal for many decades. Two approaches are dynamical modeling and statistical modeling. Dynamical models use a coupled

ocean-atmosphere model with initial conditions based on observations. Statistical models use observed parameters such as SST or heat content and winds with a regression method to forecast ENSO several months ahead. Forecasts are generally probabilistic, meaning that an ensemble (large number) of model runs is made with slightly varying initial conditions. Given the randomness of "triggering" mechanisms, Philander and Fedorov (2003) and Fedorov et al. (2003) highly recommended this approach. The International Research Institute for Climate and Society (IRI) at Columbia University currently monitors 15 dynamical and 8 statistical model forecasts (http://iri.columbia.edu/climate/ENSO/currentinfo/SST_table.html).

10.9. PACIFIC OCEAN WATER MASSES

Pacific Ocean water properties, like those of the other oceans, can be considered in four layers (Section 4.1). The upper ocean layer contains the mixed layer and main pycnocline (thermocline/halocline), and is in broad contact with the atmosphere. The intermediate layer contains two low salinity water masses that originate at the sea surface of the subpolar/subantarctic latitudes. The deep layer contains two deep water masses, one from the North Pacific and one from the Southern Ocean. The North Pacific deep water "source" is entirely internal mixing and upwelling of waters from the Southern Ocean, with no contact with the atmosphere. The Southern Ocean deep water source contains a mixture of deep waters from all three oceans (Atlantic, Indian, and Pacific) as well as waters that are locally ventilated in the Southern Ocean. The bottom layer contains the densest water that escapes northward from the Southern Ocean. The distinction between the deep and bottom layers is not sharp, and is usually based on the direction of net meridional transport in the two layers, with net southward transport in the deep layer and net northward in the bottom layer.

The Pacific Ocean is the freshest of the three main ocean basins. The Atlantic and Indian Oceans are both net evaporative basins, and therefore have high overall salinity. The Pacific evaporation-precipitation balance is nearly neutral which makes the Pacific fresher than the Atlantic and Indian.

The most important distinguishing process for Pacific Ocean water properties is the lack of a surface source of very dense water in the North Pacific. This differs entirely from the Atlantic Ocean. The densest water formed locally is the relatively light North Pacific Intermediate Water. On a global scale, the Pacific Ocean is the low density end-member of the overturning circulation. Its bottom waters, which originate in other oceans, are salty and its upper waters are relatively fresh; cooling to the freezing point, which occurs in the Bering and Okhotsk Seas in the northwest Pacific, cannot increase the surface water density to a high enough value to punch through to the deep and bottom layers.

A potential temperature-salinity (T-S) diagram that represents the major water masses is shown in Figure 10.29. Table S10.4 on the textbook Web site lists the principal water masses and an abbreviated description of the process that initially forms each water mass. The Pacific World Ocean Circulation Experiment (WOCE) Hydrographic Programme Atlas (Talley, 2007) is a comprehensive source of sections, maps, and property plots.

10.9.1. Pacific Ocean Upper Waters

Pacific surface temperature (Figure 4.1) shows the usual tropical maximum with poleward decrease in temperature in both hemispheres. The highest temperatures (>29°C) are in the equatorial warm pool. The lower temperatures of the equatorial cold tongue are also evident. Isotherms in the PCCS and CCS are deformed,

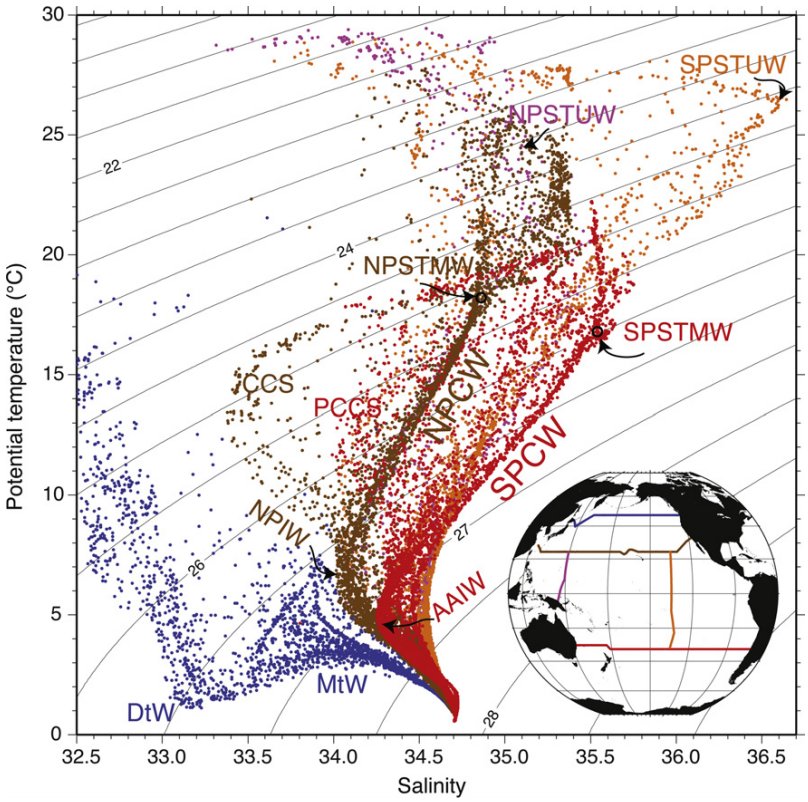

FIGURE 10.29 Potential T-S curves for selected stations (inset map). Acronyms: NPCW, North Pacific Central Water; SPCW, South Pacific Central Water; NPSTUW, North Pacific Subtropical Underwater; SPSTUW, South Pacific Subtropical Underwater; NPSTMW, North Pacific Subtropical Mode Water; SPSTMW, South Pacific Subtropical Mode Water; NPIW, North Pacific Intermediate Water; AAIW, Antarctic Intermediate Water; DtW, Dichothermal Water; MtW, Mesothermal Water; CCS, California Current System waters; and PCCS, Peru-Chile Current System Waters. This figure can also be found in the color insert.

with colder water near the coasts due to equatorward advection and upwelling. The coldest temperatures are in the sea ice areas of the Okhotsk and Bering Seas, and in the Antarctic.

Pacific surface salinity shows the typical maxima in the subtropics, in the major subtropical evaporation centers (Figures 4.14, 5.4). There is a north-south minimum in the tropics beneath the ITCZ at 5–10°N, due to excess precipitation. Salinity is also low at high latitudes due to excess precipitation. The surface salinity in the North Pacific is considerably less than in the North Atlantic, because of the greater runoff and precipitation. In the South Pacific the average surface salinity is higher than in the North Pacific but is lower than in the South Atlantic.

In the subtropics, there are two important processes for creating upper ocean waters: subduction of surface waters equatorward and downward beneath less dense, lower latitude surface waters, and production of thick, well-mixed layers on the warm side of strong current fronts such as the Kuroshio. These result in several recognized subtropical water masses (Table S10.4 on the textbook Web site) as follows.

The waters that make up the thermocline/pycnocline in the subtropics are called *Central Waters* (Figure 10.29), as also found in the Atlantic and Indian Oceans. The pycnocline, or Central Water, is created by subduction and diapycnal mixing (Section 9.8.1). "Central Water" is a T-S relation with a large range of temperatures

and salinities, rather than an extremum of some property.

North Pacific Central Water (NPCW) extends from the NECC to about 40°N and is the freshest of the Central Waters of the world's oceans (Figure 4.7). It is separated from the eastern boundary by another, yet fresher water mass that characterizes the CCS. This fresher CCS water is advected southward from the eastern subpolar gyre.

South Pacific Central Water (SPCW) is saltier than NPCW since the South Pacific is saltier overall. SPCW extends from about 10°S southward to the Subantarctic Front at about 55°S. Similar to NPCW, SPCW is separated from the eastern boundary by another, fresher water mass within the PCCS, advected northward from fresher high latitude surface waters.

A second water mass associated with subtropical subduction in both hemispheres is the *Subtropical Underwater* (STUW), or subtropical salinity maximum water. This is identified as a shallow salinity maximum on the equatorward part of the subtropical gyre (Figure 10.30). STUW results from subduction of the very high salinity surface water in the center of each subtropical gyre. STUW is found on every meridional section in the Pacific between 25°S and 25°N. It is very shallow, with its salinity extremum no more than 200 m deep, because the isopycnals that

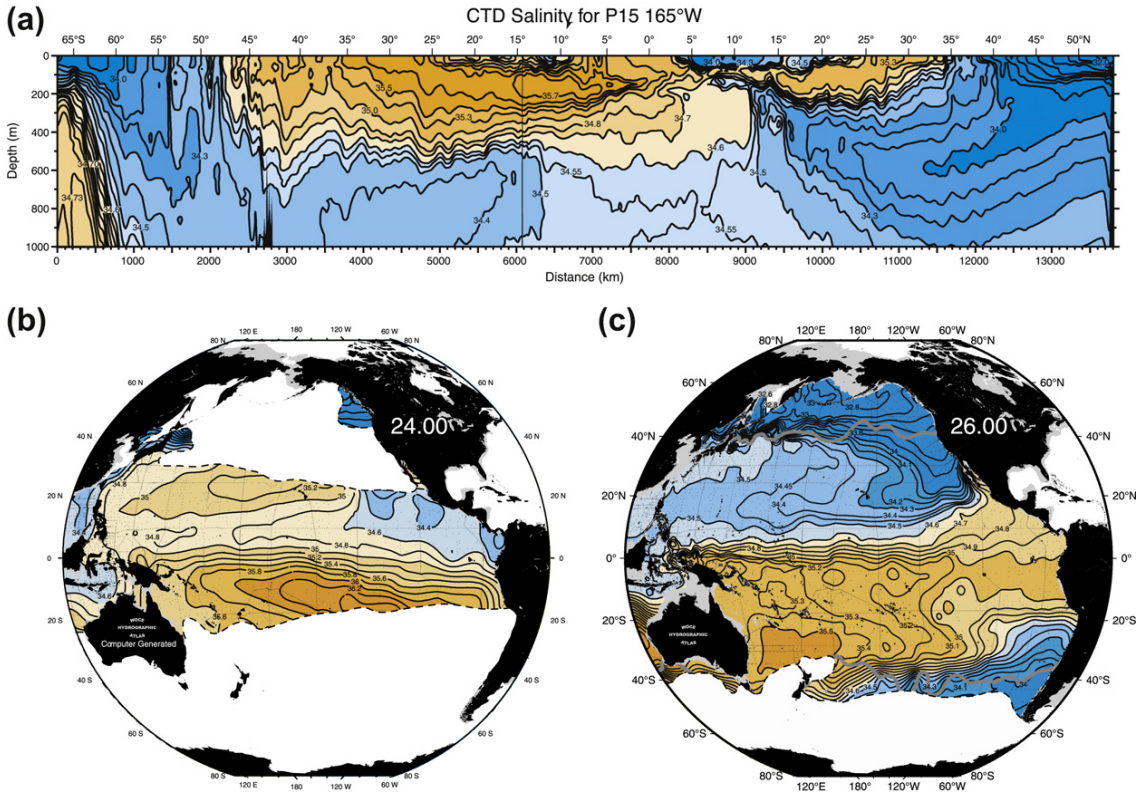

FIGURE 10.30 Salinity: (a) along 165°W (WOCE P15); (b) at neutral density 24.0 kg/m^3, characteristic of STUW; and (c) at neutral density 26.00 kg/m^3, characteristic of SPSTMW. The isopycnals intersect the surface along the dashed contours Gray contours in (c) indicate winter outcrops. *Source: From WOCE Pacific Ocean Atlas, Talley (2007).*

outcrop in the surface salinity maximum water are warm (~26 and 24°C in the South and North Pacific, respectively) and low density (σ_θ ~ 24.0 and 23.5 kg/m^3 in the South and North Pacific, respectively).

The third subtropical water mass that we single out is *Subtropical Mode Water* (STMW; Masuzawa, 1969). "Mode" means relatively large volume on a volumetric potential T-S diagram. Mode Water is a pycnostad embedded in the main pycnocline; it results from subduction of the especially thick winter mixed layers on the warm side of the separated western boundary currents (Kuroshio and EAC; Hanawa & Talley, 2001; Figure S10.26 on the textbook Web site). The STMW in the North Pacific (NPSTMW) is in the temperature range 16−19°C and centered at potential density σ_θ = 25.2 kg/m^3 (Figure 10.29 and Figure S10.26b on the textbook Web site). It originates in winter as a thick mixed layer just south of the Kuroshio. The thick layers subduct into the general region of the western subtropical gyre and are evident within the thermocline (Figures 10.31a and S10.26c on the textbook Web site). The temperature of the STMW is highest (>18°C) just south of Japan and decreases toward the east.

In the South Pacific, the South Pacific STMW (SPSTMW) is present north of the Tasman Front and East Auckland Current (Figure 10.31b and Figure S10.26c on the textbook Web site; Roemmich & Cornuelle, 1992). Its core temperature, salinity, and density are 15−17°C (just north of New Zealand) and 17−19°C (region north of 29°S), 35.5 psu, and σ_θ = 26.0 kg/m^3 (SPSTMW in Figures 10.29 and 10.30). Thus it has the same temperature range as NPSTMW. It is denser because it is somewhat more saline, because the South Pacific is saltier than the North Pacific. SPSTMW is the weakest of the global STMWs; without a supplementary vertical density gradient calculation, the widening of isopycnals and isotherms on intersecting vertical sections is somewhat difficult to discern (Figure 10.31b). The North Pacific's subpolar gyre is a region of Ekman upwelling rather than downwelling. Therefore there is no wind-driven subduction. Surface densities increase along the cyclonic path around the gyre; they are higher in the west than in the east, and are highest in the Okhotsk Sea, along Hokkaido and just south of Hokkaido. In the regions of highest surface density, the densest (intermediate) North Pacific waters are formed (Section 10.9.2).

The combination of low surface salinity and upwelling in the subpolar gyre creates a strong halocline. This supports a temperature minimum where the surface water becomes very cold in winter. The temperature minimum is called *Dichothermal Water* and is found in the western subpolar gyre and the adjacent Okhotsk and Bering Seas. Associated with the temperature minimum is very high oxygen saturation in the summertime, due to capping by warm surface water and slight warming of the subsurface T min layer. Below the Dichothermal Water, temperature increases to a maximum and then decreases to the ocean bottom. The temperature maximum layer is called *Mesothermal Water*. The maximum indicates a substantial advective component from the east or the south since otherwise it would acquire the low temperature of the surface layer.

Tropical Pacific water properties were described in Section 10.7.5. Complex vertical structure is created by interleaving of North and South Pacific waters (Figure 10.19). Nearly zonal fronts in salinity occur along the equator (Figure 10.30c). In temperature and density, the equatorial thermocline/pycnocline ascends and intensifies from 150−200 m in the west to less than 50 m in the east (Figure 10.23). The pycnocline inhibits vertical transfer of water properties. In the west, a halocline lies within the upper (warm pool) layer, above the thermocline, so the pycnocline is determined by salinity rather than temperature.

One tropical water mass that is distinguished by a name is the *Equatorial 13°C Water*

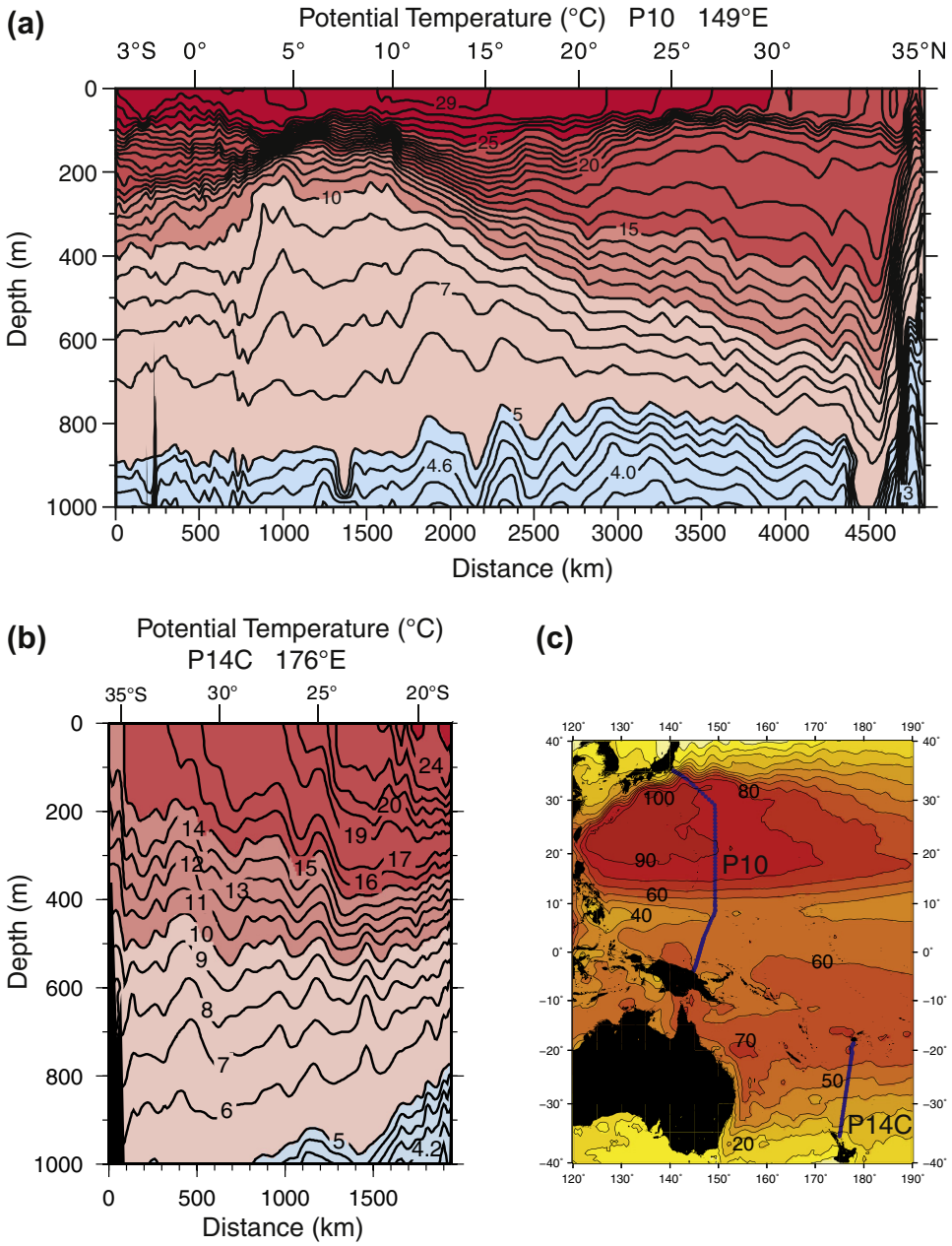

FIGURE 10.31 (a) Potential temperature (°C) along 149°E in the North Pacific. (b) Potential temperature along 170°E in the South Pacific. *Source: From WOCE Pacific Ocean Atlas, Talley (2007).* (c) Station locations superimposed on surface streamfunction. *(Data from Niiler, Maximenko, & McWilliams, 2003.)*

(Montgomery & Stroup, 1962; Tsuchiya, 1981). This is a mode water — a conspicuous thickening of the equatorial layer centered at 13°C, at about 75–300 m depth (Figure 10.19). Water at this temperature is advected eastward across the Pacific from the low latitude western boundary currents. The thickening is possibly linked to the local dynamics of the equatorial currents, as the water mass is associated with the North and South Subsurface Countercurrents (Figure 10.20b).

Finally, two large regions of remarkably low oxygen (<1 μmol/kg) are found in the eastern tropical Pacific, centered at 10°N and 7°S, and most intense near the eastern boundary (Figures 10.32 and 4.20). The most extreme oxygen minima here coincide with well-developed subsurface maxima in nitrite (NO_2; Figure 10.32b). Nitrite normally occurs within or at the base of the euphotic zone (widespread band in the upper 200 m in the figure), as part of the usual nitrification process. The strongly developed subsurface nitrite maxima are a unique feature of *denitrification*. Remarkably, chlorofluorocarbons (CFCs) are non-zero in the oxygen minima (WOCE Pacific Ocean Atlas, Talley, 2007), which means that these waters are ventilated and that oxygen is low because of high biological productivity rather than extreme age.

10.9.2. Intermediate Waters

The intermediate layer of the Pacific is occupied by two low salinity water masses, the *North Pacific Intermediate Water* (NPIW) and the *Antarctic Intermediate Water* (AAIW) (e.g., Figures 4.12b, 14.13 and S10.27 on the textbook Web site). The source waters of both are fresh, cool surface waters at subpolar latitudes. In the subtropics and equatorial Pacific, the overlying water is the higher salinity Central Water, which originates in the high salinity midlatitude surface waters. Underlying the intermediate waters is higher salinity Circumpolar Deep Water, which obtains its higher salinity from the North Atlantic. Thus the NPIW and AAIW both appear as vertical salinity minima in the subtropics and tropics.

The NPIW salinity minimum is confined to the subtropical North Pacific. The AAIW salinity minimum, in contrast, is found throughout the subtropical South Pacific, the tropical Pacific, and similar regions of the Atlantic and Indian Oceans. Both NPIW and AAIW are within the ventilated, higher oxygen part of the water column. However, neither have particularly high oxygen content in the Pacific, indicating that residence time is longer than for the overlying Central Waters.

Salinity and oxygen content on isopycnals that represent NPIW and AAIW (Figure 10.33) reflect the low salinity/high oxygen influx from (1) the Okhotsk Sea for the NPIW and (2) the southeast Pacific for the AAIW. These are the source regions of these water masses.

(Salinity at neutral density 27.30 kg/m^3 provides a straightforward example of the importance of diapycnal mixing. Throughout the tropics, salinity is higher and the water is warmer as this is an isopycnal. There is no warm, salty surface outcrop for this isopycnal, so the tropical properties must result from diapycnal mixing.)

10.9.2.1. North Pacific Intermediate Water

NPIW is the densest water that is directly ventilated on a regular basis in the North Pacific. The full NPIW density range is σ_θ = 26.7 kg/m^3 to 27.2 kg/m^3 (directly ventilated), to 27.6 kg/m^3 (ventilated through vigorous diapycnal mixing in the Kuril Island straits). The subtropical NPIW salinity minimum has potential density σ_θ = 26.7 to 26.8 kg/m^3. On an NPIW isopycnal, the lowest salinity (hence coldest) and highest oxygen, indicating the most recently ventilated water, occur in the Okhotsk Sea and adjacent subpolar gyre (Figure 10.33). The main direct ventilation process for NPIW is brine rejection during sea ice formation in a coastal (latent heat) polynya

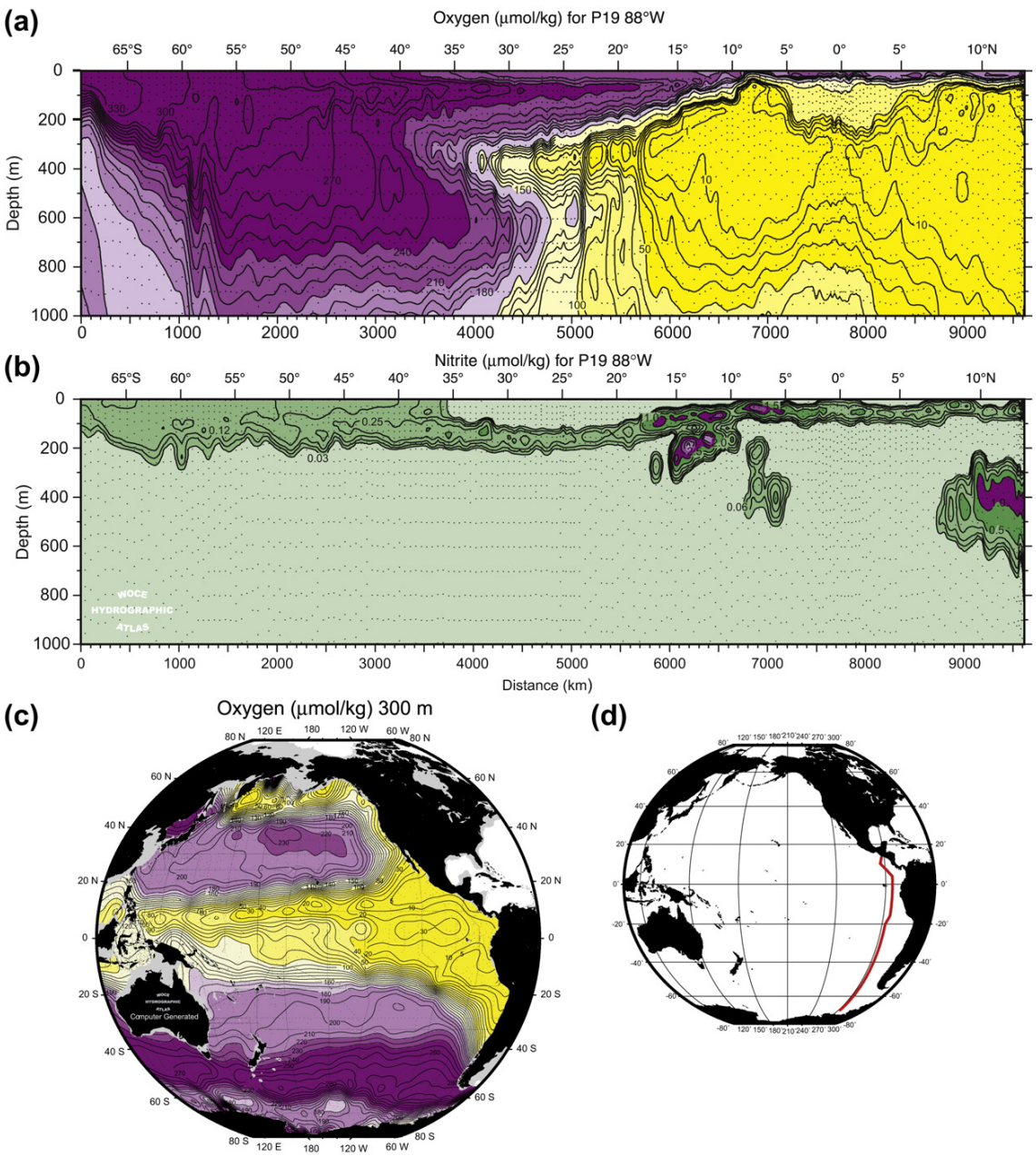

FIGURE 10.32 Tropical oxygen minima and denitrification regions. Eastern Pacific vertical sections of (a) oxygen (µmol/kg) and (b) nitrite (µmol/kg) at 88°W (WOCE P19). (c) Oxygen (µmol/kg) at 300 m depth. (d) P19 station locations. *Source: From WOCE Pacific Ocean Atlas, Talley (2007).*

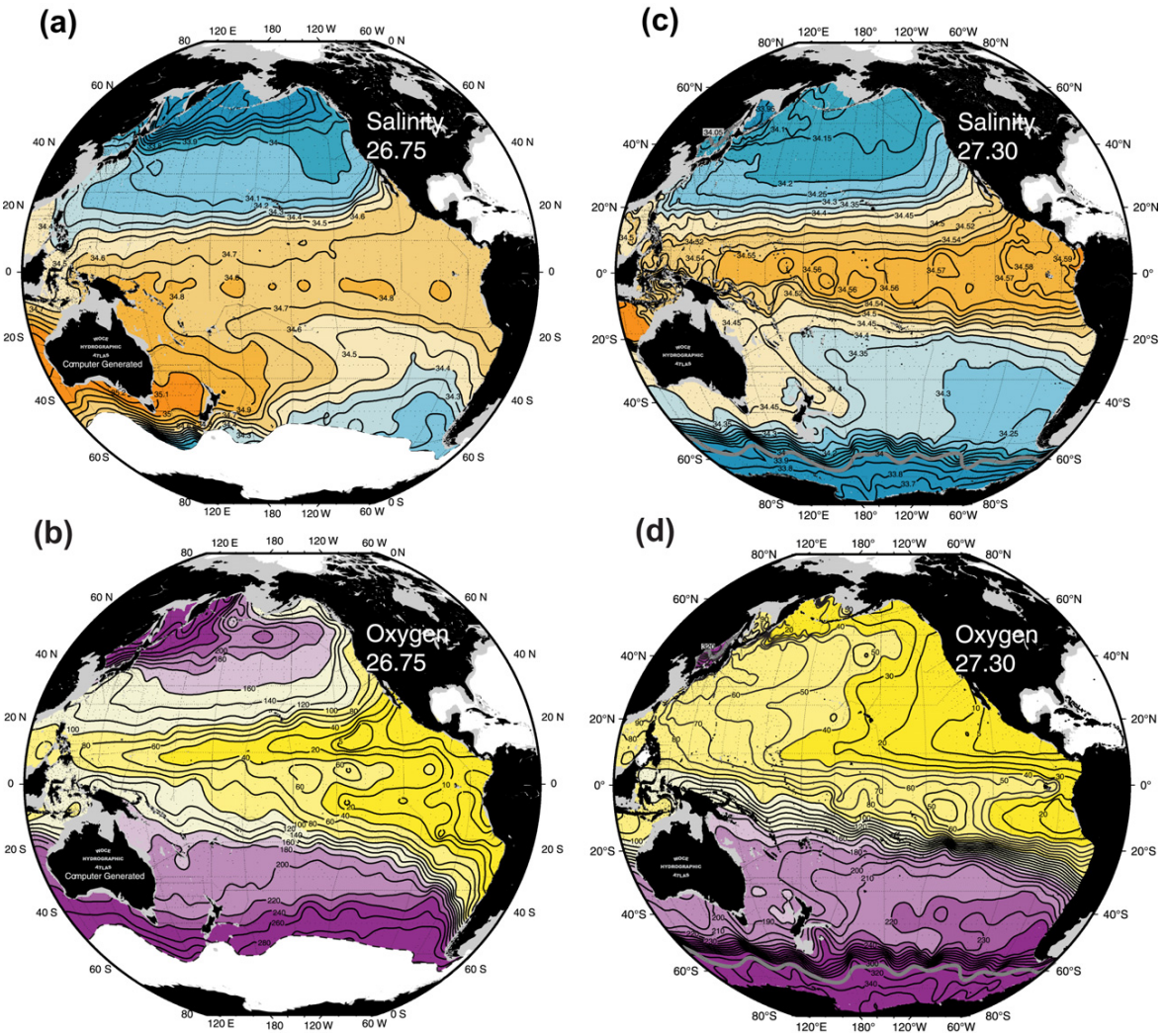

FIGURE 10.33 (a, c) Salinity and (b, d) oxygen (μmol/kg) at neutral densities 26.75 kg/m^3 and 27.3 kg/m^3, characteristic of NPIW and AAIW, respectively. In the Southern Ocean, white at 26.75 kg/m^3 shows the isopycnal outcrops; the gray curve in (c) and (d) is the winter outcrop. Depth of the surfaces is shown in the WOCE Pacific Ocean Atlas. This figure can also be seen in the color insert. *Source: From WOCE Pacific Ocean Atlas, Talley (2007).*

in the northwestern corner of the Okhotsk Sea ("NWP" in Figure 10.34b). Polynyas all along the shelf create brine rejection; the NWP is at the end of the cyclonic circulation, so the water has accumulated the most brine. Historical data suggest that brine rejection can affect densities up to about $\sigma_\theta = 27.1$ kg/m^3. See also the online supplement Section S8.10.6 on the Okhotsk Sea.

A sensible heat polynya maintained by tidal mixing (Figure 3.12b) almost always occurs over Kashevarov Bank ("KBP" in Figure 10.34b). The subsurface temperature maximum is mixed upward, melting the sea ice and fluxing

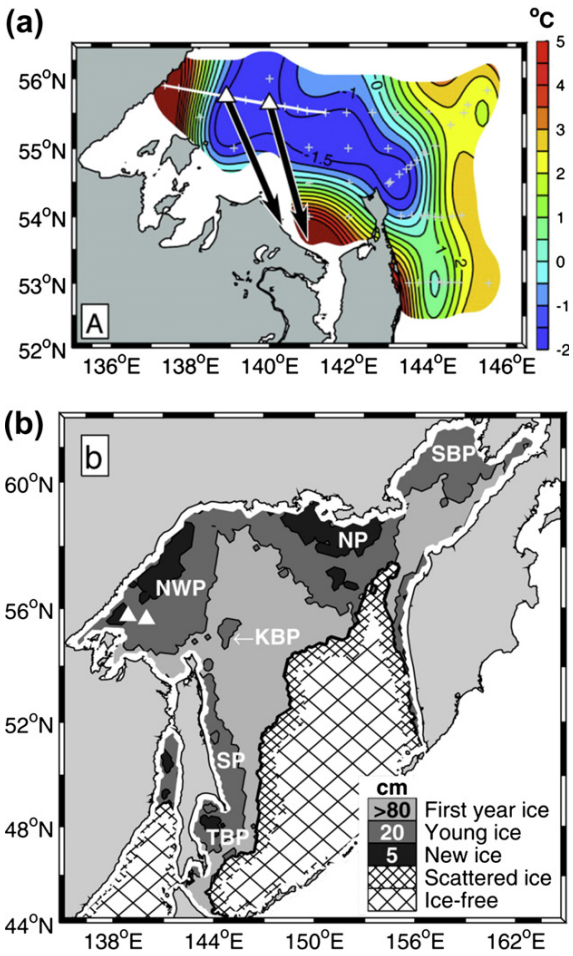

FIGURE 10.34 Dense water formation in the Okhotsk Sea. (a) Bottom potential temperature in September, 1999, and mean velocity vectors at the two moorings. (b) Ice distribution on February 1, 2000, from the SSM/I microwave imager. "NWP" is the northwest polynya where the densest water is formed. Figure 10.34a can also be found in the color insert. *Source: From Shcherbina, Talley, and Rudnick (2003, 2004).*

nutrients to the surface layer; this is a highly productive region biologically. The Okhotsk Sea waters exit back to the northwest Pacific through a deep strait in the Kuril Islands (depth ~ 1500 m). Vigorous tides complete the process of mixing the high oxygen down to the maximum density at the sill, σ_θ ~ 27.6 kg/m^3 (Talley, 1991). The renewed waters that exit into the Oyashio do not have a subsurface salinity minimum; instead, salinity is lowest at the sea surface. The NPIW salinity minimum forms as the renewed Oyashio waters encounter the warmer, saltier, lighter surface waters of the Kuroshio in the transition region between the separated Oyashio and Kuroshio.

The NPIW formation rate based on meridional overturn across 24°N is 2 Sv, which is small compared with the other low salinity intermediate waters. If measured locally, within the subpolar gyre, where most of the newly ventilated water remains, the recycling rate could be higher.

Export of the low salinity NPIW southward into the subtropics balances the net precipitation in the subpolar region and net evaporation in the subtropics. Part of the subpolar freshwater input also exits northward through the Bering Strait, where it eventually becomes part of the North Atlantic Deep Water and is exported to the low latitude North Atlantic (Talley, 2008).

10.9.2.2. Antarctic Intermediate Water

AAIW is the low salinity intermediate layer in all of the Southern Hemisphere oceans north of the ACC (Figure 14.13; Section 13.4.2).

The Pacific AAIW salinity minimum is at a depth of about 700–1000 m through most of the South Pacific. Its potential density is between σ_θ = 27.05 and 27.15 kg/m^3 in the southeast Pacific, where it originates in the thick surface layer (Subantarctic Mode Water) just north of the Subantarctic Front. Its potential temperature and salinity in this region are 4–6°C and 34.1–34.5 psu. The salinity minimum is just the top of the AAIW layer. We generally identify the layer down to approximately σ_θ = 27.5 kg/m^3 as AAIW, based on properties that indicate an identifiable water mass separate from Circumpolar Deep Water (Section 13.5.2).

AAIW circulates anticyclonically around the South Pacific's subtropical gyre. Tongues of low salinity, high oxygen water on the neutral density surface 27.30 kg/m^3 (σ_θ = 27.15 kg/m^3)

originate in the southeast Pacific and stretch northwestward across the South Pacific (Figure 10.32c, d). The AAIW salinity minimum becomes slightly warmer, saltier, and denser along its path. It enters the tropics in the western Pacific, where its density becomes distinctly higher due to higher salinity (mean values of 5.4°C, 34.52 psu, 27.25 kg/m^3 between 15°S and the equator).

The northern boundary of the AAIW is at the Northern Hemisphere tropical-subtropical transition at about 15°N (Figure 14.13); that is, AAIW does not enter the North Pacific subtropical gyre as a salinity minimum. AAIW does extend northward along the eastern boundary to about 35°N, in the "shadow zone" outside the subtropical gyre.

The formation rate of Pacific AAIW is approximately 5–6 Sv based on air–sea fluxes (Cerovecki, Talley, & Mazloff, 2011). A slightly smaller rate of 4 Sv was obtained by Schmitz (1995a), with an additional 10 Sv of AAIW formation for the Atlantic/Indian.

10.9.3. Deep Waters

Two deep waters, distinct from the bottom waters, are identified in the Pacific: Pacific Deep Water and Circumpolar Deep Water. Historically, Sverdrup thought (essentially by analogy with the Atlantic) that a slow southward movement of deep water must occur in the South Pacific. This is the case, but for a different reason than in the Atlantic, which has active deep water formation in the north. PDW, also known as Common Water, originates within the Pacific from upwelled bottom waters and modified UCDW. UCDW originates in the Southern Ocean as a mixture of PDW and Indian Deep Water (IDW; both marked by low oxygen) and deep waters that are formed locally in the Southern Ocean. PDW and UCDW occupy approximately the same density (and depth) range in the Pacific, with UCDW flowing into the Pacific and PDW flowing out. The net transport is southward, hence dominated by PDW (Figure 10.18).

UCDW is described in Section 13.5.3 so is only referred to here where it interacts with PDW.

PDW is one of the major deep waters of the global ocean, with many similarities to IDW (Chapter 11). PDW has no surface sources, unlike North Atlantic Deep Water. PDW is formed entirely internally from upwelling and diffusion. Because PDW is formed internally from waters that flow in from the Southern Ocean, the waters in the PDW are the oldest of the global ocean. PDW is marked by low oxygen, high nutrients, no CFCs, and large Δ^{14}C age (Figures 10.35, 4.12, 4.22, 4.24). The vertical extrema indicating greatest age are centered at 2000–2500 dbar, with the most extreme values in the mid- to high-latitude North Pacific. These signals of age extend southward down the length of the Pacific toward the Southern Ocean. Because the PDW mixes with the younger surrounding waters as it moves south, its age appears to decrease toward the south. These age tracers, especially the low oxygen, mark the presence of PDW in the Southern Ocean. Because it is very old, PDW is well mixed in T-S properties. It includes the highest peak by far in the global volumetric T-S diagram (Figure 4.17), at 1.1–1.2°C, 34.68–34.69 psu (corresponding to σ_4 = 45.87 kg/m^3). (PDW encompasses a wider range of T-S than this.) For this reason, Montgomery (1958) named it the (Oceanic) Common Water. In sections of Figure 4.12, these T-S properties are found in the North Pacific north of 20°N from about 3500 m to the bottom.

In the North Pacific, north of 40°N, the most extreme PDW is found on the isopycnal in Figure 10.35, as indicated by highest silica and lowest salinity (and also the most negative Δ^{14}C in Figure 4.24b). This is the "new" PDW, which is formed of very old waters. The low salinity is acquired through downward diffusion from above. The high silica in the northern

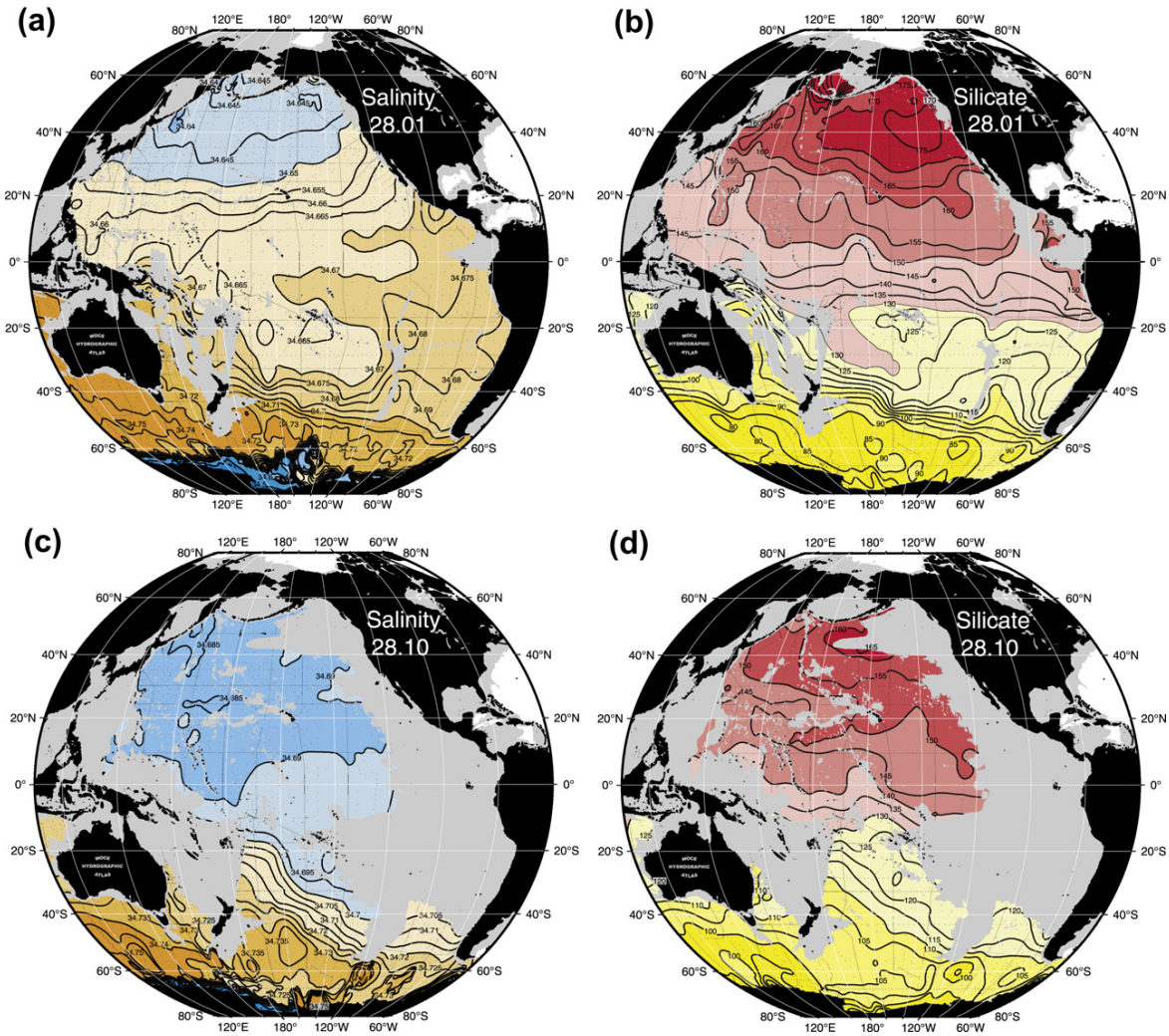

FIGURE 10.35 (a, c) Salinity and (b, d) silicate for PDW/UCDW ($\gamma^N = 28.01$ kg/m^3; $\sigma_2 \sim 36.96$ kg/m^3) and LCDW ($\gamma^N = 28.10$ kg/m^3; $\sigma_4 \sim 45.88$ kg/m^3). Depths of the two surfaces are approximately 2600–2800 m and 3500–5200 m, respectively, north of the ACC. Maps of Δ^{14}C (/mille) and δ^3He (%) at $\gamma^N = 28.01$ kg/m^3 and depth and potential temperature at $\gamma^N = 28.10$ are found in Figures S10.31 and S10.32 on the textbook Web site. *Source: From WOCE Pacific Ocean Atlas, Talley (2007).*

North Pacific, which is also a marker of PDW, comes from both aging of the waters and dissolution from the underlying silica-rich sediments (Talley & Joyce, 1992).

PDW and UCDW are horizontally juxtaposed, especially in the South Pacific. Salinity and silicate on an isopycnal (Figure 10.35a, b) show the higher salinity/lower silicate UCDW entering in the southeast, and the contrasting low salinity/high silicate PDW moving southward in the west.

There is also southward flow of PDW along the South American boundary, evidenced by the higher silica in Figure 10.35b, but much

more obvious in the vertical section of oxygen at 32°S (Figure 10.15b). Salinity in Figure 10.35a does not reflect this southward flow because of the small but noticeable impact of geothermal heating from the East Pacific Rise. The geothermally affected waters are beautifully marked by δ^3He plumes (Talley, 2007). These match the two westward-extending plumes of higher salinity in the tropics in Figure 10.35a. (On an isopycnal, warmer water must be more saline.) The higher salinity at the eastern boundary in the South Pacific is consistent with East Pacific Rise heating, which masks the salinity signature of southward flow.

When it leaves the Pacific and enters the Southern Ocean, PDW joins the IDW, which has a similar density range and is also marked by low oxygen and high nutrients. The layer is then referred to as UCDW, which upwells to the sea surface in the ACC. This upwelled UCDW is the most likely source of the surface waters that are transported northward out of the Southern Ocean (Chapter 14).

10.9.4. Bottom Water (LCDW)

The densest water in the Pacific comes from the Southern Ocean. Its source is a mixture of the deep waters of all three oceans (Atlantic, Indian, and Pacific) that is modified by production of dense waters around the Antarctic continent (Section 13.5.3). In the Pacific and Indian Oceans, it is common to refer to this dense bottom water mass as Lower Circumpolar Deep Water (LCDW). The similar layer in the Atlantic is usually called Antarctic Bottom Water (AABW), which is the nomenclature we use when we discuss this bottom layer globally (Chapter 14).

LCDW is recognized in the Pacific by low temperatures and higher salinity than the overlying PDW (vertical section in Figure 4.12). Its higher oxygen and lower nutrients reflect its somewhat younger age than the very old PDW (Figures 4.12 and 4.22).

At the southern end of the Pacific sections, LCDW is marked by the vertical salinity maximum within the ACC. The higher salinity is a long-distance tracer of North Atlantic Deep Water (Reid & Lynn, 1971). The salinity maximum, which approximately follows an isopycnal, extends northward into the deep Pacific; eventually the maximum salinity is at the ocean bottom. On the 165°W section, this grounding occurs at about 5°S, but in the far eastern Pacific at 88°W, it has already occurred by 45°S (section P19 in the WOCE Pacific Ocean Atlas, Talley, 2007).

LCDW enters the Pacific in the DWBC in the southwest, east of New Zealand (Section 10.6). This inflow is apparent in northward extension of high salinity and low silica in the southwestern Pacific on a deep isopycnal surface characterizing LCDW (Figure 10.35). Some of this signal succeeds in passing through the Samoan Passage at 10°S and crosses into the Northern Hemisphere hugging the western boundary. Silica in particular shows evidence of northward flow all the way along the western boundary to the northern North Pacific.

LCDW properties change to the north as the layer erodes and upwells across isopycnals into the PDW, with downward diapycnal diffusion of heat and freshwater as the source of buoyancy. The upwelling transports were described in Section 10.6, with the budgets suggesting most of the upwelling occurs in the South Pacific and tropics. Evidence of diapycnal diffusion is abundant in the property changes along the LCDW pathway. Salinity on the characteristic LCDW isopycnal decreases to the north, and is lowest in the central North Pacific near the Hawaiian Ridge and in the northwestern North Pacific (with temperature, of course, the mirror image). Similar patterns are apparent on constant depth surfaces and in bottom properties (Figure 14.14).

The bottom water is subject to low levels of geothermal heating that increase its temperature gently, by about 0.05°C from the tropics to the

northern North Pacific. This change is consistent with geothermal heating, and affects a bottom layer of about 1000 m thickness (Joyce, Warren, & Talley, 1986). This buoyancy source could be important for the deepest upward flux in the northern North Pacific, where overturn does not extend much higher above the bottom than this (Section 5.6; Figure 10.18).

10.10. DECADAL CLIMATE VARIABILITY AND CLIMATE CHANGE

The Pacific Ocean represents a large fraction of the global ocean's surface and therefore a large potential for coupled atmosphere–ocean feedbacks. The interannual ENSO (Section 10.8), which has maximum amplitude in the tropics, is an excellent example of efficient coupling. The decadal and longer timescale climate modes are characterized by much larger north-south spatial patterns, with extratropical amplitudes that are similar to tropical amplitudes. Outside the tropics, coupling of the ocean and atmosphere is much weaker and so feedbacks are much weaker and harder to discern.

All of the text, figures, and tables relating to climate variability other than ENSO are located in Chapter S15 (Climate Variability and the Oceans) on the textbook Web site. Chapter S15 covers the following modes of decadal climate variability that most directly affect the Pacific: *Pacific Decadal Oscillation* (PDO), *North Pacific Gyre Oscillation* (NPGO), *Pacific North American* teleconnection pattern (PNA), *North Pacific Index* (NPI), *Southern Annular Mode*. It concludes with a discussion of climate change (trends in temperature, salinity, and oxygen).